Insights on Coarse Sediment Routing in Tributaries of the Buffalo National River, AR

by

Ryan James Brooks

A thesis submitted to the Graduate Faculty of
Auburn University
in partial fulfillment of the
requirements for the Degree
of Master of Science

Auburn, Alabama
December 9th, 2023

[Gravel-Bed Rivers, Tributaries, Provenance, RFID, Sediment Tracking, Buffalo National River]

Approved by

Dr. Stephanie L. Shepherd, Associate Professor, Auburn University
Dr. Ashraf Uddin, Robert B. Cook Professor, Auburn University
Dr. Robert C. Mahon, Assistant Professor, University of New Orleans

Abstract

Sediment routing studies are of particular importance to understanding geomorphic changes in fluvial systems. Although tributary-derived sediment inputs serve as primary sources of sediment in main stems, few in-situ studies analyze controls that dictate these inputs. Thus, gravel caliber and provenance variability in major tributaries of the Buffalo National River (BNR) of northwest Arkansas have been analyzed to identify how lithology and basin morphometrics influence tributary gravel routing in a gravel-mantled bedrock stream. Analyses identified significant coarse sediment inputs from 3 of the 4 study tributaries, with basin area and drainage density appearing to be the most influential morphometric controls on tributary sediment routing processes. Additionally, a pilot study on reach-scale gravel movement was conducted in one of the headwater tributaries of the BNR. This RFID project identified that most bedload movements occur in only the largest peak discharge events, with sediment caliber and channel flow patterns influencing localized sediment entrainment. This study better constrains watershed-scale gravel routing patterns and controls in the BNR, which is critical for understanding channel and basin morphology in this ever-changing fluvial system.

Acknowledgements

I am very thankful for my mentor and advisor, Dr. Stephanie Shepherd, for providing me with the opportunity to further my education and contribute to scientific discovery in my own backyard. Her expertise was appreciated, and I feel as though her guidance and development of my skills as a scientist have truly prepared me to be successful in my future endeavors. I am also thankful for my other committee members, Dr. Ashraf Uddin and Dr. Robert Mahon, for their time, support, and feedback to make my project the best it could be. A special thank you to Dr. Frances O'Donnell for her assistance with running non-parametric statistical analyses in RStudio, as these analyses were of integral importance to this work. I am also very appreciative of Chuck Bitting for coming to the field and sharing his expertise on BNR lithology. Taryn Hicks provided immeasurable support for this project, having assisted with data collections on multiple trips to the field and always supporting my efforts along the way. I also want to thank my wonderful parents, James and Ellen Brooks, for their unwavering support and assistance in the field. It was truly an honor to share my research experiences and field excursions with my parents throughout this project. Another thanks to Abrianna Lance and Taylor Wynn for their assistance in the field. My sincerest gratitude to Bill Cochrane and the National Park Service for granting me permission to research and access field sites included in this study. Shawn Hodges of the National Park Service is also appreciated for allowing us to use the Steel Creek Research Station for one of my trips to the field. This project would not have been possible without research and travel support from the Auburn University Geosciences Advisory Board (GAB) and the Geological Society of America (GSA), to which I am very thankful. Finally, I am incredibly thankful for my family and friends at Auburn University and elsewhere for their constant support and encouragement. I have the most incredible support group and I am truly beyond blessed!

Table of Contents

Abstract ii

Acknowledgments iii

List of Tables vii

List of Figures viii

List of Abbreviations ix

Chapter 1: Introduction 1

Objectives 3

Study Area 3

Stream Classification 4

Geologic Setting 4

Lithology 6

Lithologic Heterogeneity and Valley Width 9

Tributary Basin Morphometrics 10

BNR Bedload Character 11

Ongoing Basin Morphologic Evolution 11

Chapter 2: Theoretical Framework 13

The Morphologic System – Basin Morphometrics 13

Basin Area and Stream Order 14

Basin Shape 16

Topographic Relief and Slope 19

Drainage Density 21

The Cascading System – Water and Sediment 22
Stream Power 22
Stream Competence 23
Channel Roughness 24
Channel Slope 25
Sediment Transport Mechanisms 25
Stream Classifications 27
Bedload Transport in Gravel-Mantled Bedrock Streams 30
Semi-Controlled Stream Bed Considerations 32
Using Coarse Sediment Characteristics to Distinguish Sediment Yields 32
Conclusions 33
Chapter 3: Methods 34
Tributary Selection 34
Gravel Bar Sampling 37
RFID Pilot Project 38
Tributary Morphometric Analyses 41
Chapter 4: Results 43
Gravel Bar Caliber 43
Gravel Bar Provenance 50
Basin Morphometrics 54
Transport in Beech Creek 56
Chapter 5: Discussion 61
Gravel Bar Caliber & Provenance 61

Basin Morphometrics 64
Transport in Beech Creek 70
Conclusions 72
Future Directions 73
Significance 74
References 76
Appendices 85
Appendix A: Beech Creek 86
Appendix B: Cave Creek 101
Appendix C: Calf Creek 114
Appendix D: Clabber Creek 127
Appendix E: Caliber Statistics 140
Appendix F: Basin Morphometrics 145
Appendix G: RFID Data 151

List of Tables

Table 2.1: Alluvial Channel Classification Diagram 29

Table 3.1: DEM, DRG, and Geologic Map DRG's 36

Table 3.2: Basin Morphometrics Calculated 42

Table 4.1: Gravel Caliber Data and Watershed Lithology 44

Table 4.2: Coarse Sediment Provenance Data 52

Table 4.3: Mean Basin Morphometric Values for Northern and Southern Basins 54

Table 4.4: Study Tributary Basin Morphometric Data 55

Table 4.5: RFID Survey Detection Rates and BNR Average Peak Discharge Values 56

Table 4.6: Total Cobble Movement and Average Caliber 59

List of Figures

Figure 1.1: Ozark Plateaus Physiographic Province and BNR Watershed Map 6

Figure 1.2: BNR Stratigraphic Sequence 8

Figure 1.3: Main Stem Lithology and Valley Width Data 10

Figure 2.1: Strahler Stream Order Diagram 15

Figure 2.2: Common Basin Shapes and Associated Hydrographs 17

Figure 2.3: Sediment Loss vs. Relief Ratio Plot 20

Figure 2.4: Regression Plot of the Relationship Between Re and Rr 21

Figure 2.5: Hjulstrom's Diagram 26

Figure 3.1: Map of Study Tributaries 35

Figure 3.2: RFID Cobble Preparation Images 38

Figure 3.3: View of the Beech Creek Confluence Area 39

Figure 3.4: OregonRFID Equipment Demonstration 40

Figure 4.1: Beech Creek Confluence Gravel Size Distribution Graphs 46

Figure 4.2: Cave Creek Confluence Gravel Size Distribution Graphs 47

Figure 4.3: Calf Creek Confluence Gravel Size Distribution Graphs 48

Figure 4.4: Clabber Creek Confluence Gravel Size Distribution Graphs 49

Figure 4.5: Cave, Calf, and Clabber Creek Confluence Provenance Visualizations 53

Figure 4.6: RFID Cobble Detection Time-Series Data 57

Figure 4.7: Log Graph of USGS BNR Daily Peak Discharge Data 59

Figure 4.8: RFID Cobble Placement Grid with Associated Gravel Movements 60

Figure 5.1: Tributary Drainage Density Percentile Ranges 67

Abbreviations

ANOVA	Analysis of Variance
BNR	Buffalo National River
Dd	Drainage Density
DEM	Digital Elevation Model
Dolo	Dolostone
DRG	Digital Raster Graphics
EHS	Einstein-Hubbell-Sayre Model
ESRI	Environmental Systems Research Institute, Inc.
Fm	Formation
GEM	Yang-Sayre Gamma-Exponential Model
GIS	Geographic Information System
GNSS	Global Navigation Satellite System
GPS	Global Positioning System
HCl	Hydrochloric Acid
Ls	Limestone
Miss-Penn	Mississippian-Pennsylvanian Periods
Ord	Ordovician Period
ORSR	OregonRFID Single Reader
PIT	Passive Integrated Transponder
Rc	Circularity Ratio
Re	Elongation Ratio

Rf	Form Factor
RFID	Radio-Frequency Identification
Rr	Relief Ratio
Ss	Sandstone
USGS	United States Geological Survey

Chapter 1: Introduction

Sediment routing studies are of particular importance to landscape evolution, as routing processes result in a myriad of geomorphic changes in fluvial systems. Since channelized sediment loads affect the availability of material to erode and incise the channel floor, sediment volume, caliber, and routing have a profound influence on channel morphology, valley width, and basin morphometry (Foley, 1980; Whipple, 2004; Imhoff and Wilcox, 2016; Keen-Zebert et al., 2017). In gravel-mantled bedrock streams, bedload serves as the primary tool for channel incision, thus controlling the aforementioned geomorphic attributes (Cook et al., 2012). Downstream fining of bedload in gravel-bed rivers is well established and attributed to a combination of abrasion, sorting, and inputs from tributaries and hillslopes (Knighton, 1980). With this being said, however, mathematical models consistently underestimate the degree of fining in natural systems because of the complexity of natural river systems at multiple scales (Pizzuto, 1995). Specifically, existing models poorly account for sediment inputs from tributaries (Rice and Church, 1998).

In the highest reaches of the longitudinal profile of a stream, hillslopes primarily source sediment inputs, as they are directly coupled with the channel in these reaches (Verstraeten, 2006). As a fluvial valley widens downstream, however, tributaries and channel banks become the primary source of sediment in the main stem (Rice, 1998). Further complicating this picture is the degree of lithologic heterogeneity within a watershed. Variations in lithology determine a rock unit's susceptibility to weathering and erosion, which influences both the caliber and volume of coarse sediment produced within a watershed (Beer and Turowski, 2015). Multiple studies have noted that more resistant units will dominate channelized bedload in watersheds with heterogenous lithology (Hack, 1957; Keen-Zebert et al., 2017).

In addition to lithology, tributary basin morphometrics – basin size, shape, relief, slope, and drainage density - also influence watershed-scale coarse sediment routing. Tributary basin characteristics control hillslope sediment production mechanisms (creep, landslides, and overland flow) and channelized sediment routing in tributaries, which directly influence the volume of tributary-derived sediment inputs in the main stem (Leopold et al., 1964; Foley, 1980; Araújo, 2007). Basin form is widely variable based on climate, tectonics, and lithology (Huang et al., 2002; Caracciolo, 2020). Climate directly influences the amount of rainfall in a drainage basin, which impacts overland flow and subsequent erosive processes that produce sediment (Huang et al., 2002). Tectonics and lithology can also influence sediment production and erosion rates as a byproduct of their effect on basin morphometrics and outline form (Horton, 1941; Rigon et al., 1993). These two controls can influence groundwater infiltration rates and basin shape, which both impact peak streamflow discharges necessary for coarse sediment entrainment (Horton, 1945; Strahler, 1964).

The variety of controls on sediment production and routing necessitates in situ studies that can identify specific controls and their direct effect on coarse sediment yields (Caracciolo, 2020). This makes the Buffalo National River (BNR) of northwest Arkansas an ideal field site for studying lithologic controls on coarse sediment production, as the watershed's sub-basins are tectonically stable and share the same climate (Keen-Zebert et al., 2017). Since these other two main controls on sediment production and basin morphometrics are consistent in the BNR, lithologic differences between tributary basins can be evaluated to determine their relative influence on basin morphometrics and tributary-derived coarse sediment inputs in the main stem.

Objectives

Previous work in the BNR has documented both downstream fining and the dominant presence of more resistant bedrock lithologies in the modern gravel bars and terrace deposits (Keen-Zebert et al., 1997). Thus, this thesis builds on the existing body of work in the BNR to investigate the influence of tributaries on gravel caliber and provenance in the main stem. The variation in tributary watershed morphometrics was characterized to provide context for understanding gravel inputs and identifying potential controls on watershed-scale coarse sediment routing. Additionally, a pilot study was conducted in a tributary of National Park Service interest to determine the feasibility of using radio-frequency identification (RFID) technology to track course sediment routing at the reach scale. These results not only add to our understanding of the controls on bedload within the watershed, but also provide insight for future management of the BNR as a natural resource.

To meet these objectives, this study will address the following questions:

1. Do BNR tributary sediment yields have a strong signal in the main stem?
2. To what extent do tributary lithology and basin morphometrics affect coarse sediment production and inputs?
3. How does gravel move at the riffle-pool scale in a gravel-mantled bedrock stream?

Study Area

The BNR of northwest Arkansas was designated as our nation's first National Scenic River in 1972 for its unique geologic features and historical importance to the region. Meandering ~238 kilometers across the Ozark Plateaus to its confluence with the White River (Keen-Zebert et al., 2017), the BNR is one of the longest free-flowing rivers in the continental United States. Since the

BNR is protected, it has avoided subsequent sediment routing and deposition disturbances that accompany dam construction, rendering the unique opportunity to study a fluvial system with primarily natural controls on sediment routing. With this said, however, late 20th century land use changes in the region are thought to have increased sediment loads in the modern system (Scott and Udouj, 1999). Thus, human influence is not entirely obsolete in the watershed, though it is likely more limited than dammed streams in the region.

Stream Classification

Both the BNR and its tributaries classify as gravel-mantled bedrock streams, which incise through relatively flat lying Ordovician, Mississippian, and Pennsylvanian sedimentary units (Keen-Zebert et al., 2017). Downcutting in the main stem mobilizes predominantly gravel-sized sediments (2-256 mm; Wentworth, 1922), which then interact with the channel bed and influence channel form. The BNR is primarily bedload transport dominated (following Kondolf et al., 2003) and can be described as a semi-controlled stream with locally determined material constraints on morphology (following Schumm, 1963, 1985), as main stem and tributary channel reaches will alternate between gravel-mantled bedrock beds and bedrock pavement. Additionally, main stem and tributary channels are occasionally constrained in reaches that flow against bedrock cliffs.

Geologic Setting

The BNR watershed is situated within the Ozark Plateaus physiographic province of northern Arkansas and southern Missouri. This province is a structural dome that was uplifted from the Pennsylvanian to Early Permian in conjunction with the Ouachita Orogeny (Fenneman, 1928; Hudson, 2000; Hudson and Turner, 2022). The Ozark Plateaus province includes four

differentiated regions: the Boston Mountain Plateau, the Salem Plateau, the Springfield Plateau, and the St. Francois Mountains (Figure 1.1). The BNR watershed is primarily located within the Springfield Plateau, though some overlap occurs with the Boston Mountain Plateau to the south and the Salem Plateau to the north. Each of the three plateau surfaces have distinguishable escarpments that lie between them (Knox, 1966). Ultimately, the combination of the Eureka Springs Escarpment (forming the boundary between the Salem Plateau and the Springfield Plateau) and the Boston Mountain Escarpment (distinguishing the Springfield Plateau from the Boston Mountain Plateau to the south) has led to the exposure of sedimentary units from the Early Ordovician to Middle Pennsylvanian in the BNR watershed (Purdue and Miser, 1916; Knox, 1966; Keen-Zebert et al., 2017).

In addition to these escarpments, fault systems stemming from the Ouachita Orogeny of the Middle Mississippian are present in the region (Hudson, 2000). These include both normal and transform faults, with the normal faults generally striking to the east and the transform faults striking roughly northeast (Hudson, 2000). These faults add complexity to understanding sediment provenance in the watershed.

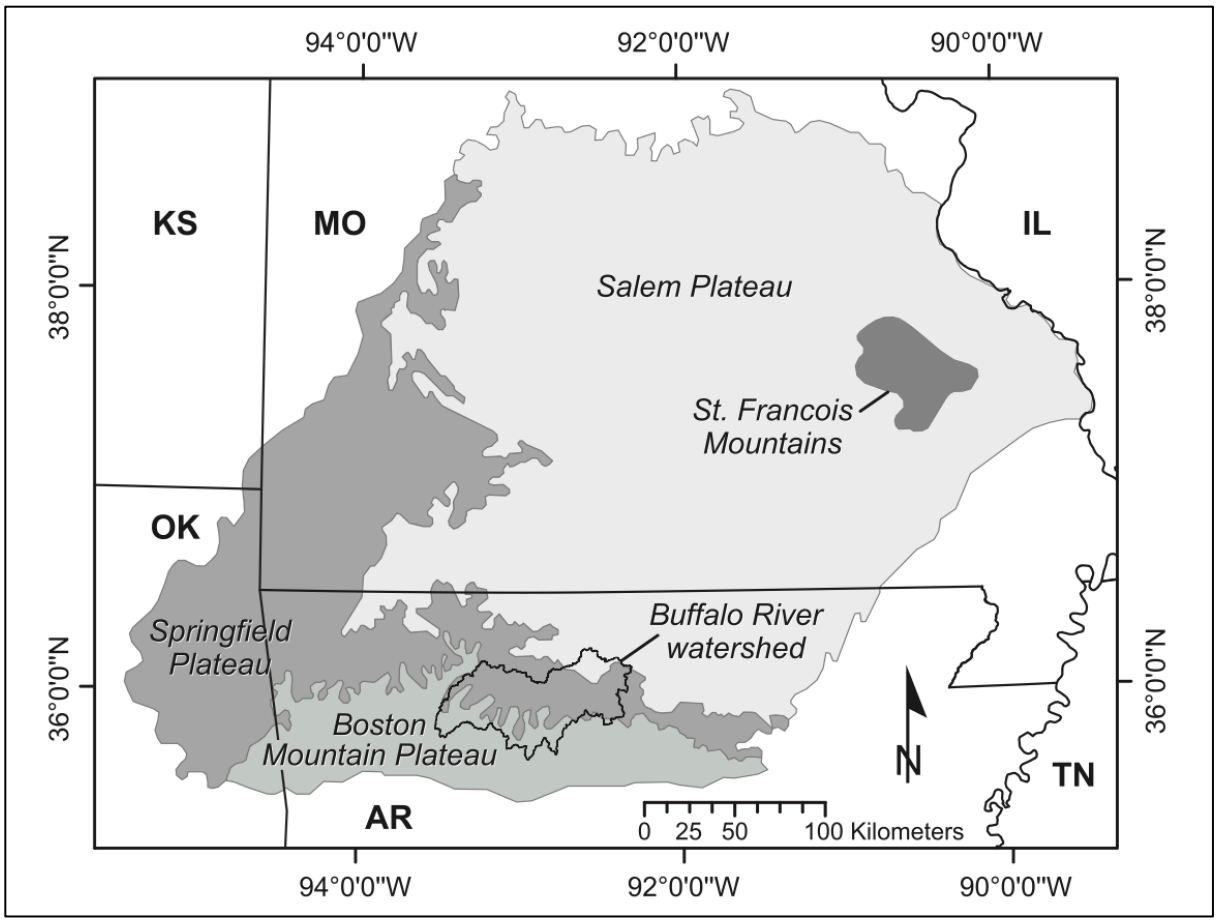

Figure 1.1: Map of the extent of the BNR watershed within the Ozark Plateaus Physiographic Province and the specific regions that comprise the Ozark Dome; from Keen-Zebert et al. (2017).

Lithology

While Ordovician-aged Salem Plateau units are exposed in tributary watersheds along the lower BNR, the main stem of the BNR and most tributaries incise Ordovician and Mississippian-aged rock units within the Boston Mountain and Springfield Plateaus (Keen-Zebert et al., 2017; Figure 1.2). The Everton Formation is composed of interbedded Ordovician-aged limestones, dolostones, and sandstones (Hudson and Murray, 2003). The Newton Sandstone Member, a well-rounded and well-sorted sandstone unit, separates the Everton into upper and lower units (McKnight, 1935). As a primary cliff former in the watershed, the Everton is exposed at river level

in sections of the main stem and many tributaries. The St. Peter Sandstone (Giles, 1932) is also of Ordovician age and sits conformably above the Everton. This unit, much like the Newton Sandstone member of the Everton Formation, is quite friable and distinctive from the younger sandstones in the watershed (Ausbrooks et al., 2012b). The St. Peter is often exposed in thin bands on hillslopes that cap the upper boundaries of the Everton.

Exposed Mississippian units in the watershed are dominated by the Boone Formation's interbedded cherty limestone and thinner units of sandstone and shale (McFarland, 1998). The Boone is the most wide-spread unit in the watershed, as it underlies most of the surrounding hillslopes and, like the Everton, is a common bluff-forming unit with exposures at river level along reaches of the main stem and tributaries. Thinner units that overlie the Boone Formation include the Batesville Sandstone and Fayetteville Shale, which are mostly present in the higher elevation portions of the watershed where other Mississippian and Pennsylvanian sandstones are exposed (Keen-Zebert et al., 2017). Although the Batesville Sandstone is relatively thin (~1.5-9 meters thick; Hudson and Turner, 2007) and not widely exposed in the watershed, this unit is rather resistant to weathering and presents itself in channelized coarse sediment deposits.

Lastly, the Upper Mississippian to Middle Pennsylvanian units commonly found in the upper portion of the watershed include sandstones, shales, and siltstones (Hudson and Turner, 2007). Higher elevation areas in the Boston Mountain Plateau are commonly capped by the resistant Atoka and Upper Bloyd Formation sandstones. The Upper Bloyd is rather distinctive due to extensive bioturbation borrows, which are easy to identify in hand sample.

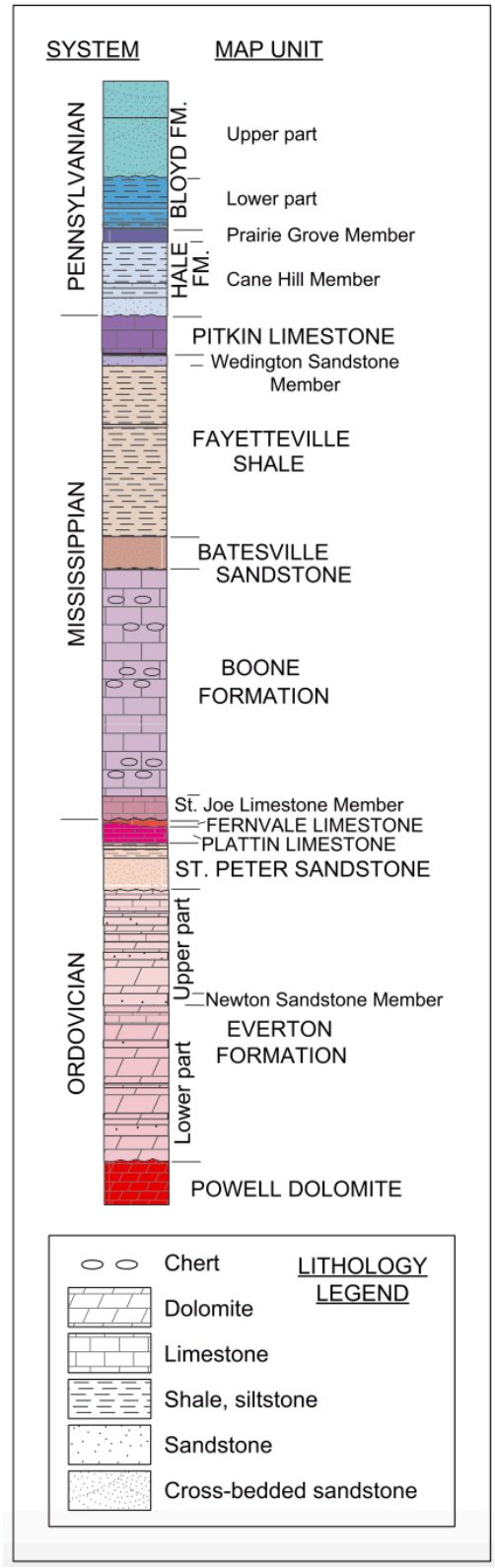

Figure 1.2: Stratigraphic sequence of rock units present in the BNR watershed; from Keen-Zebert et al. (2017).

Lithologic Heterogeneity and Valley Width

Ongoing work in the BNR has identified heterogenous lithology as a primary control on valley form variability due to differences in weathering resistance (Keen-Zebert et al., 2017; Rodrigues et al., 2023). The headwaters of the BNR incise the Boone Formation and have relatively wide, flat valley floors. As the river cuts into the Everton Formation 30 kilometers downstream, however, the valley abruptly decreases in width (Figure 1.3). This pattern is repeated where Paleozoic faulting at river kilometer 114 brings the Boone Formation back to the surface, allowing for increased lateral erosion through river kilometer 153. The Boone reaches likely create a situation in which it becomes more physically difficult for hillslope processes to move gravel to the main stem, as the wide and flat valley floors of limestone reaches cannot provide adequate gravitational potential for sediment movement due to a lack in slope. Additionally, due to increased valley width (Keen-Zebert et al., 2017), sediment sources in limestone reaches are further from the river than those in sandstone reaches. BNR reaches that incise the Everton sandstone, however, form narrower valleys with step-like terraces that dominate hillslope morphometry (Keen-Zebert et al., 2017). Because of these differences, gravel inputs from tributaries may be of greater influence on gravel composition and caliber within the main stem of the BNR in the wider limestone reaches. Thus, while hillslope processes can dominate sediment production, local lithology may dictate the prevalence of tributary-derived sediment yields over hillslope-derived sediment yields due to significant differences in valley width and form.

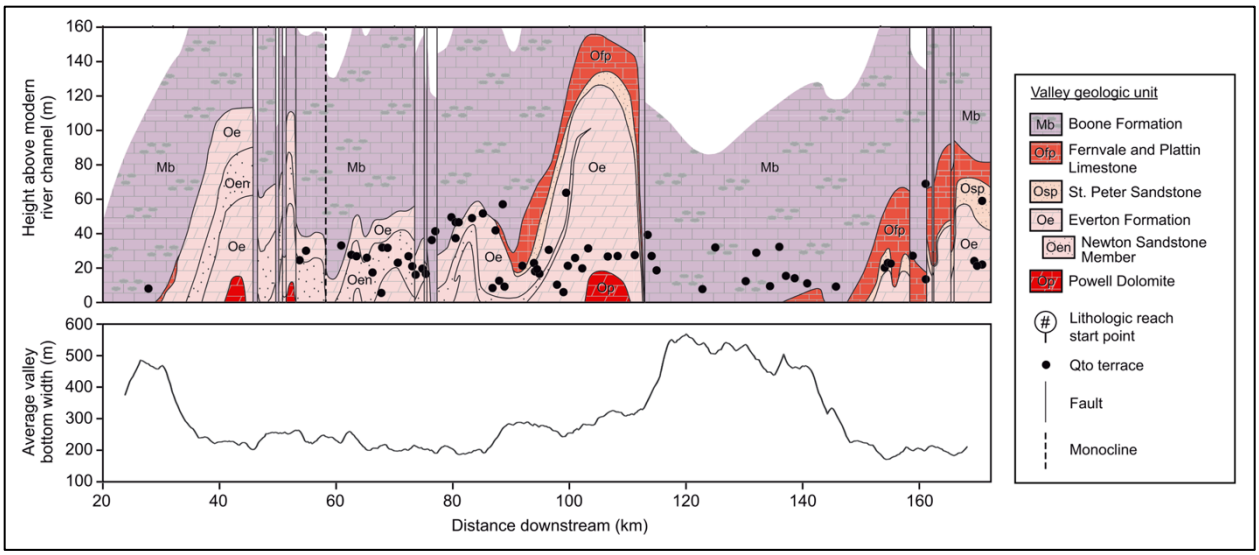

Figure 1.3: Valley width and terrace distribution along the main stem of the BNR with surface lithology. Notice the valley width trends in relation to the most-prominent valley lithology; modified from Keen-Zebert et al. (2017).

Tributary Basin Morphometrics

The possibility that main stem valley width dictates the relative influence of tributary sediment inputs on main stem gravel compositions further necessitates the importance of studying controls on tributary inputs when evaluating sediment routing in a watershed. Tributary basins can have varying degrees of sediment production due to morphometric factors that influence the effectiveness of hillslope processes and channelized sediment routing (Griffiths and Topping, 2017). These factors include drainage outline forms, basin area, basin topographic relief, drainage density, flow competence, channel slope, and more (Horton, 1945; Strahler, 1957, 1964; Komar, 1987; Booth, 1990; Sólyom and Tucker, 2004; Sukristiyanti et al., 2018). Quantifying tributary basin morphometrics can help to identify why particular tributary basins may be more efficient in providing coarse sediment inputs in the main stem.

Of these morphometrics, tributary basin shape and area appear to be spatially different on either side of the BNR. Tributary basins north of the main stem have a smaller surface area than

the basins that flow from the south. Additionally, the southern basins visually appear to be more elongated, while the northern basins appear to be more rounded. These differences are generally attributed to the greater relief of the Boston Mountain Plateau in the southern portion of the watershed (Quinn, 1958). Hence, tributary basin morphometrics were analyzed to provide context for interpreting gravel routing patterns in the BNR.

BNR Bedload Character

As previously mentioned, the BNR includes granule-to-cobble-sized (2-256 mm) bedload, which requires a higher flow velocity threshold to be met to stay in transport (Jacobson and Gran, 1999). Since coarse sediments remain stationary during typical daily discharges, coarse material can only move as bedload during infrequent, high-flow events (Jacobson and Gran, 1999). This is particularly the case in basins with rainfall-dependent hydrologic systems like the BNR, as periods of runoff tend to cause abbreviated high-flow events. Previous work in the region has documented that bedload material moves in waves of storage and remobilization across multiple drainage basins in the Ozark Plateaus (including the BNR), causing erosion and alterations in channel form overtime (McKenney and Jacobson, 1996; James, 1997; Jacobson and Gran, 1999).

Ongoing Basin Morphologic Evolution

Though the Ozark Plateaus province is structurally stable, recent work by Beeson et al. (2017) indicates that the region has experienced topologic reform, or the reorganization of stream networks, by way of stream capture and migrating drainage basin boundaries. These processes have continued to influence basin form and stream channel networks in the BNR region, as the

Ozark Plateaus have yet to reach an equilibrium state. Thus, basin evolution is currently occurring in the BNR region, which will potentially change basin morphometrics over time.

Chapter 2: Theoretical Framework

As this study primarily focuses on coarse sediment routing, it is important to understand how basin morphometrics and channel characteristics can act as controls on sediment production and routing within the fluvial system. To approach this theoretical discussion, Piégay and Schumm's (2003) framework for categorizing fluvial systems is employed. This framework differentiates the fluvial system into two interconnected components: the morphologic system and the cascading system. The morphologic system includes the hillslopes, floodplains, and other landscape features and their associated characteristics within a drainage basin, while the cascading system focuses on the channel characteristics that dictate transfers of mass and energy – i.e. water and sediment movements - within the system. Put simply, the morphologic system encompasses basin characteristics that are interdependent on the flow processes of the cascading system. Together, the interplay of these geomorphic components dictates sediment routing in a fluvial system.

The Morphologic System – Basin Morphometrics

Drainage basins possess a variety of key morphometric characteristics that directly influence geomorphic landscape evolution (Piégay and Schumm, 2003). Basin area, basin shape, topographic relief, average slope, drainage density, channel network topology, lithology, and a variety of other physical characteristics greatly influence how water and sediment move through a watershed (Horton, 1932, 1945; Strahler, 1964; Shreve, 1969; Piégay and Schumm, 2003). Thus, understanding each of these morphometrics and their controls on sediment production and routing

can help to better inform landscape evolution interpretations and provide context for understanding the cascading system.

Basin Area and Stream Order

Drainage basins are defined as the total land area in which overland flow contributes to a defined main stem and includes the tributaries or sub-basins of each lower-ordered stream (Strahler, 1964). Intrinsically linked to this definition, stream order is a dimensionless metric that defines a stream's position in relation to the watershed (Horton, 1945; Strahler, 1964; Scheidegger, 1965). Though there are a variety of approaches for determining stream order, Strahler's (1964) system is the most used in fluvial geomorphic applications. For classification, the smallest streams at the edge of a drainage basin are given an order of one (Figure 2.1). Once two first-order streams meet, the stream becomes a second-order stream. When two second-order streams meet, it becomes a third-order stream, and so on. Stream order classification systems imply that the main stem, of which all overland flow in a specific basin flows through, is of the highest order (Strahler, 1964; Scheidegger, 1965). Furthermore, it is implied that as stream order increases, other characteristics like channel cross-sectional area, discharge, and stream power will increase. Different stream orders at tributary confluences can, therefore, indicate a stream's relative ability to entrain and transport sediment, i.e., stream power (Bagnold, 1960). With this said, however, stream order is limited as a metric for comparison, as it is very generalized and does not correlate with specific cross-sectional areas or discharges within a single basin or between different basins. This means that streams of different orders in different drainages can still have net equal discharge, stream power, and other characteristics. Thus, stream order should be used in combination with other basin morphometrics when comparing different drainage networks.

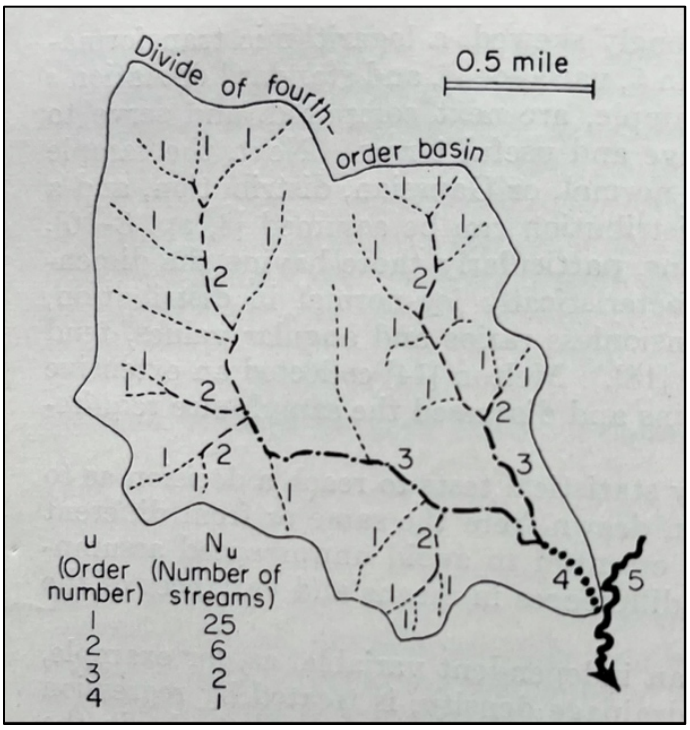

Figure 2.1: Schematic illustrating Strahler's method of determining stream order; from Strahler (1964).

Regardless of this limitation, basin areas are directly proportional to stream order, channel lengths, and discharge at pour points (Schumm, 1956; Strahler, 1957, 1964). This generalization suggests how interconnected each of these basin morphometrics are, which necessitates researchers to compare basins of the same magnitude (Strahler, 1957). If this is not done, then there is no correspondence to base comparisons upon, as the magnitudes of these geomorphic characteristics will differ greatly between small and large drainage basins (Strahler, 1957).

Strahler's (1957) work emphasized basin area as a major factor in discharge, and therefore, sediment yields. Hack (1957) supports this theory by displaying how discharge and basin area were directly proportional in data from different gaging stations along the Potomac River. Strahler's theory on sediment yields in this context is derived from the notion that larger basin areas collect more runoff, thus allowing for greater stream power for sediment routing. The

proportional relationships between area and other basin characteristics mean that larger basins should also have longer channels, greater stream network complexity, and greater discharge, which equips these basins with a greater potential for sediment entrainment. This theory will be analyzed in this study.

Basin Shape

Basin shapes, and their capability to change dynamically over relatively short geologic time-scales, affect basin hydrology and erosion rates (Strahler, 1964; Sólyom and Tucker, 2004). Basins begin to take shape when a channel is initiated from adequate overland flow on an inclined land surface, which forms a rill that bifurcates over time. The rills widen and deepen into channels, extending in length through headward erosion, until a drainage basin develops (Horton, 1941, 1945; Strahler, 1964). While an ovoid shape is the most common form, tectonic activity, heterogenous lithology, topographic relief differences, and other physical features can result in more elongated or more rounded shapes (Horton, 1941; Strahler, 1964; Rigon et al., 1993). These basin shape variations can influence peak flood-discharge rates at a basin's outlet (Strahler, 1964; Das et al., 2022). Per Strahler (1964), elongated basins tend to have reduced peak flood-discharges at their confluence, while circular basins have much greater flood-discharges at their confluence (Figure 2.2). Since peak flood-discharges directly influence stream power in this context (Booth, 1990), basin shape may influence the ability of tributaries to entrain and transport coarse sediment to a main stem.

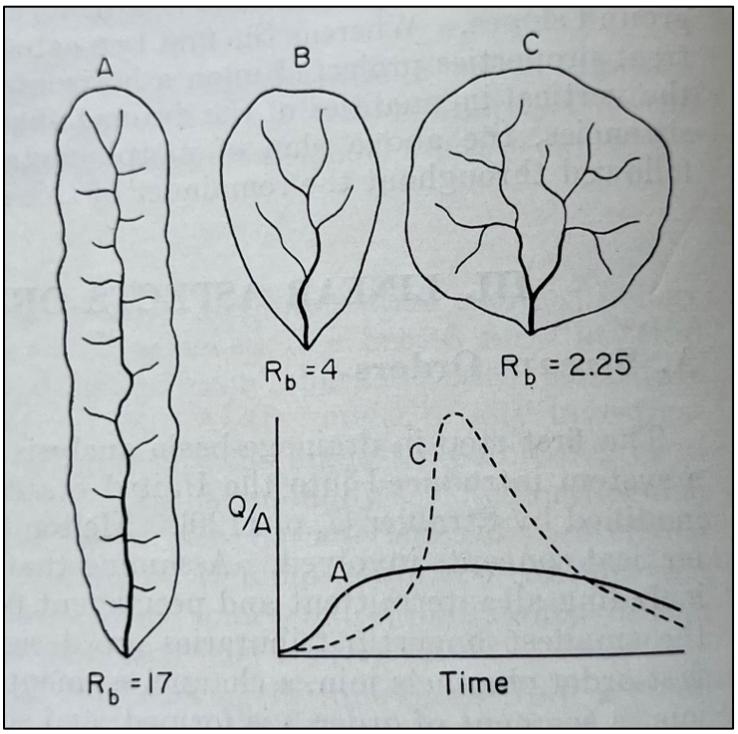

Figure 2.2: Example basin shapes and their associated hydrographs (R_b represents bifurcation ratio). **A** is an elongated basin, **B** is an ovoid basin, and **C** is a circular basin; from Strahler (1964).

A variety of quantitative metrics can be used to define basin shape. Specifically, form factor, the circularity ratio, and the elongation ratio are particularly useful for this assessment (Horton, 1932; Schumm, 1956; Strahler, 1964). These quantitative comparison metrics can assist in identifying differences between drainage basins and their subsequent influences on sediment transport.

Form factor (Rf) represents the ratio between basin area and the squared basin length (Strahler, 1964; Sukristiyanti et al., 2018). Greater Rf ratio values signify basins with high peak flood discharges during a shorter time interval, while lower Rf values represent elongated basins with lower peak flood discharges over a longer period of time (Sukristiyanti et al., 2018). Consequently, lower peak flood discharges do not allow for coarse sediment to be entrained as

easily as high peak flood discharges, thus decreasing the ability of elongated sub-basins to contribute coarse sediment to a main stem.

The circularity ratio (Rc) is a dimensionless ratio between the basin area and a circle area possessing a circumference that equals the basin perimeter (Strahler, 1964). Typically, Rc values are indicative of a basin's degree of dendritic development and are commonly used to identify tectonically controlled drainage shapes and patterns (Magesh et al., 2011; Sukristiyanti et al., 2018). This metric is very useful in tectonically active basins, as neighboring basin forms can differ drastically in response to structural controls.

Of these ratios, the elongation ratio (Re) is perhaps the most suitable metric for defining basin shape (Gray, 1961). Schumm (1956) identifies Re as the ratio between the diameter of a circle of equal area to that of the basin and the basin's maximum length. This longest length can be interpreted to be the length from the basin outlet to the furthest point upland in the basin that is parallel to the main stem (Schumm, 1956). Lower Re values represent elongated basins with larger topographic reliefs, while higher values represent circular basins with less topographic relief (Kumar, 2011; Sukristiyanti et al., 2018).

Sukristiyanti et al. (2018) analyzed the interrelationships between Rf, Rc, and Re in nine east Indian watersheds and discovered a positive correlation between each. This correlation can be generalized across different physiographic settings – as low values of each metric tend to indicate an elongated basin shape with greater topographic relief (Ansari et al., 2012). While the ratios should be correlated with one another across various drainages, each metric should also be analyzed individually, as each ratio is informed by specific basin controls (peak discharge for Rf, topographic relief for Re, tectonic activity/dendritic stage for Rc). Identifying large deviations from average ratio values can indicate specific controls that dictate basin shape more than others

in a watershed. Thus, relating and analyzing these factors can help to identify how specific basin controls act together to influence basin shape and, subsequently, geomorphic processes (peak discharge, steeper slopes, etc.) that directly influence sediment transport. Once these metrics are compared to one another in a specific region, they can be compared to basins of a different region, thus highlighting the differences between each.

Topographic Relief and Slope

Topographic relief in drainage basins has a documented relationship with basin shape (Kumar, 2011; Sukristiyanti et al., 2018). Generally, basins with a more elongated shape tend to have greater relief and, thus, greater average slopes than circular basins in the same physiographic region (Schumm, 1956; Sukristiyanti et al., 2018). Additionally, elongated basins have greater potential for erosion via hillslope processes, as average basin slopes tend to be greater (Sukristiyanti et al., 2018). To examine relief and slope, a dimensionless Relief Ratio (Rr) between topographic relief (difference between the highest and lowest elevations in a watershed) and the longest basin length can be calculated (Strahler, 1957). Rr values effectively represent average slope in a drainage basin, which can be linked to hillslope erosional potential (Strahler, 1957; Sukristiyanti et al., 2018). For example, Schumm (1954) found a statistically significant relationship between mean sediment yield and relief ratio across varying lithologies (Figure 2.3). Of the basins studied, resistant underlying lithologies tended to exhibit lower sediment losses and lower relief ratios, while less resistant lithologies were tied to greater sediment loss and higher relief ratios. This relationship suggests that relief ratios and sediment inputs are dependent on lithologic resistance in a watershed. These interrelationships suggest that relief ratio can be utilized

with other factors to better understand hillslope-derived sediment inputs (Schumm, 1954; Strahler, 1957).

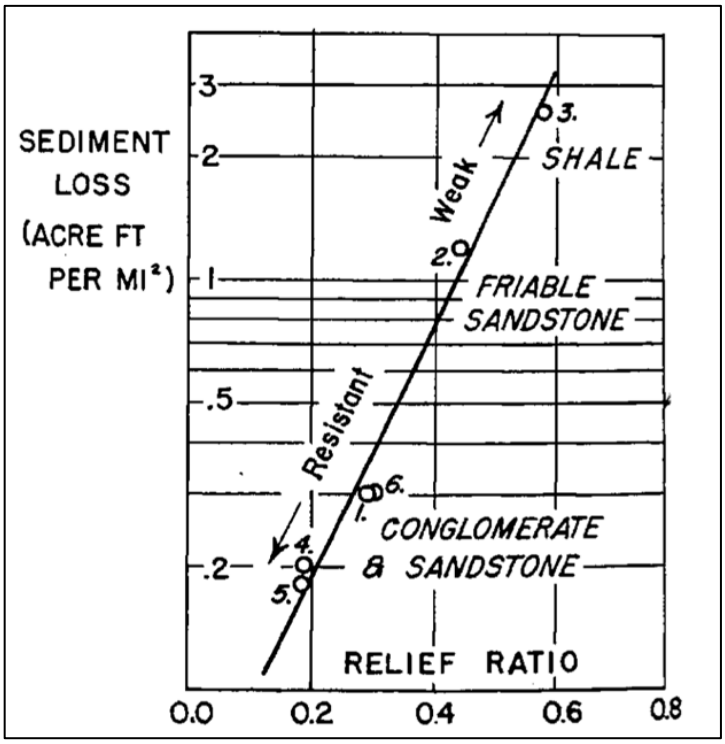

Figure 2.3: Plot of relationship between sediment loss and relief ratio; from Strahler (1957).

Additionally, Schumm (1956) provided quantitative evidence that elongated basins tend to have greater relief, as he explored the relationship between Re and Rr in eight different North American watersheds (Figure 2.4). In his research, Schumm found that relief ratio is inversely proportional to the elongation ratio. This linear regression further exemplifies the role that topographic relief plays in basin morphology, as topographic relief directly influences basin shape and other processes that directly influence sediment routing.

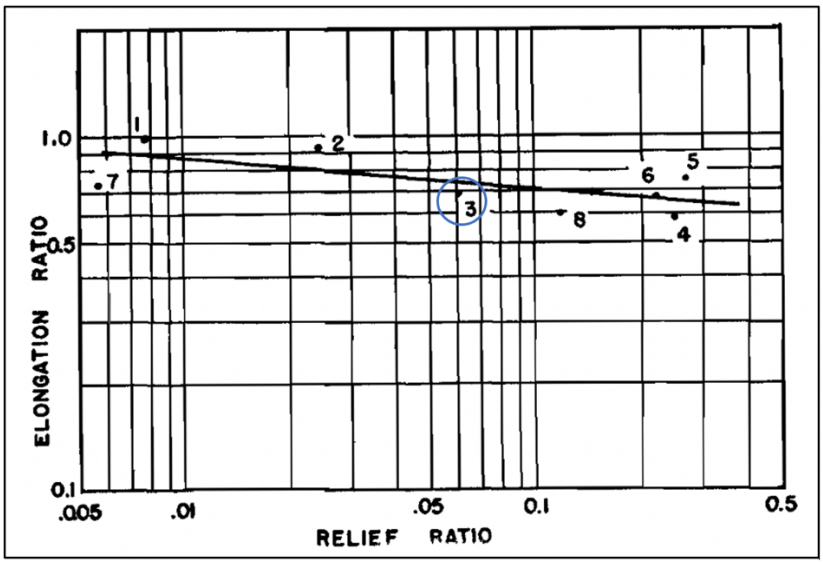

Figure 2.4: Regression plot of the relationship between Re and Rr utilizing data from a variety of drainages in the United States. Note that the Ozark Plateau is #3 (circled in blue); from Schumm (1956).

Drainage Density

Horton's (1945) drainage efficiency metric, known as drainage density (Dd), is defined as the ratio between the sum of stream lengths and the overall drainage area. Greater Dd values tend to indicate basins with more complex stream networks, while lower Dd values are associated with simpler networks of less channels. While this seems to be a simple metric, there are a variety of geomorphic factors that influence Dd. Of these, lithology, climate, and topographic relief are primary controls (Strahler, 1964). Specific to lithology, lower Dd values tend to be located in areas in which the regolith and underlying lithology are highly permeable or resistant to erosion, which causes fewer channels to be present to transport runoff and, subsequently, an increased opportunity for water to infiltrate the subsurface (Horton, 1945; Strahler, 1964). Basins with higher Dd values are likely dominated by surface runoff due to the presence of an impermeable subsurface and/or weaker lithology, which results in the incision of more channels for runoff to flow into (Strahler, 1964). Thus, Dd more closely measures a basin's ability to drain surface runoff as stream

discharge, as heavily influenced by a basin's subsurface infiltration capacity and erosive resistivity (Horton, 1945; Strahler, 1964). This metric is important for inferring whether tributary basins are dominated by surface runoff or interflow, as this distinction is of great importance to sediment routing mechanisms. If tributaries exhibit low Dd values that suggest the basin may have increased subsurface infiltration, then less streamflow would be present to allow for channelized sediment routing, and vice versa.

The Cascading System – Water and Sediment

Piégay and Schumm's (2003) cascading system encompasses the flow of mass and energy within a watershed, which directly influences fluvial channels and their ability to transport sediment. Characteristics such as stream power, flow competence, sediment caliber, channel slope, stream type, lithology, and more directly influence channel form and morphometry, as well as previously described basin morphometric parameters.

Steam Power

Sediment transport serves as a major component of the cascading system, as well as a primary control on channel form (Kondolf et al., 2003; Piégay and Schumm, 2003). This control necessitates the need to understand sediment routing when evaluating channel morphology, and vice versa. Since sediment transport is both temporally and spatially variable, however, it is complicated to quantify (Hicks and Gomez, 2003). Therefore, it is important to understand transport mechanisms and controls that generate this variability, such as the basic fluid mechanics that mobilize sediment (Knapp, 1938). Channelized sediments require energy to be entrained and transported (Bagnold, 1960). Thus, the stream power equation quantifies the ability of a stream to

do work, which is derived from the transition of potential, gravitational energy to turbulent, kinetic energy (Knapp, 1938; Bagnold, 1960). Total stream power can be described by the following equation:

$$\Omega = \gamma Q s \qquad \text{Eq. 2.1}$$

where γ is the specific weight of water, Q is discharge, and s is the channel slope (Knighton, 1999). In theory, the greater the stream power, the greater the ability to mobilize sediment (Knighton, 1999).

Stream Competence

While adequate stream power is a prerequisite to sediment transport, the stream power equation does not account for the character of the sediment itself. Thus, stream power is related to sediment caliber by a channel's competence metric, which is a measure of the largest sediments that a stream can transport (Gilbert and Murphy, 1914; Komar, 1987; Booth, 1990). Stream competence represents the ability of a turbulent flow to overcome the critical shear stress required for sediment entrainment via the flow's basal shear stress (Booth, 1990; Hayes et al., 2002). The equation for basal shear stress is as follows:

$$\tau_b = \rho_w g d S \qquad \text{Eq. 2.2}$$

where basal shear stress (τ_b) is the product of the relationships between water density (ρ_w), acceleration by gravity (g), depth of flow (d), and slope (S). Due to the correlation between flow depth (d) and discharge (Q), as well as the subsequent correlation between discharge and basin area, theory supports the idea that basal shear stress can generally be tied to basin area (Begin and Schumm, 1979; Booth, 1990). As a result, this equation establishes a linkage between channel characteristics and basin morphometrics, which further exemplifies the importance of studying

each when analyzing basin-wide sediment routing. More significant, however, is the positive relationship between basal shear stress and channel slope that this equation establishes (Booth, 1990).

Channel Roughness

Though basal shear stress is an important flow metric in overcoming critical shear stress for entrainment, it must be considered in relation to the shear stress associated with channel roughness (Hayes et al., 2002). Channel roughness is a measure of the friction created by channel bed and bank materials, which restrict streamflow and sediment transport. The difference between basal shear stress (as defined above) and the counteracting shear stress resulting from roughness is defined as the effective basal shear stress enacted upon sediments (Hayes et al., 2002). Since channel roughness can reduce this effective basal shear stress by increasing the basal shear stress required for sediment entrainment, channel roughness acts to decrease sediment entrainment, as roughness counteracts the stress sediments receive from streamflow. This relationship indicates the importance of analyzing flow resistance as a result of channel roughness, as sediment transport decreases with increasing flow resistance (Cowan, 1956; Hayes et al., 2002).

Channel roughness is calculated using Manning's Equation (Cowan, 1956; Marcus et al., 1992). Manning's Equation is as follows:

$$v = R^{2/3} S^{1/2} / n \qquad \text{Eq. 2.3}$$

where v = velocity (in m/s), R = the hydraulic radius, and S = slope. Manning's roughness coefficient (n) increases with increasing grain size. Though the literature has introduced a variety of quantitative and qualitative methods for assessing the roughness coefficient, the majority of methods agree that sediment caliber has the greatest influence on channel roughness (Limerinos,

1970; Marcus et al., 1992). Additionally, multiple studies identify that the roughness coefficient is positively correlated with channel slope, as is established by Manning's Equation (Jarrett, 1984; Hayes et al., 2002; Prancevic and Lamb, 2015). This conclusion is logical, as an increase in slope increases the frictional effect of channel roughness, as more cobbles encounter turbulent flow in steeper streams.

Channel Slope

As previously mentioned, channel slope is directly correlated to stream power, basal shear stress, and Manning's roughness coefficient (Booth, 1990; Hayes et al., 2002). Thus, when all other stream power variables are equal, steeper stream channels will have greater gravitational pull and greater effective shear stress on sediments, increasing the stream's competence to transport sediment (Bagnold, 1960; Booth, 1990; Knighton, 1999).

Regarding the evolution of channel slopes in drainage basins, Horton (1945) identified the Law of Stream Slopes to compliment the stream order classification system. This quantitative law states that average stream slopes decrease with increasing stream order (Horton, 1945; Strahler, 1964). Though discharge increases with increasing stream order, lower-order streams have steeper slopes and, therefore, greater gravitational potential that can transport coarser sediments (Strahler, 1964; Scheidegger, 1965; Hayes et al., 2002).

Sediment Transport Mechanisms

Sediment loads are dependent on a stream's transport capacity, sediment availability, primary sediment routing mechanism, and other channel characteristics (Hicks and Gomez, 2003). There are two primary modes of sediment transport commonly discussed in the literature:

suspended load and bedload (Hicks and Gomez, 2003; Kondolf et al., 2003). Streamflow velocity and sediment caliber dictate which transport mechanism will dominate under specific conditions (Figure 2.5).

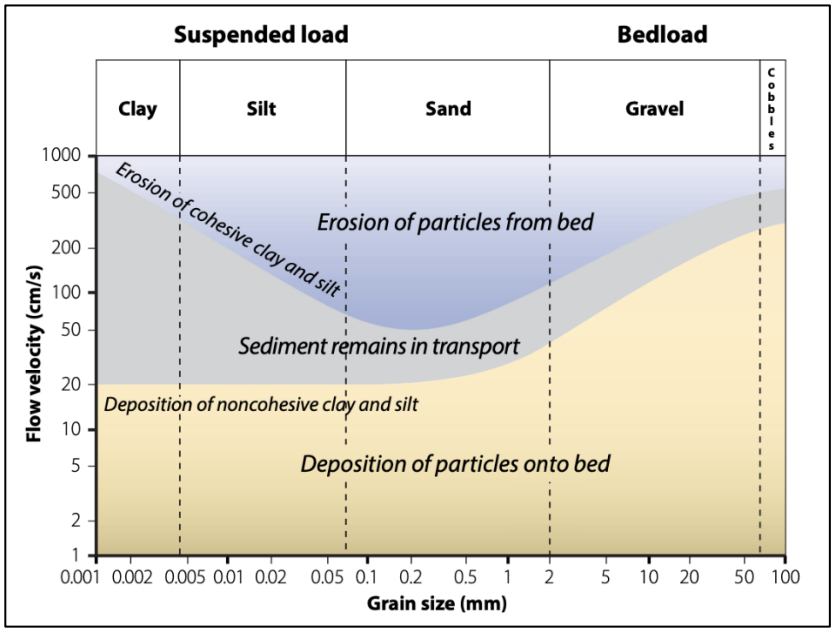

Figure 2.5: Hjulstrom's Diagram illustrates the relationship between flow velocity (cm/s) and sediment caliber (mm), as well as the associated transportation state in each scenario (deposition, entrainment, or erosion); from Bierman and Montgomery (2014).

Suspended loads typically include clay, silt, and sand-sized sediments that are circulated through the stream's turbulent flow (Horton, 1945; Hicks and Gomez, 2003). Though sand-sized particles can sometimes be circulated as suspended loads, these sediments tend to saltate in flowing water, which serves as the middle ground between suspended load and bedload transport mechanisms. Bedload includes coarser, gravel-sized sediments that move in connection with the channel floor (Hicks and Gomez, 2003). These sediments roll, saltate, slide, and bombard the channel floor, abrading and eroding the channel (Cook et al., 2012). The bedload transport rate (q_b) can be quantified using the following equation:

$$q_b = \alpha(\tau' - \tau_c)^{\beta} \qquad \text{Eq. 2.4}$$

This rate is predicated on the effective basal shear stress (τ') being greater than the critical shear stress of entrainment (τ_c) (Marcus et al., 1992; Hayes et al., 2002). Bedload transport rates are of particular importance in gravel-mantled bedrock streams (Cook et al., 2012), as bedload is the principal transport mechanism.

As previously mentioned, both the bedload and suspended load transport mechanisms are dependent upon flow velocity, as certain thresholds must be met to keep coarse sediments in transport (Figure 2.5) (Jacobson and Gran, 1999; Bierman and Montgomery, 2014). Since lower discharge results in the deposition of coarse sediments, bedload material is not transported as often as suspended load material (Jacobson and Gran, 1999). This causes bedload to move in infrequent, high-flow events that exceed the transport threshold (Jacobson and Gran, 1999). This process has been supported by the observation of bedload material moving in waves across various drainage basins in the Ozark region (McKenney and Jacobson, 1996; Panfil and Jacobson, 2001). These waves of cobble movement have been found to have a variety of implications on channel form, including the decrease of channel capacity and increase in channel instability. Therefore, understanding and quantifying bedload transport is of critical importance to stream management decisions.

Stream Classifications

Through time, a variety of stream classification systems have been introduced in the literature for the purpose of identifying specific geomorphic controls and management strategies for specific stream types (Kondolf et al., 2003). Classifications have been based on geomorphic processes, stream power, system hierarchy, and more (Schumm, 1963; Kondolf et al., 2003). Of particular interest to this study, however, is the classification of streams based on both their transport mechanisms (Table 2.1) and primary materials (Schumm, 1963, 1985). While this

transport-based classification model is useful, it does not account for differences in channel bed material. Thus, this model should be used in combination with a material-based model to best address important material distinctions and comprehensively classify streams.

Mode of sediment transport	Channel sediment (M, %)	Proportion of total sediment load		Channel Stability		
		Suspended load %	*Bed load %*	*Stable (graded stream)*	*Depositing (excess load)*	*Eroding (deficiency of load)*
Suspended load	30-100	85-100	0-15	Stable suspended load channel. Width-depth ratio less than 7; sinuosity greater than 2.1; gradient relatively gentle.	Depositing suspended load channel. Major deposition on banks cause narrowing of channel; streambed deposition minor.	Eroding suspended-load channel. Streambed erosion predominant; channel widening minor.
Mixed load	8-30	65-85	15-35	Stable mixed-load channel. Width-depth ratio greater than 7, less than 25; sinuosity less than 2.1, greater than 1.5; gradient moderate.	Depositing mixed-load channel. Initial major deposition on banks followed by steam bed deposition.	Eroding mixed-load channel. Initial streambed erosion followed by channel widening.
Bedload	0-8	30-65	35-70	Stable bedload channel. Width-depth ratio greater than 25; sinuosity less than 1.5; gradient relatively steep.	Depositing bedload channel. Streambed deposition and island formation.	Eroding bedload channel. Little streambed erosion; channel widening predominant.

Table 2.1: Table classifying alluvial channels based on sediment transport mechanisms. *M* represents the percentage of silt-clay particles in the channel, which can dictate a stream's alluvial channel classification; from Schumm (1963).

The material-based classification system differentiates streams into bedrock streams, semi-controlled streams, and alluvium streams (Schumm, 1985). While bedrock streams are fixed in position, alluvium streams can undergo rapid channel migration. In the middle of these extremes are semi-controlled streams, which possess characteristics of both bedrock and alluvium rivers.

Considering each of these two classification schemes, the BNR is a bedload dominated, semi-controlled stream with locally determined material constraints on morphology. Though the main stem has lower reaches where suspended loads and/or sands dominate, most main stem and tributary channel beds are overlain by gravel-sized sediments (Keen-Zebert et al., 2017). The semi-controlled material designation also fits the BNR and its tributaries in that channel reaches will alternate between gravel-mantled bedrock beds and bedrock pavement. Additionally, the main stem and tributary channels occasionally flow against bedrock bluffs, which constrain the channel on a specific side in various locations.

Bedload Transport in Gravel-Mantled Bedrock Streams

While a wide variety of literature exists on gravel-mantled bedrock streams, few in-situ studies have focused on coarse sediment routing in these streams due to the mechanical difficulties of tracking bedload transport in the field (Wilcock, 2001). For the most part, existing methods for sampling bed materials in alluvial or bedrock streams do not accommodate for their semi-controlled nature (Schumm, 1985; Wilcock, 2001; Bartels et al., 2021). Bartels et al. (2021) tested the applicability of pre-existing bedload transport equations in a semi-controlled stream and found that flow resistance was underestimated in the models. Ferguson (2017) also came to the same result in a different semi-controlled stream study.

Since mathematical approaches have not been able to effectively account for bedload transport in the field, innovative tracer tracking studies have been implemented in bedrock streams to try to better constrain coarse sediment routing. Pryce and Ashmore (2003) attempted to re-analyze existing sediment tracer experiments in gravel-bed streams, as transport from the entrainment point is key in determining bedload transport rates. This analysis found that bedload in gravel-bed channels mobilized in observable surges to temporary areas of deposition in some studies, as controlled by channel form. The overall comparison of pre-existing tracer studies presented inconclusive results, however, as methods in these studies were inconsistent and movements were not consistently tied to single threshold events.

More recently, a successful tracer study was conducted in Halfmoon Creek, Colorado by Bradley and Tucker (2012). This four-year tracer study presented results that best matched Yang and Sayre's (1971) GEM model. While the GEM (gamma distribution) and EHS (exponential distribution) models each accounted for the study's greater transport distances in larger peak flood discharge years (2008 and 2010), the GEM's gamma distribution of transport lengths did not overestimate nor underestimate transport of slower-moving tracers like the exponential EHS model, rendering it as the best fit. Though some preliminary conclusions could be identified from one year of cobble movement data, this study indicates the necessity of comprehensive datasets from multiple water-years for understanding annual variances in bedload transport and modeling bedload transport rates in the field. The success of this work supports the idea that long-term tracer studies may provide better constraints of bedload transport rates in field-based experiments than previous methodologies.

Semi-Controlled Stream Bed Considerations

Channel morphology in semi-controlled, gravel-mantled bedrock streams is influenced by the presence of alluvium atop exposed bedrock pavement in stream channels, as the volume of this alluvial cover can have a profound influence on channel incision rates (Fernández et al., 2019). If aggradation of coarse alluvium outpaces degradation, then the erosive potential of bedload would decrease, as maximum erosive potential cannot be reached when sediment loads approach a stream's transport capacity (Gilbert, 1877; Fernández et al., 2019). As a result, channel incision rates would decrease, causing a slowing of downcutting in the fluvial system.

Due to land use changes in the BNR watershed in the late 20th century, large volumes of sediment have been deposited in portions of the modern system from land clearing activities by the logging industry (Scott and Udouj, 1999). Thus, there is a chance that this influx of sediment could have caused incision rates to slow in the watershed in areas where alluvial cover is experiencing a net increase in volume. Though Fernández et al.'s (2019) study was completed in a flume, field notes of alluvial cover will be an important consideration in estimating the BNR's morphologic future.

Using Coarse Sediment Characteristics to Distinguish Sediment Yields

Provenance and caliber studies have also been completed in western streams of similar characteristics to the BNR and its tributaries (steep stream gradient headwaters, terrace-forming gentle main stems, etc.). Lindsey et al. (2007) exemplifies the usefulness of roundness, lithology counts, and pebble counts in determining how sediment provenance relates to specific drainage areas, as each method allowed for coarse sediment in terraces and alluvial fans to be linked to specific tributary sources and transport distances. While the BNR does not have as much lithologic

diversity as the western watersheds incorporated in that study, the combination of lithology and caliber counts will still be useful in differentiating tributary sediment inputs from main stem sediments, as the combination of these methods can likely allow for differences to be distinguished above and below each study tributary.

Conclusions

Each of the aforementioned geomorphic mechanisms, characteristics, and relationships inform our current understanding of stream and basin morphology in fluvial systems. Basin morphometrics of Piégay and Schumm's (2003) morphologic system and flow characteristics of the cascading system inform one another and combine to directly influence sediment production and transport in gravel-mantled bedrock streams. Thus, each of these mechanisms should be comprehensively analyzed and related to one another in in-situ studies so specific sediment routing controls can be identified in a particular watershed.

While in-situ sediment routing controls can be analyzed in fluvial systems, a major complicating factor of streams is the scale at which these processes occur, as well as the scale of influence specific morphologic characteristics have on a watershed (Phillips, 1988). Though other tracer and provenance studies are present in gravel-mantled bedrock stream literature, few in-situ studies have analyzed bedload transport at varying scales. Thus, the synopses of proven methods described in the previous literature above will be utilized to analyze sediment routing controls at varying scales in the BNR. We hope to obtain results that inform reach-scale, tributary-scale, and watershed-scale patterns and controls on coarse sediment transport in this gravel-mantled bedrock stream.

Chapter 3: Methods

To better understand course sediment routing in the BNR watershed, I utilized a combination of field data collections at the reach to tributary scale, spatial analyses at the watershed scale, and statistical analyses. Within four selected tributaries, pebble counts and provenance data were collected from gravel bars to study the influence of tributaries on gravel populations in the main stem of the BNR. One tributary, Beech Creek, was selected to test the feasibility of using RFID technology to track bedload movement patterns in the BNR. Finally, to provide context of how the study tributaries compare to the BNR watershed as a whole, basin morphometrics for all third order or greater tributaries were compiled from a five-meter Digital Elevation Model (DEM) in ArcMap 10.8.2 (Arkansas GIS Office, 2006; ERSI, 2021).

Tributary Selection

The four tributaries selected for the study include Beech Creek on the Boston Mountain Plateau, Cave Creek and Calf Creek on the Springfield Plateau, and Clabber Creek on the Salem Plateau (Figure 3.1). These tributaries were selected based on the lithology within their watersheds, their location in the overall watershed, National Park Service research and management priorities, as well as accessibility constraints. Geologic maps, digital raster graphics (DRGs), and a 5-meter digital elevation model (DEM) were used to identify primary lithologies present in each tributary basin and calculate preliminary basin morphometrics in ArcMap 10.8.2 (ESRI, 2021) (Table 3.1). The analyses of these materials informed tributary selections for this study.

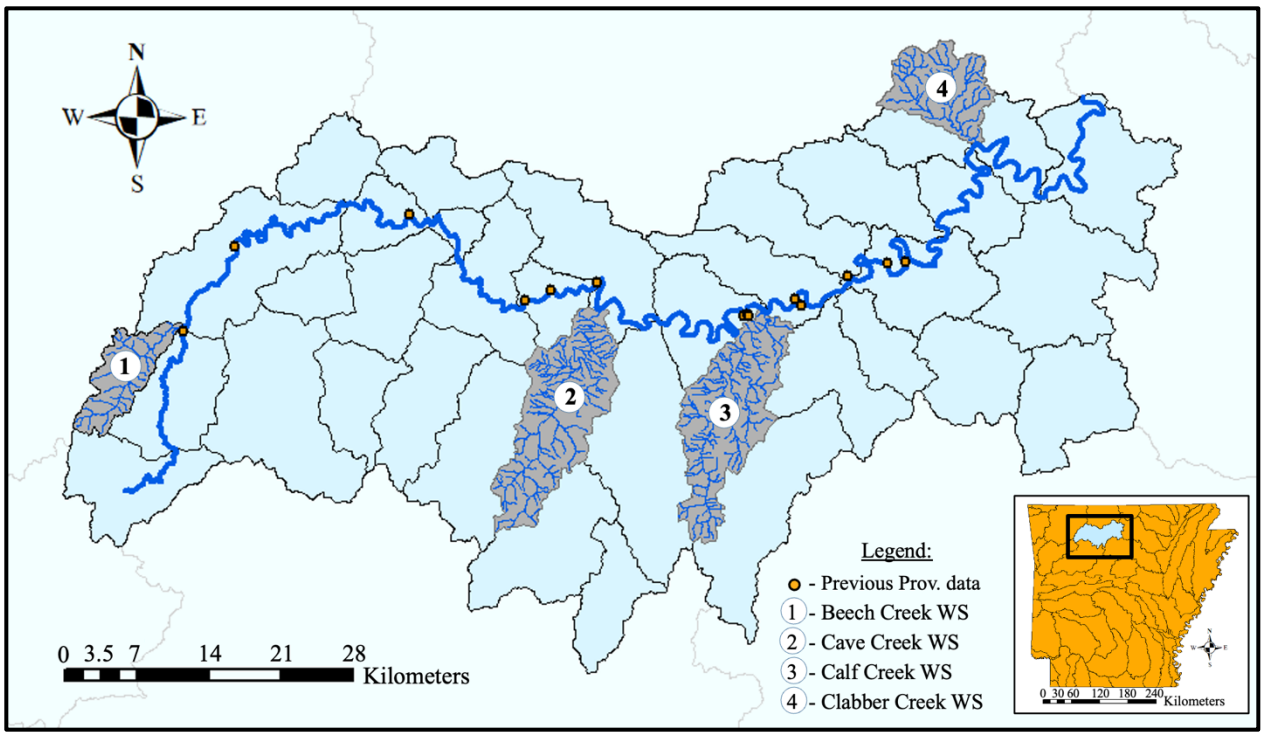

Figure 3.1: Map of the four tributary watersheds selected for the study. Moving from upstream (west) to downstream (east) are the watersheds of Beech Creek (1), Cave Creek (2), Calf Creek (3), and Clabber Creek (4). This map utilized USGS delineated basins.

Digital Elevation Models (DEM):		
Publisher	*Year*	*Name*
AR GIS Office	2006	2006 Five Meter Resolution Digital Elevation Model
Digital Raster Graphics (DRG):		
Publisher	*Year*	*Name*
USGS	2017	Boxley Quadrangle. Arkansas. 7.5-minute series
USGS	2014	Eula Quadrangle. Arkansas. 7.5-minute series
USGS	2011	Rea Valley Quadrangle. Arkansas. 7.5-minute series
USGS	2014	Snowball Quadrangle. Arkansas. 7.5-minute series
Geologic Map DRG's:		
Publisher	*Year*	*Name*
USGS	2007	Geologic Map of the Boxley Quadrangle, Newton and Madison Counties, Arkansas
AGS	2012	Geologic Map of the Cozahome Quadrangle, Marion and Searcy Counties, Arkansas
AGS	Revised 2015	Geologic Map of the Eula Quadrangle, Newton and Searcy Counties, Arkansas
USGS	2004	Geologic Map of the Lurton Quadrangle, Newton County, Arkansas
USGS	2004	Geologic Map of the Moore Quadrangle, Newton and Searcy Counties, Arkansas
AGS	Revised 2015	Geologic Map of the Mt. Judea Quadrangle, Newton County, Arkansas
USGS	2003	Geologic map of the Ponca Quadrangle, Newton, Boone, and Carroll County, Arkansas
AGS	2012	Geologic Map of the Rea Valley Quadrangle, Madison County, Arkansas
AGS	Revised 2015	Geologic Map of the Snowball Quadrangle, Searcy County, Arkansas
USGS	2007	Geologic Map of the Witts Springs Quadrangle, Searcy County, Arkansas

Table 3.1: Table displaying the DEM, DRG's, and geologic maps analyzed for study site selections. Each DRG and geologic map analyzed had a scale of 1:24,000.

Gravel Bar Sampling

In each of the four study tributaries, one to two gravel bars approximately one reach up from each confluence with the BNR were sampled. The cross-sectional area of the active channel was measured at each gravel bar's mid-point, following Imhoff & Wilcox (2016). Flow velocities were also collected for these cross-sectional surveys using a pygmy current meter. Wolman (1954) pebble counts were conducted on each gravel bar to determine sediment grain size distributions. The number of measurements collected per survey was based on the size of the bar, ranging from 75-250 measurements each. Additionally, 20 samples along 1-meter transects were measured and broadly classified by lithology (sandstone, limestone, or chert) and/or geologic period in three locations on each gravel bar, following previous sampling efforts in the BNR by Keen-Zebert et al. (2017). Similarly, pebble counts and provenance data were collected on gravel bars in the main stem of the BNR just upstream and downstream of each tributary confluence.

The mean, D50, and D84 grain sizes were calculated for grain sizes from < 2 mm (sand-sized) to > 256 mm (boulder-sized) for each gravel bar. Additionally, non-parametric statistical analyses were conducted using RStudio (v. 4.1.2) to quantitatively compare gravel bar sediment size distributions (RStudio Team, 2021) (Appendix E). Boulder-sized coarse sediments (> 256 mm) were not included in these analyses, as some of the tests are more sensitive to outliers. According to the Shapiro-Wilk Test and the Bartlett Test, these data are not normally distributed and have unequal variances. Therefore, a Kruskal-Wallis Test was used to determine if at least one group was significantly different from others at each tributary confluence. Since statistical differences were present in each confluence, Wilcoxon Rank Sum Tests were completed to make pairwise comparisons between each gravel bar in each confluence. These statistical analyses were used to recognize tributary fingerprints in the main stem, while also providing a visualization of

the variability in grain size distributions of gravel bars in the watershed.

RFID Pilot Project

To measure gravel movement at the reach scale, thirty-three Beech Creek gravel samples were collected and fitted with passive-integrated transponder (PIT) tags for the radio-frequency identification (RFID) pilot project in the BNR (Figure 3.2). The tagged gravel were then placed in a grid with approximately one-meter spacing in the active channel at the upstream end of the Beech Creek study reach (Figure 3.3A). Each gravel placement location was documented with both a Trimble Geo 7X GPS unit and OregonRFID ORSR single antenna reader and mobile reader kit (Figure 3.4).

Figure 3.2: Preparing cobbles for the RFID tracer experiment in Beech Creek. Each cobble was indented with a portable angle grinder and fitted with a passive-integrated transponder (PIT) tag (**A**) and water-resistant epoxy (**B**).

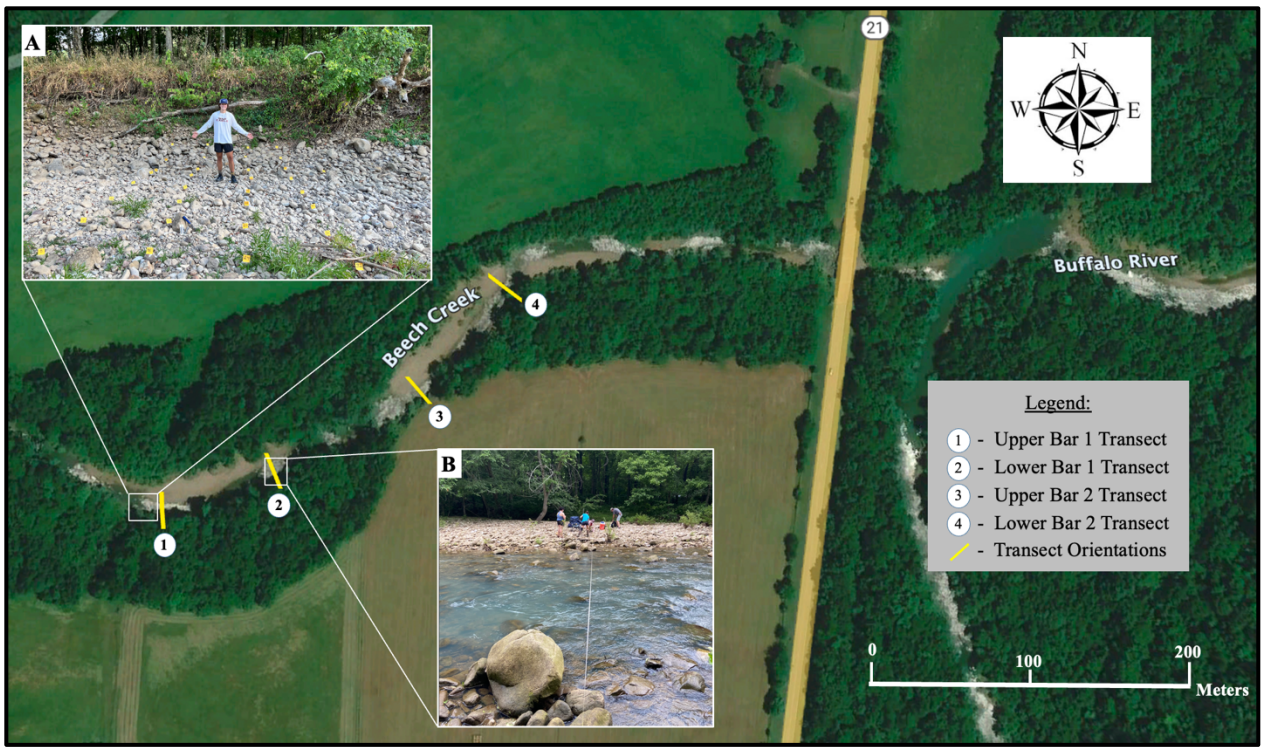

Figure 3.3: View of the Beech Creek confluence area. Stream surveys and gravel counts were collected across each of the four transect localities displayed in the figure. **A**: Picture of PIT-tagged RFID cobbles placed in the active channel in a grid-like pattern. This image is looking from river left to river right (looking ~S). **B**: Image of the Lower Bar 1 Transect set-up. This image is looking from river right to river left (looking ~N-NW). Satellite imagery from Google Earth Pro (v. 7.3.6.9345), June 4, 2020 (Google Earth, 2023).

Figure 3.4: Utilizing the OregonRFID equipment in the field. Tagged objects are passively identified via emitted radio waves from the antenna to the tag and vice versa. The antenna communicates with the GNSS receiver and then transmits location-based data to the reader, which can then be downloaded and analyzed.

After the initial placement of the tagged gravel on July 27, 2022, gravel locations were measured six additional times through May 9, 2023 to track gravel movement after periods of high flow. For each return trip, RFID data was collected starting from the initial placement location and moving downstream until no further RFID detections were acquired by the reader. Additionally, main stem streamflow data were downloaded from the USGS *Buffalo River Near Boxley, AR – 07055646* gage upstream of the Beech Creek confluence and the *Buffalo River Near Ponca, AR – 07055660* gage downstream of the confluence to compare daily average flows between site visits (USGS, 2023a, 2023b) (Appendix G.4).

Since the RFID reader often collected multiple detections with slightly different coordinates for some cobbles, coordinates associated with the longest detection time were selected as the primary coordinate for each cobble on that date. Longer detection times likely produce more accurate location data due to increased GNSS triangulation times, thus supporting this decision. After processing, selected detection data from each collection date was exported to ArcMap (v. 10.8.2) for spatial analysis.

Tributary Morphometric Analyses

Watershed boundaries and drainage networks for all third order or greater (Strahler method) BNR tributary watersheds were delineated from the five-meter DEM (Arkansas GIS Office, 2006) in ArcMap (v. 10.8.2) using the hydrology toolset (ERSI, 2021). Resulting basins were overlain upon USGS geologic maps to identity and compare surface lithologies in each tributary confluence study area. Additionally, tributary basin morphometrics were calculated for each study tributary to identify potential in situ controls on tributary sediment routing (Table 3.2; Appendix F.1). Morphometrics for all third order or greater streams were also calculated and grouped based on position relative to the BNR to analyze potential differences between northern and southern tributary basins.

Morphometric:	Units
Drainage Area	km^2
Position relative to BNR (N or S)	-
Pour order into BNR	-
Perimeter	km
Slope Mean	degrees
Strahler Order	-
Flowline length total	km
Drainage Density	-
Circularity Ratio (Rc)	-
Elongation Ratio (Re)	-
Relief Ratio	-
Tributary main stem length	km

Table 3.2: Basin morphometrics calculated and analyzed for each third order or greater BNR tributary watershed. These data can be found in Appendix F.1.

Chapter 4: Results

Gravel Bar Caliber

Coarse-grained gravel bar sediments are highly variable in the main stem of the BNR (mean values range from 19 mm to 57 mm) and do not exhibit the expected downstream fining pattern (Table 4.1). However, mean grain sizes in each study tributary decrease by 45.6% from upstream to downstream in the BNR watershed. Though all pebble counts were conducted at base flow conditions in these intermittent and perennial streams, visual bankfull indicators suggest that all selected bars are occasionally inundated at higher flows. Gravel bars range in size from 463 m^2 to 2,027 m^2 in the tributaries, and 253 m^2 to 8,959 m^2 on the main stem, with averages of 1,146 m^2 and 4,382 m^2, respectively (Appendices A.2, B.2, C.2, and D.2). Additionally, gravel bars are armored, and gravel imbricated – meaning gravel is stacked at an angle in alignment with the dominant streamflow direction. While the majority of streams in the BNR are gravel-mantled, portions of the BNR main stem, Beech Creek, and Clabber Creek contain sections of exposed bedrock in the active channel above or below sampling locations. This pattern is typical in the BNR system.

Comparing gravel size distributions between the tributary and main stem bars above and below each confluence exhibit grain size differences that indicate tributary gravel input influence. Signatures of tributary gravel inputs in the BNR are interpreted from relationships in which tributary bar caliber data more closely resembles that of the downstream main stem bar. The gravel bars sampled on Beech Creek, Cave Creek, and Calf Creek all have greater mean caliber, D50, and D84 values than the gravel bars sampled upstream from their confluences. While main stem gravel bars downstream of the Cave Creek and Calf Creek confluences see mean grain size

increases of 10.5% and 11.5% (respectively) from the upstream main stem bars, the mean grain size of the main stem bar downstream of Beech Creek unexpectedly decreases 5.9% from its upstream main stem bar. The Clabber Creek gravel bar has the opposite relationship with its upstream main stem bar, as mean caliber, D50, and D84 values are all lower on the tributary bar. As a result, the main stem saw a 13.3% decrease in mean gravel caliber below the Clabber Creek confluence.

	Gravel Bar Location	n	Mean (mm)	D50 (mm)	D84 (mm)	Confluence Lithology	Tributary Major Lithology
Beech Creek	Main Stem Upstream	100	34	25	58	Boone	Highest elevations Pennsylvanian Atoka Fm. to Mississippian Boone Fm. at river level
	Tributary Bar 1	100	57	36	125		
	Tributary Bar 2	130	46	29	90		
	Main Stem Downstream	75	32	28.5	47		
Cave Creek	Main Stem Upstream	200	19	16	34	Everton	Highest elevations Mississippian Boone Fm. to Ordovician Everton Fm. at river level
	Tributary Bar	150	43	36	75		
	Main Stem Downstream	150	21	34	79		
Calf Creek	Main Stem Upstream	150	26	22	43	Boone	Highest elevations Pennsylvanian Bloyd Fm. to Mississippian Boone Fm. at river level
	Tributary Bar	103	33	29	47		
	Main Stem Downstream	200	29	25	45		
Clabber Creek	Main Stem Upstream	200	45	33	71	Everton	Highest elevations Mississippian Boone Fm. to Ordovician Powell Dolomite
	Tributary Bar	100	31	25	50		
	Main Stem Downstream	120	39	25	74		

Table 4.1: Gravel caliber data and watershed lithology for tributary study sites. Maps of each bar above are presented in Appendices A.2, B.2, C.2, and D.2.

Percent finer graphs and histograms for each bar (Figures 4.1-4.4) display non-normal distributions and variability in caliber within each confluence area, as evidenced by Shapiro-Wilk Tests ($p < 0.05$) and Bartlett Tests ($p < 0.05$), respectively (Appendix E.3). Though variance differences are present, tributary and main stem bars are generally dominated by pebble-sized sediments (4 – 64 mm). These graphs also display boulder-sized outliers (> 256 mm) in most gravel bars, which were not included in the statistical analyses. At least one gravel bar is significantly different from the other two confluence gravel bars (Kruskal-Wallis, $p < 0.05$) at all four study sites (Appendix E.3). Pair-wise comparisons, using a Wilcoxon Rank Sum test, identified which bars are statistically different (Appendix E.4). At the Beech Creek confluence, the upstream BNR bar is significantly different ($p < 0.05$) from each Beech Creek bar (Beech Creek Bar 1: $p = 0.0078$; Beech Creek Bar 2: $p = 0.017$). The downstream bar is not statistically different from the upstream bar ($p = 0.28$), nor either of the Beech Creek bars (Beech Creek Bar 1: $p = 0.25$; Beech Creek Bar 2: $p = 0.44$). At Cave Creek, very significant statistical differences were found between the upstream main stem bar and both the tributary bar ($p = 3.84e-15$) and downstream main stem bar ($p < 2.2e-16$). The Cave Creek tributary bar and downstream main stem bar are not statistically different ($p = 0.917$). Though the Calf Creek tributary bar is significantly different from the upstream main stem bar ($p = 0.0040$), the downstream bar is not statistically different from the tributary bar ($p = 0.12$), nor the upstream bar ($p = 0.058$). It is worth noting that the p-value between the upstream and downstream main stem bars ($p = 0.058$) is very close to the < 0.05 significant difference threshold, however. Similar to Cave Creek, the main stem bar upstream of Clabber Creek exhibits a very significant difference from the tributary bar ($p = 0.00083$) and the downstream bar ($p = 0.0030$). In summary, these data provide strong evidence that the tributary is influencing sediment caliber in the main stem below the confluences of Cave

Creek and Clabber Creek. Calf Creek confluence data also provides evidence of tributary-derived sediment inputs – though this relationship is less robust. Statistical evidence for Beech Creek influence is the least robust of the four.

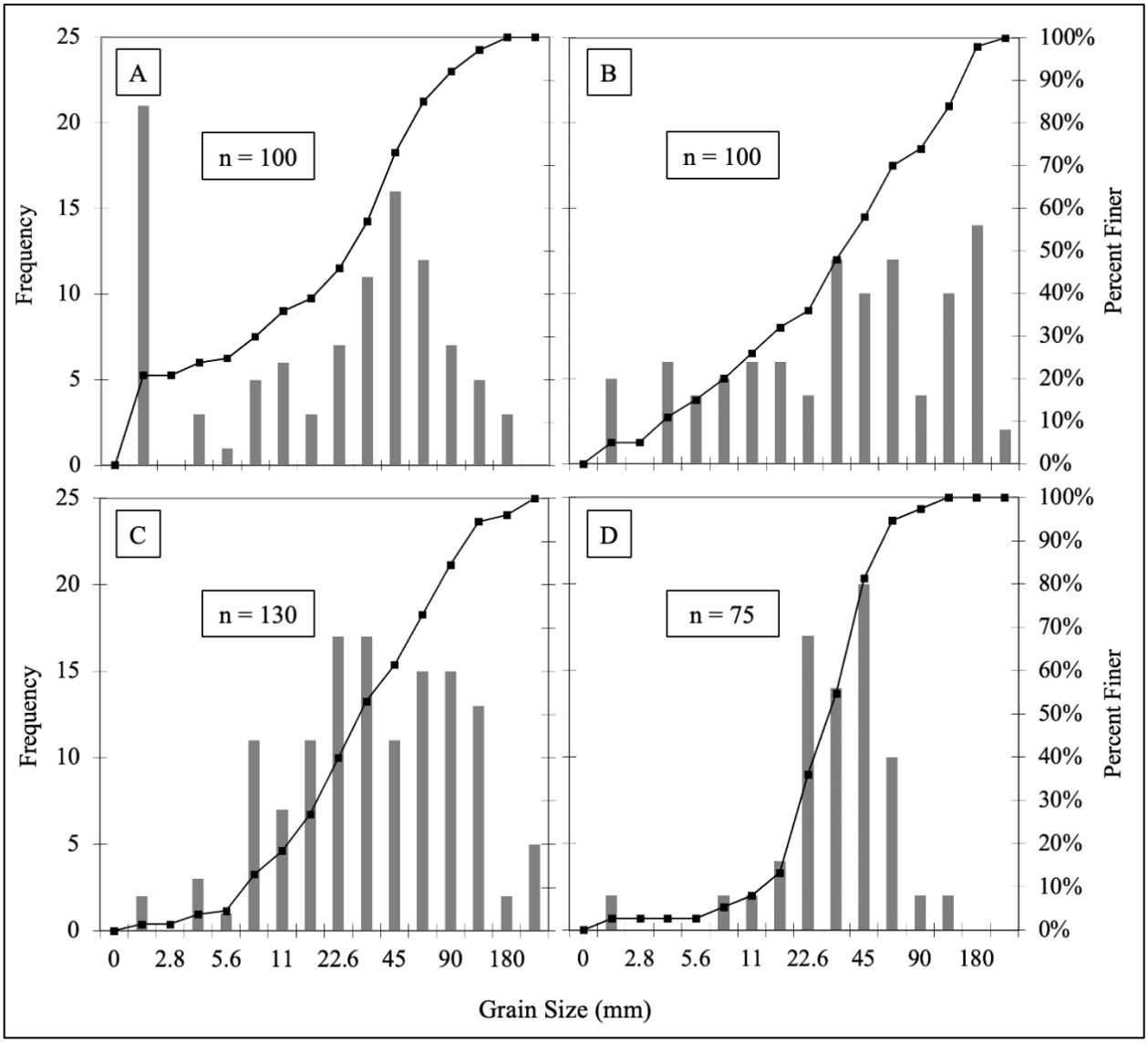

Figure 4.1: Gravel size distributions for Beech Creek confluence area gravel bars. **A**: Main stem BNR gravel bar just upstream of the Beech Creek confluence. **B**: Beech Creek gravel bar 1. **C**: Beech Creek gravel bar 2 (downstream of Beech bar 1). **D**: Main stem BNR gravel bar just downstream of the Beech Creek confluence.

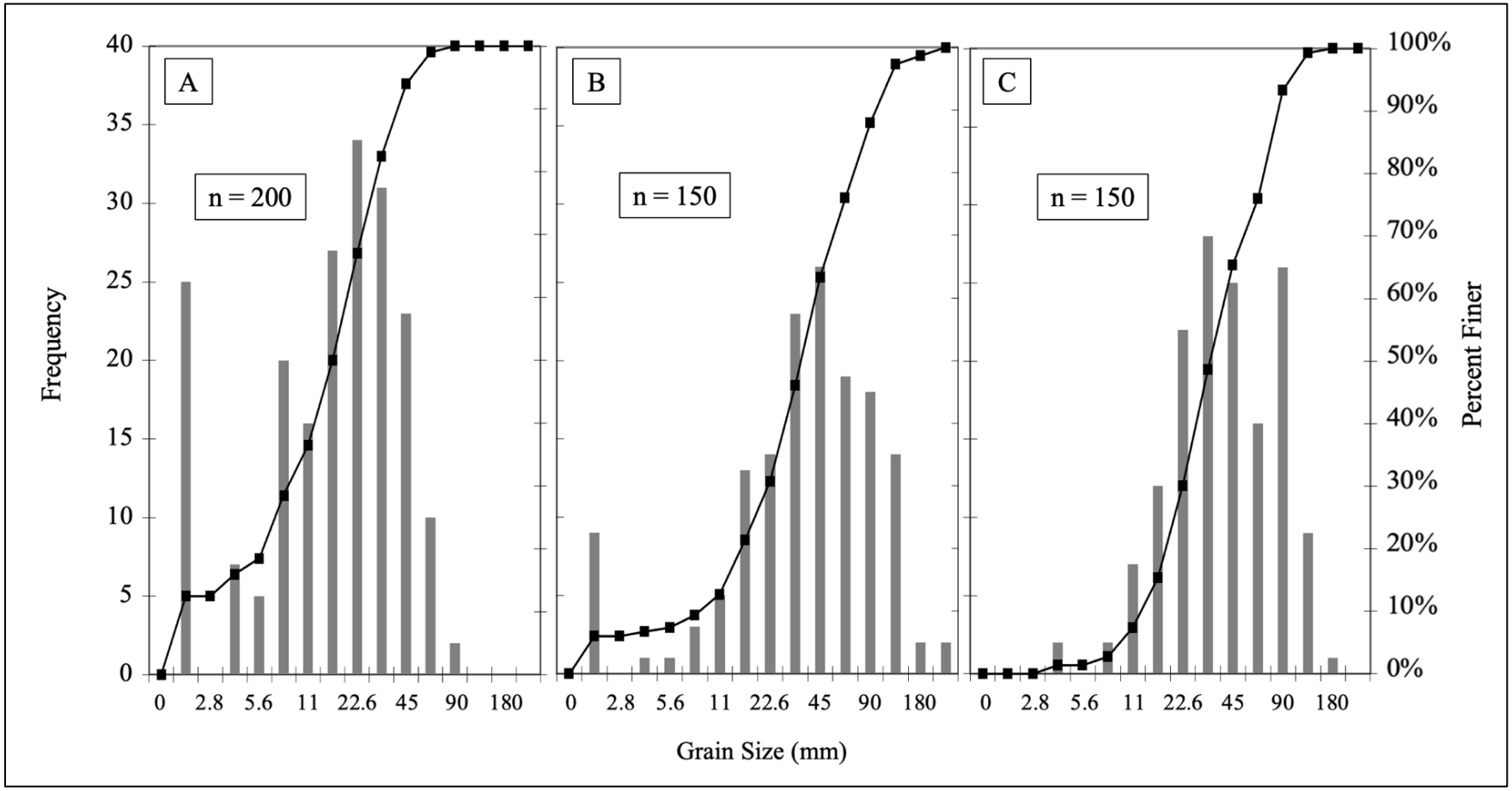

Figure 4.2: Gravel size distributions for Cave Creek confluence area gravel bars. **A**: Main stem BNR gravel bar just upstream of the Cave Creek confluence. **B**: Cave Creek gravel bar data. **C**: Main stem BNR gravel bar just downstream of the Cave Creek confluence.

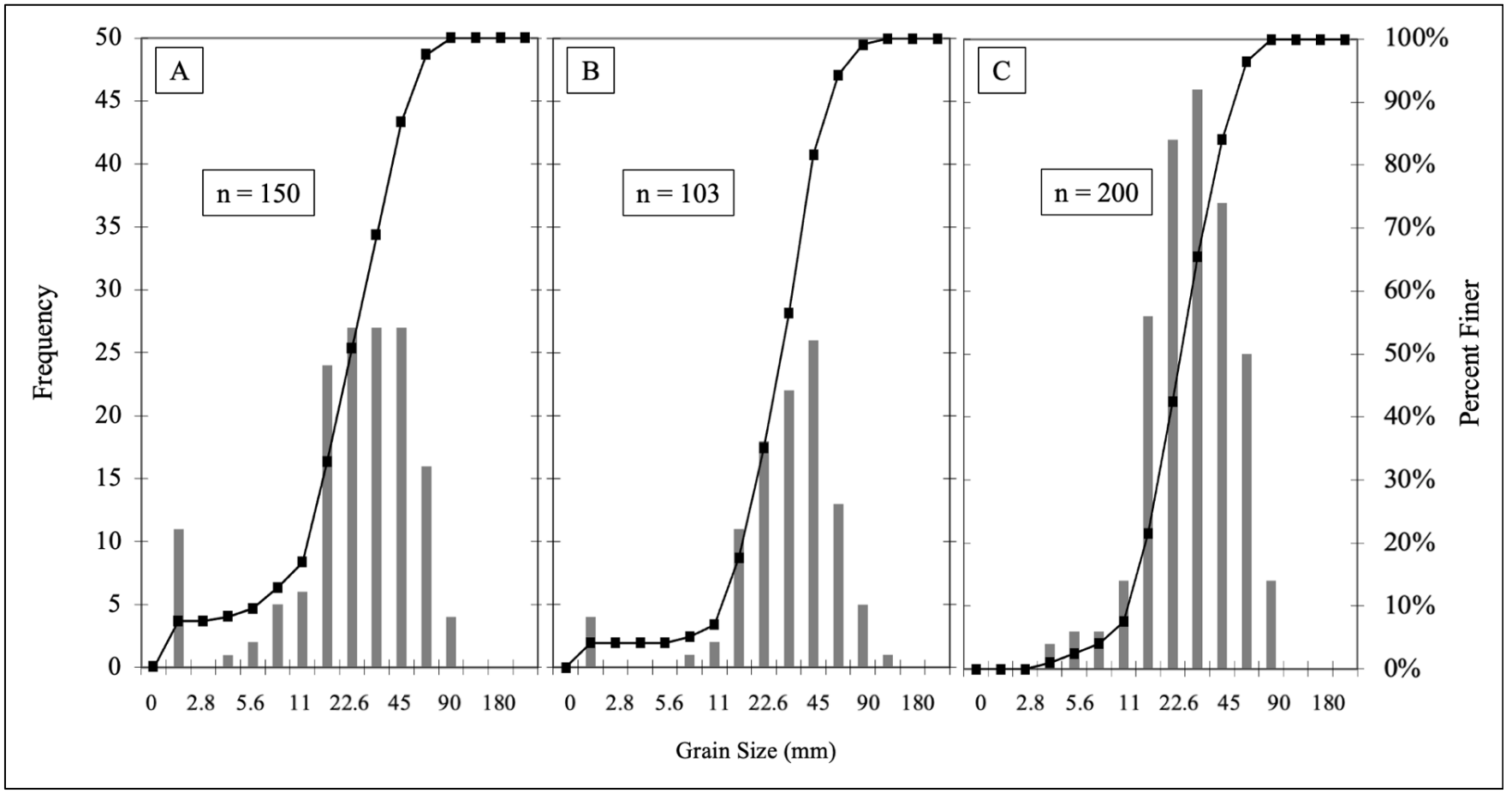

Figure 4.3: Gravel size distributions for Calf Creek confluence area gravel bars. **A**: Main stem BNR gravel bar just upstream of the Calf Creek confluence. **B**: Calf Creek gravel bar data. **C**: Main stem BNR gravel bar just downstream of the Calf Creek confluence.

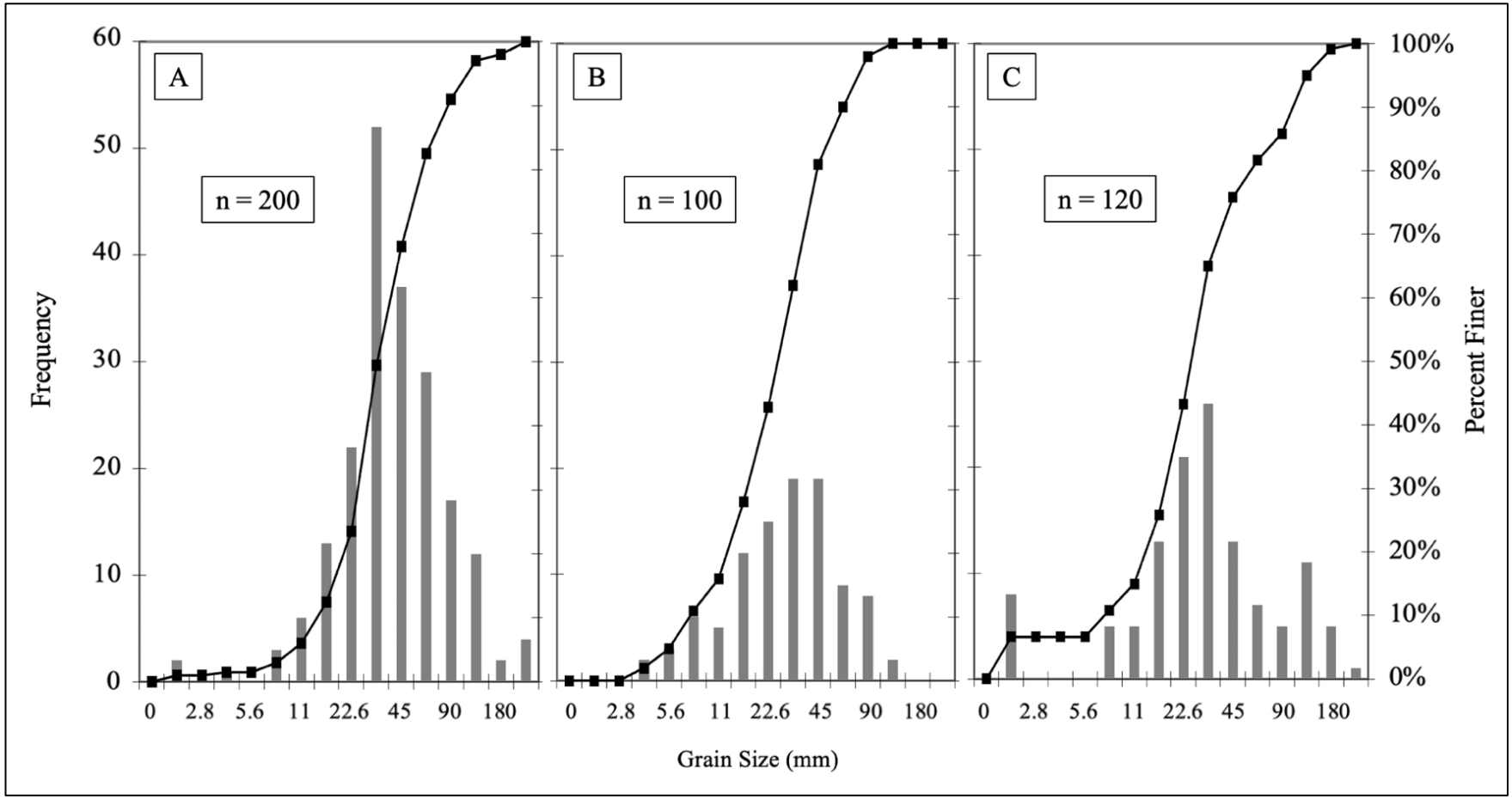

Figure 4.4: Gravel size distributions for Clabber Creek confluence area gravel bars. **A**: Main stem BNR gravel bar just upstream of the Clabber Creek confluence. **B**: Clabber Creek gravel bar data. **C**: Main stem BNR gravel bar just downstream of the Clabber Creek confluence.

Gravel Bar Provenance

Comparing provenance data from the main stem and tributary bars support the interpretation that gravel inputs from Cave Creek, Calf Creek, and Clabber Creek have distinguishable signals in the main stem gravel bar populations just below each confluence (Table 4.2; Figure 4.5). For each of these three tributaries, the dominant coarse sediment lithology identified in the tributary gravel bar is also the dominant lithology of the main stem bar just downstream of each associated confluence. Conversely, these dominant lithologies in each tributary and downstream bar are not dominant in the upstream main stem bars. At the Cave Creek confluence, main stem gravel bars see a 47.85% increase in sandstone sediments from upstream to downstream. This increase can reasonably be associated with the 74.58% sandstone provenance value identified on the Cave Creek gravel bar. This relationship is even more pronounced in Calf Creek, as limestone/dolostone sediments increase by 93.70% from the upstream to downstream main stem bars, which can likely be tied to the 63.33% limestone provenance value identified in Calf Creek. Similarly, main stem bars above and below the Clabber Creek confluence see a 47.63% increase in limestone/dolostone coarse sediments, likely derived from the 78.33% presence of limestone/dolostone sediments in Clabber Creek.

Though Beech Creek does not share the dominant lithology trend described above, gravel inputs from Beech Creek appear to have a weak, yet distinguishable signal in the main stem. The downstream main stem bar is comprised of 15% chert and 7.50% cherty limestone, which is an increase from 1.67% for both provenance categories from the upstream main stem bar (Table 4.2). These two categories only comprise 22.50% of the coarse sediments sampled on the downstream main stem bar and are not the dominant lithologies in either main stem bar, suggesting a weak tributary sediment input signal in comparison to the other tributaries. Additionally, though

sandstones dominate Beech Creek gravel bars (65.00%), sandstone coarse sediments decrease 29.59% from the upstream to downstream main stem bars (from 81.67% to 57.50%). Since sandstone sediments dominate each Beech Creek gravel bar at a higher percentage than the downstream bar, it seems counterintuitive for sandstone provenance values to drop as low as they did based on the gravel bars that were surveyed, thus convoluting any signal from the tributary.

Overlaying the 1:24,000 Geologic Maps for the BNR watershed display that the confluences of Beech and Calf Creeks incise the Boone Formation, while the confluences of Cave and Clabber Creeks incise the Everton Formation (Appendices A.1, B.1, C.1, and D.1). The Cave Creek and Clabber Creek confluences incise different portions of the Everton, which has variable lithology in the vertical section. Cave Creek and the main stem near its confluence incise through the upper contact of the Everton, exposing mainly dolostone and friable sandstones (Chandler and Ausbrooks, 2015). As expected, these lithologies dominate modern bedload near the Cave Creek confluence. The Clabber Creek confluence area incises the entire Everton Formation, including dolostone, friable sandstone, chert, and limestone interlayers. Of these, limestone/dolostone and sandstone appear to dominate modern bedload provenance near Clabber Creek. In contrast, the Beech Creek and Calf Creek confluence areas incise the interbedded cherty limestone of the Boone Formation (McFarland, 1998; Keen-Zebert et al., 2017). While the main stem near Calf Creek exclusively incises the Boone Formation before and after the confluence (which dominates provenance data in the Calf Creek and downstream main stem gravel bars), the BNR begins to incise the Boone just before encountering the Beech Creek confluence. This upper portion of the watershed includes much steeper topography and plateau tops capped by younger Mississippian-Pennsylvanian sandstones, which are numerous in the provenance gravel bar data at this site. Shale sediments are also minimally present in the Beech Creek and Clabber Creek areas.

	Provenance	Upstream Main Stem	Tributary	Downstream Main Stem
Beech Creek		n=60	n=120	n=40
	Limestone	13.33%	10.00%	17.50%
	Sandstone	81.67%	65.00%	57.50%
	Chert	1.67%	17.50%	15.00%
	Cherty LS	1.67%	-	7.50%
	Shale	1.67%	7.50%	2.50%
Cave Creek		n=60	n=60	n=60
	Limestone/Dolostone	43.33%	11.86%	30.00%
	Sandstone	38.33%	74.58%	56.67%
	Chert	13.33%	11.86%	8.33%
	Cherty LS	5.00%	1.69%	5.00%
	Shale	-	-	-
Calf Creek		n=60	n=60	n=60
	Limestone/Dolostone	26.67%	63.33%	51.66%
	Sandstone	45.00%	18.33%	18.33%
	Chert	28.33%	15.00%	30.00%
	Cherty LS	-	3.33%	-
	Shale	-	-	-
Clabber Creek		n=60	n=60	n=60
	Limestone/Dolostone	35.00%	78.33%	51.67%
	Sandstone	35.00%	10.00%	31.66%
	Chert	15.33%	10.00%	15.00%
	Cherty LS	8.33%	0.00%	1.67%
	Shale	3.33%	1.67%	-

Table 4.2: Coarse sediment provenance data for all study tributaries and the BNR main stem above and below each tributary confluence.

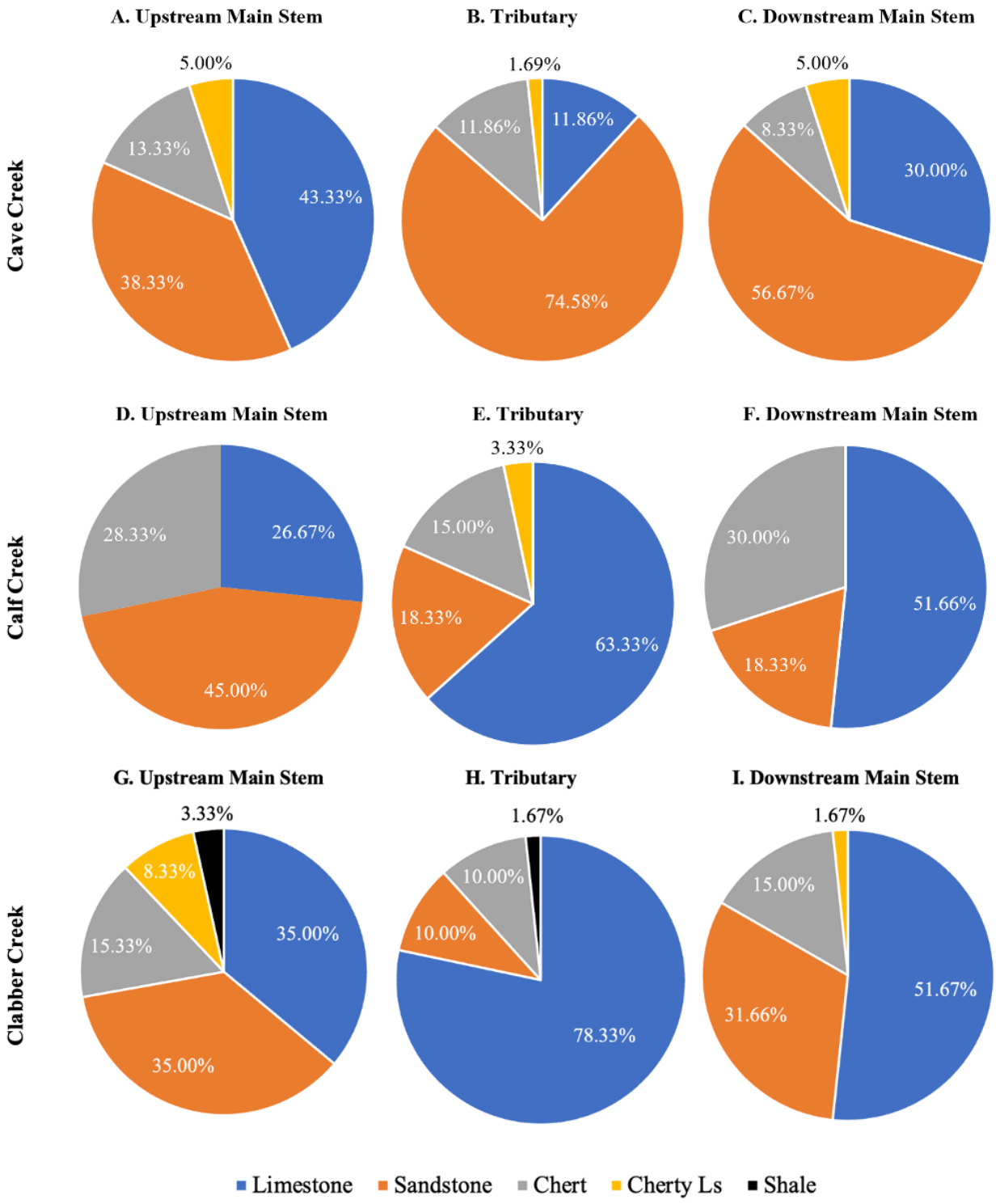

Figure 4.5: Coarse sediment provenance data for Cave Creek (**A-C**), Calf Creek (**D-F**), and Clabber Creek (**G-I**) confluence areas. These three tributaries are displayed from Table 4.2 since they have more pronounced sediment inputs in the main stem.

Basin Morphometrics

The tributary basins within the BNR have distinctly different areas depending on their position north or south of the main stem, as was hypothesized. Specifically, tributaries north of the main stem are more than 50% smaller on average (Table 4.3). Other basin morphometrics that can influence sediment production and routing according to the literature - drainage density (Dd), slope, relief ratio (Rr), and elongation ratio (Re) – have similar averages regardless of position. These results support the idea that the greater relative relief of the Boston Mountain Plateau in the southern portion of the watershed serves as a physiographic control on watershed size (Quinn, 1958). The minor differences in the other morphometrics analyzed can likely be attributed to localized controls (lithology, faulting, etc.) or natural variability rather than regional physiography, since substantial differences in these metrics are not present based on north-south orientation.

Metric	North Sub-basins	South Sub-basins
Area (km^2)	34.27	86.88
Dd	1.47	1.51
Slope	12.60	12.70
Rr	0.044	0.050
Re	0.78	0.76

Table 4.3: Mean basin morphometric values for northern and southern BNR tributary basins of third order (Strahler) or greater. These metrics were selected from a wide range of basin morphometric data, as these factors seem to best inform sediment production and routing in the literature.

Following this spatial trend, the northern study tributaries of Beech Creek and Clabber Creek each have smaller basin areas and, by inference, less surface area to capture rainfall (Table 4.4). In contrast, the southern study tributaries of Cave Creek and Calf Creek have almost twice the land area. Additionally, the northern study basins have shorter main stem lengths and total

flowline lengths. These northern study basins also have lower drainage densities and higher elongation ratios than those to the south, with Beech Creek having the lowest drainage density.

Although the southern and northern study tributaries have some similarities, this does not hold true for slope. For instance, the average slope is higher in Beech Creek and Cave Creek than the two downstream tributaries (Table 4.4), which is expected due to their higher relative position in the BNR watershed. Of these tributaries, Beech Creek has the highest average slope, as well as the highest relief ratio. Additionally, Beech Creek is a stream order smaller than the other three, has the smallest area, and is just the fifth of 48 tributary basins (stream order of three or greater) to empty into the BNR – which is much higher than the other three study tributaries.

	upstream → downstream			
	Beech Creek	**Cave Creek**	**Calf Creek**	**Clabber Creek**
Strahler Order	3	4	4	4
PourOrder	5	22	28	40
Area (sq. km)	50.88	135.46	127.39	68.44
Perimeter (km)	46.13	74.48	77.95	43.08
Slope mean (degrees)	13.03	12.55	9.76	10.55
Flowline Length Total (km)	63.44	209.75	198.60	97.49
Drainage Density	1.25	1.55	1.56	1.42
Circularity Ratio (Rc)	0.30	0.31	0.26	0.46
Elongation Ratio (Re)	0.76	0.60	0.55	0.80
Relief Ratio	0.04	0.02	0.02	0.02
Main Stem Length (km)	12.26	29.36	31.39	16.09

Table 4.4: Basin morphometric data for each study tributary. Pour order denotes the order in which tributaries (of third order or greater) drain into the main stem. There are 48 tributaries of third order or greater in the BNR.

Transport in Beech Creek

RFID tracer location data were collected over ~10 months from July 2022 to May 2023 (Table 4.5; Appendix G). Detection rates of the 33 cobbles averaged 91.9% for all six RFID surveys, – including a 100% retention rate on the final survey. Unfortunately, the GNSS signal failed to collect location data for some of the gravel in surveys two through five (Appendix G.2). These failed detections likely occurred due to Beech Creek's remote location in a confined valley, which limits satellite visibility.

	Date	Detection Rate	Peak Q (Boxley)	Avg. Q (Boxley)	Peak Q (Ponca)	Avg. Q (Ponca)
Survey 1	07/27/2022	100%	n/a	n/a	n/a	n/a
Survey 2	09/11/2022	81.81%	2.37	0.17	87.22	1.14
Survey 3	11/24/2022	93.93%	8.78	0.20	64.00	0.84
Survey 4	12/30/2022	84.84%	42.19	4.38	69.09	9.04
Survey 5	02/12/2023	90.90%	104.21	4.63	141.30	7.99
Survey 6	05/09/2023	100%	180.10	5.96	233.05	10.43

Table 4.5: Detection rates for all RFID surveys with average peak discharge values (cms) from the Boxley and Ponca stream gages for the time since the previous survey (USGS, 2023a, 2023b).

Between surveys one and five, at least 32 of the 33 tagged gravel only moved a maximum of one to three meters downstream from their placement locations (Figure 4.6). This result is known because all detections through survey five were taken within 3-meters of each gravel's original placement position. Though three cobbles were not detected during survey five, two of these three cobbles were detected within 3 meters of their placement locations in survey six, thus limiting the distance they could have moved beforehand. The greatest downstream movement for the gravel was between surveys five and six. In fact, many cobbles were transported out of the

placement riffle to various locations downstream (Figure 4.6F).

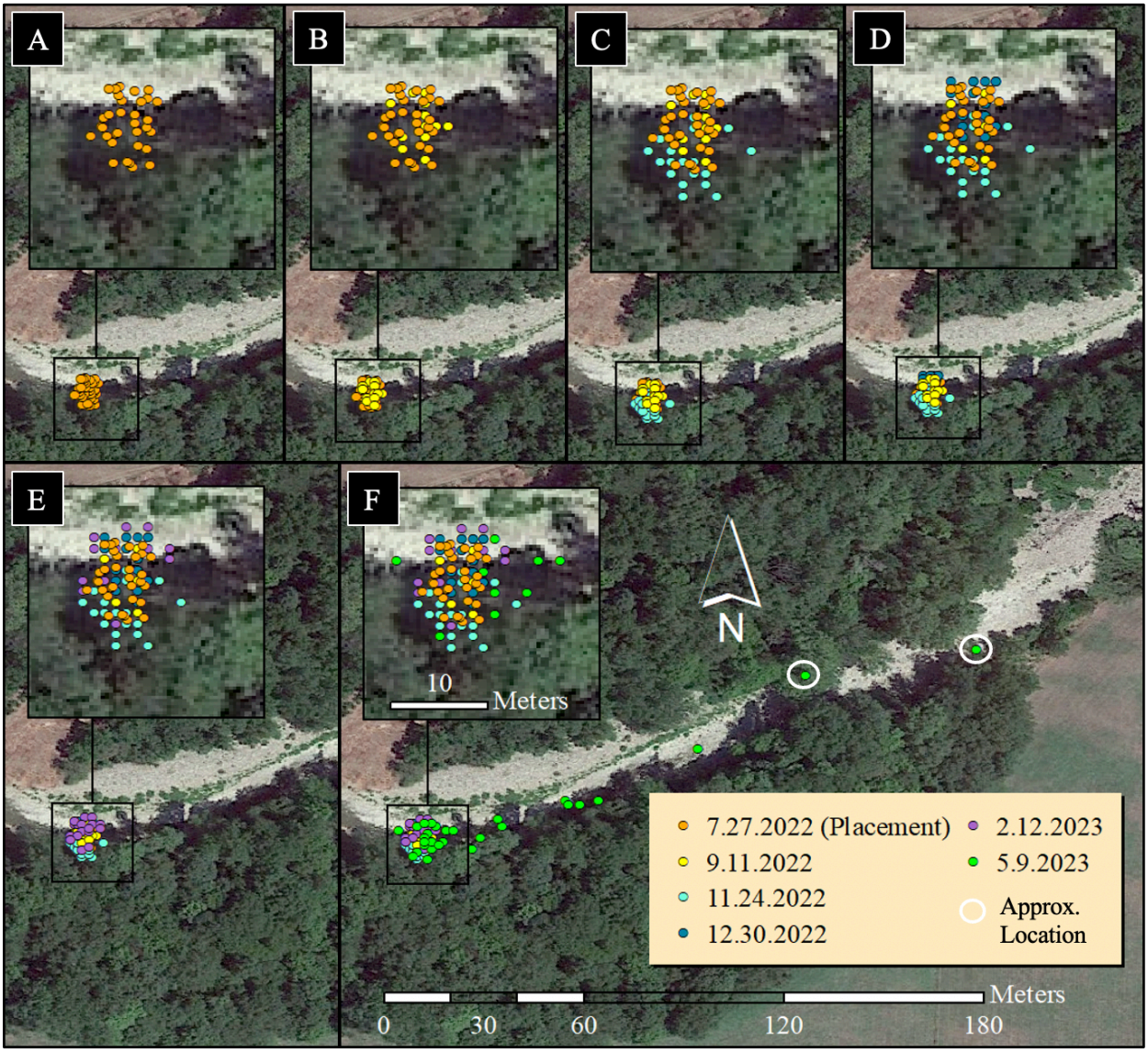

Figure 4.6: RFID cobble detection time-series data from each collection date (six total trips). **A**: Original cobble placement location data from survey 1; 7.27.2022. These data were collected with the Trimble Geo 7X GPS unit, while the rest of the data in this figure was collected with the OregonRFID equipment. **B**: Cobble location data from survey 2; 9.11.2022. **C**: Cobble location data from survey 3; 11.24.2022. **D**: Cobble location data from survey 4; 12.30.2022. **E**: Cobble location data from survey 5; 2.12.2023. **F**: Cobble location data from survey 6; 5.9.2023. Since the two furthest cobbles in survey six did not render coordinates, they have been given approximate locations in the figure. Satellite imagery from Google Earth Pro (v. 7.3.6.9345), July 10, 2022 (Google Earth, 2023).

Main stem discharge data from USGS gages above and below the Beech Creek confluence were evaluated to compare relative flow magnitudes between surveys (Figure 4.7; Appendix G.4). The Boxley USGS gage is located ~3.5 km upstream of Beech Creek, while the Ponca gage is located ~9 km downstream (USGS, 2023a, 2023b). Each gage generally trends together with varying magnitudes depending on local rainfall. Regardless of these slight differences, these data support the inference that peak discharges from surveys one through five in Beech Creek were not great enough to transport gravel past the riffle in which they were originally placed. Between survey five and six, however, the occurrence of the study's two highest peak flows corresponds with the greatest observed downstream movement of gravel (Figure 4.6F). These data show that coarse-grained bedload generally only moves during the highest peak flow events and not during typical streamflows or lower magnitude peak flows.

Due to minimal movement through the first five surveys and the 100% detection rate in survey six, movement distances were calculated over the entire experimental period (Table 4.6; Appendix G.3). As expected, the seven samples that moved the furthest (20+ meters) have the smallest average caliber. In relation to the original placement grid, the gravel placed in downstream positions tended to be transported greater distances downstream (Figure 4.8). Additionally, gravel on the edges of the active channel tended to move greater distances than those in the thalweg of the channel. In contrast, the sample that moved the furthest – sample 12 (PIT tag ID: 994) – was originally placed near the thalweg. Lastly, while gravel was sporadically distributed downstream of the placement area in survey six (Figure 4.6F), there appeared to be two small clusters of four samples in portions of the stream that contain larger boulders (potentially greater resistance) and potentially very little flow at base flow conditions.

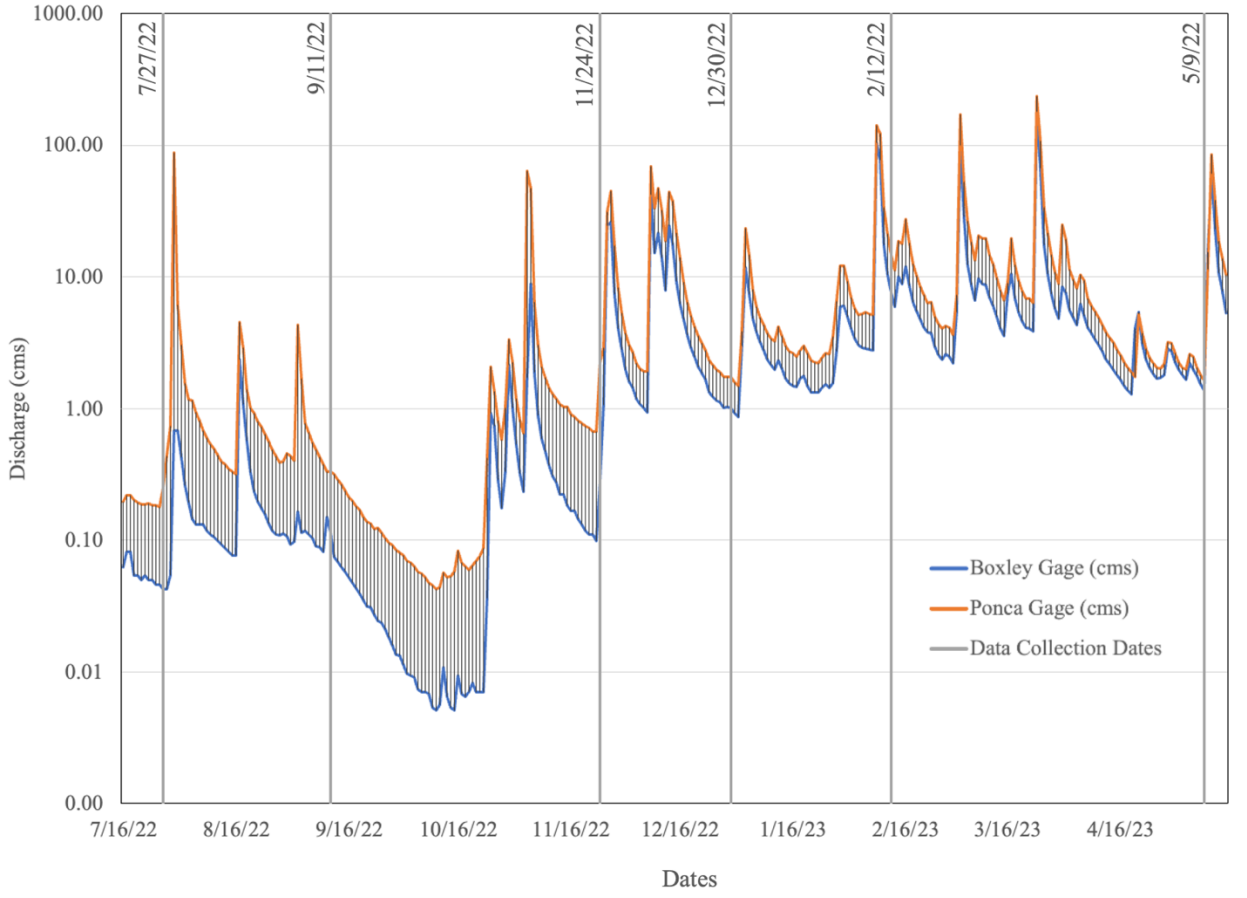

Figure 4.7: Log graph of USGS BNR daily peak discharge data from the Boxley (upstream of the Beech Creek confluence) and Ponca (downstream from the Beech Creek confluence) gage stations.

Movement (meters)	# of cobbles	% of total	Avg. cobble size (cm)
0-1	6	18.18%	9.5
1-5	6	18.18%	9.0
5-20	10	30.30%	9.9
20+	7	21.21%	7.8
unknown	4	12.12%	n/a

Table 4.6: Total cobble movement from placement (07.27.2022) to survey six (05.09.2023).

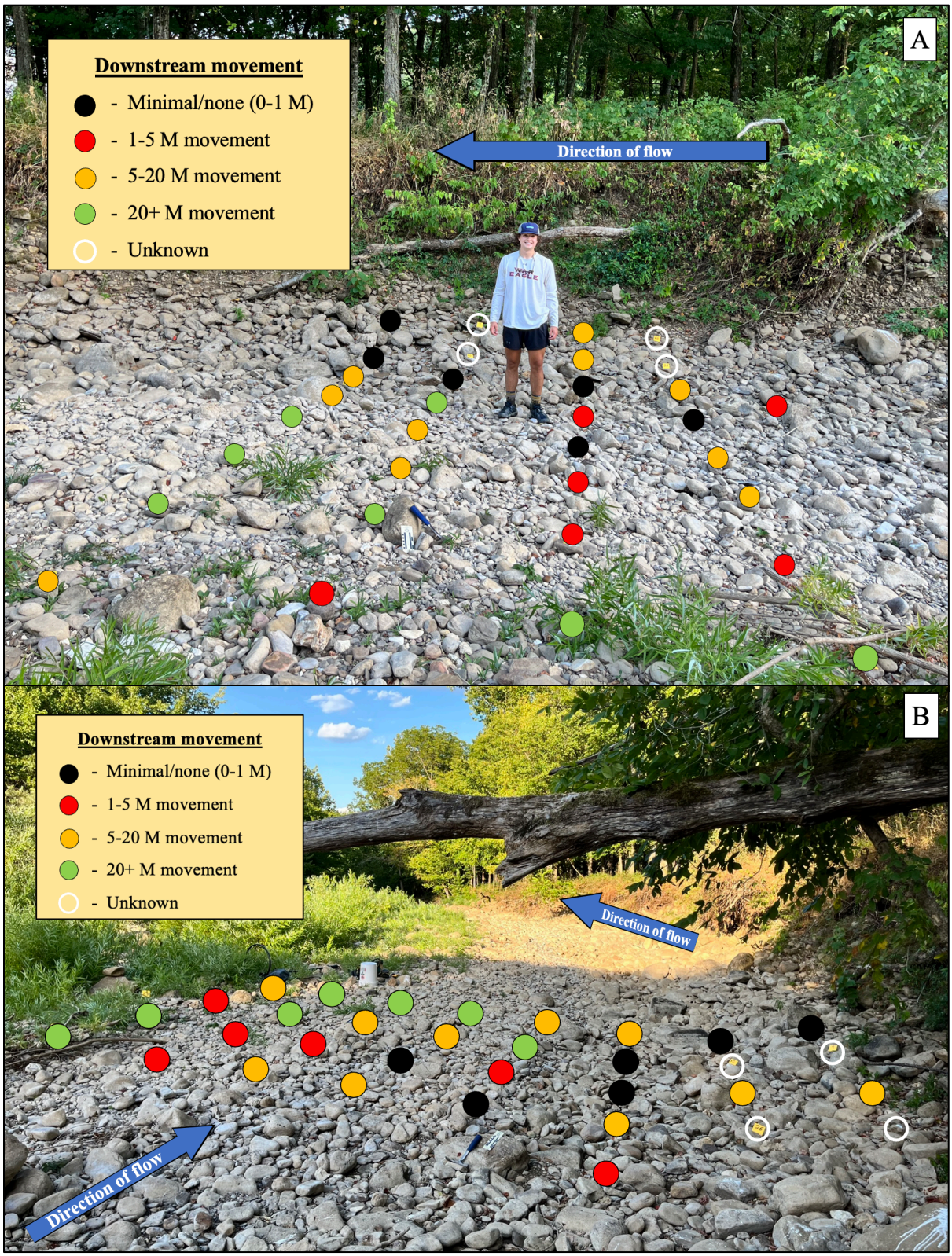

Figure 4.8: RFID cobble placement grid with associated movement over the length of the study (**A**: View from river left; **B**: View from the thalweg).

Chapter 5: Discussion

Gravel Bar Caliber & Provenance

Gravel bar caliber and provenance data each provide evidence of tributary-derived sediment inputs in the main stem. Specifically, strong signals from Cave, Calf, and Clabber Creeks have been identified. Statistically significant differences between main stem bar caliber data just upstream and downstream of the Cave and Clabber Creek confluences - combined with the fact that the tributary bars are not significantly different from the corresponding downstream bars - suggest that tributary-derived sediment inputs have directly influenced surface grain size distributions of gravel bars on the main stem (Figures 4.2, 4.4). Additionally, significant statistical differences were identified between Cave and Clabber Creek bars and their corresponding upstream main stem bars, suggesting that tributary gravel caliber is different from main stem distributions above each confluence (Appendix E). Provenance results reinforce Cave and Clabber Creek sediment input fingerprints in the main stem (Table 4.2; Figure 4.5). Both confluence areas show a dramatic rise in the dominant lithologies of each tributary bar directly below the confluence, neither of which dominate in the upstream main stem bars. Thus, Cave and Clabber Creek sediment input fingerprints in the main stem are supported by multiple lines of evidence.

Though Cave and Clabber Creek tributary inputs have been identified on the main stem, the caliber data statistics suggest that Cave Creek may have a greater influence on main stem surface distributions than Clabber Creek. Since the p-values associated with Cave Creek Wilcoxon tests were 11 and 13 orders of magnitude smaller than those associated with Clabber Creek, differences in Cave Creek confluence gravel populations were of greater significance than those

in the Clabber Creek confluence (Appendix E.4). Thus, caliber data suggest that Cave Creek sediment inputs are more pronounced in the main stem than those derived from Clabber Creek.

While statistically significant differences were identified between Beech and Calf Creek bars and their corresponding upstream main stem bars, a lack in statistically significant differences between the upstream and downstream main stem bars of each confluence suggests that these tributary sediment inputs are not pronounced enough to be detected by caliber data alone. However, the main stem upstream-downstream relationship associated with Calf Creek has a p-value ($p = 0.058$) that is very close to the $p < 0.05$ threshold used to support a significant difference between the two, suggesting that there likely is a relatively significant relationship here. Furthermore, Calf Creek provenance data provides evidence of a sediment input fingerprint from Calf Creek in the main stem, as limestone sediments dominate the tributary and downstream main stem gravel bars (Table 4.2, Figure 4.5). Since Calf Creek derived gravel inputs are well-supported by provenance data, the statistical relationship comparing upstream-downstream main stem caliber differences is likely significant enough to also support Calf Creek inputs in the main stem. Beech Creek, on the other hand, does not have a p-value near the statistically significant threshold for its upstream-downstream main stem sediment caliber relationship. Additionally, Beech Creek provenance data suggest a weak signal at best in the main stem. Although there is a distinguishable lithologic change from upstream to downstream of the Beech Creek confluence, the observed differences below the confluence do not appear to be significantly tied to Beech Creek tributary inputs since the magnitude of the decrease in sandstone sediment content does not appear to be possible from the tributary gravel bars surveyed. With this said, however, Beech Creek may still have a weak sediment fingerprint in the main stem, as the observed increase in chert content downstream from Beech Creek is potentially caused by tributary inputs. This signal is weak,

however, since the chert content comprises a relatively small percentage of the gravel at this location.

The provenance and caliber data in this study do not support a strong fingerprint in Beech Creek for two potential reasons related to sampling locations and foreign gravel influence. For one, the surveyed Beech Creek gravel bars were one bend further upstream than the other tributary bars analyzed in this study. Between the sampling site and confluence, Beech Creek continues to incise the Boone formation and younger terrace deposits (Hudson and Turner, 2007). Though Boone-derived sediments (Ls, cherty Ls, and chert) could be more dominant further downstream, Beech Creek tributary provenance data just before the confluence would have to see a drastic and unlikely increase in Boone-derived sediments to cause the large observed increase in Boone sediments on the main stem bar downstream of the confluence. Additionally, the Highway 21 bridge crosses Beech Creek just upstream of its confluence. To mitigate erosion, boulders from a foreign source were introduced along the banks and bridge structure. These boulders may serve as armor and as a barrier to gravel movement from upstream. Furthermore, since the lithology and caliber of this foreign sediment is unknown, the extent to which this foreign sediment has influenced the main stem sediment inputs is also unknown. Therefore, these considerations may influence why neither caliber nor provenance data were able to provide strong lines of evidence that Beech Creek sediment inputs can be distinguished in the main stem.

The evidence of tributary-derived sediment inputs contributes to high variability of gravel caliber in the main stem (Table 4.1). Instead of following Knighton's (1980) expected downstream fining pattern, results more closely align with Rice and Church's (1998) observations of negligible downstream fining due to the influence of lateral sediment sources. Though the lateral sources of sediment in that study are tied to both tributary and legacy glacier sediment inputs, our study

suggests that the presence of tributary sources appear to be sufficient in influencing gravel distribution variability downstream. Similarly, these results validate Pizzuto's (1995) assertion that mathematical models of downstream fining must account for variable gravel sources in addition to abrasion and entrainment of finer sediments.

Basin Morphometrics

In addition to field-based results, spatial analyses of tributary basin morphometrics provide context for how watershed form and position within the watershed may affect coarse sediment production and transport. Specifically, basin morphometric differences were identified between Beech Creek and the other study tributaries to further diagnose why it did not have a strong signal in the main stem. Beech Creek, as one of the highest tributaries in the watershed, is a headwater stream. It has the smallest area, stream order, and drainage density of the four study tributaries (Table 4.4). Beech Creek's position as the highest study site in the watershed likely exerts control on its small drainage size, as the highest tributaries in a watershed are typically the youngest and smallest since watersheds expand through headward erosion (Horton, 1945; Schumm, 1977). Because of this, we can infer that Beech Creek is the youngest of the four study tributaries. As the smallest study tributary, Beech Creek does not have as much physical area contributing rainwater and sediment to the channel. Since stream power and stream competence are proportional to stream order and basin area (Strahler, 1957, 1964), Beech Creek is at a disadvantage for coarse sediment entrainment. Though a smaller stream order may not imply less discharge for sediment transport than greater order streams in different basins, watershed area is a major factor in discharge, and subsequently, sediment transport (Strahler 1964). Even though Beech Creek has the largest relief ratio and average slope to drive sediment production (as is evidenced by the amount of hillslope-

derived Mississippian-Pennsylvanian coarse sediments in Beech Creek), the effects of the small basin area on limiting stream network complexity and discharge appear to be more influential in Beech Creek's sediment transport capabilities. Beech Creek's steeper slopes produce coarser material to its channel than the other study tributaries, which may require greater stream power and competence for entrainment than Beech Creek can provide due to its small area.

Another factor to consider about Beech Creek's position in the watershed is that the main stem of the BNR is also a headwater stream at this location. There are very few tributaries above Beech Creek and all – including Beech Creek and the main stem – are incising the same rock units. Therefore, it may not be possible to obtain a strong input signal from Beech Creek provenance data, as the gravel sources for Beech Creek and the main stem are the same in the upper BNR. As previously mentioned, however, Beech Creek confluence caliber datasets differ drastically between the tributaries and main stem (with no significant difference between the main stem bars), meaning tributary sediment inputs are not detectable from the caliber data. Thus, even if detecting a strong signal from provenance data was possible, the caliber data suggests that a strong signal from Beech Creek provenance data would have been rather unlikely.

Beech Creek's low drainage density appears to be another limiting control on tributary gravel routing and sediment inputs to the main stem. Drainage density (Dd), or a basin's ability to drain surface runoff as stream discharge, signifies the relative length of pathways and channel area for sediment to be transported to the main stem. Since Beech Creek has the lowest Dd of the study tributaries, it has the shortest sum of channel lengths per area, meaning less pathways are available for sediment entrainment. While the Dd metric is influenced by a watershed's lithology, climate, and topographic relief, Dd differences within a watershed can also be indicative of a tributary basin's stage of development (Roberts and Archibold, 1978). This is because younger tributaries

have not had as much time for their drainage networks to mature and develop (Schumm, 1977). As previously mentioned, the youngest tributary basins in a watershed are those furthest upstream (Horton, 1945; Schumm, 1977). Dd values support this assertion, as eight of the first eleven basins introduced in the BNR system have Dd values below the 25th percentile in the watershed (Figure 5.1; Appendix F.2). Since the vast majority of the lowest Dd values are found in the watershed's upper limits, low Dd values in the BNR appear to be controlled by tributary position in the watershed – as influenced by said basin's relative drainage-network maturity. Further supporting this assertion, headwater streams typically have steeper slopes and smaller basins due to upstream to downstream scaling (Tarboton et al., 1992), which generally match the morphometric data for these tributaries as well (Appendix F.1). Since Beech Creek is similar to other upper tributaries (similar basin area, exposed lithologies, Dd, slope), it is likely that these other tributaries would also be limited in their sediment transport capacity and main stem sediment inputs.

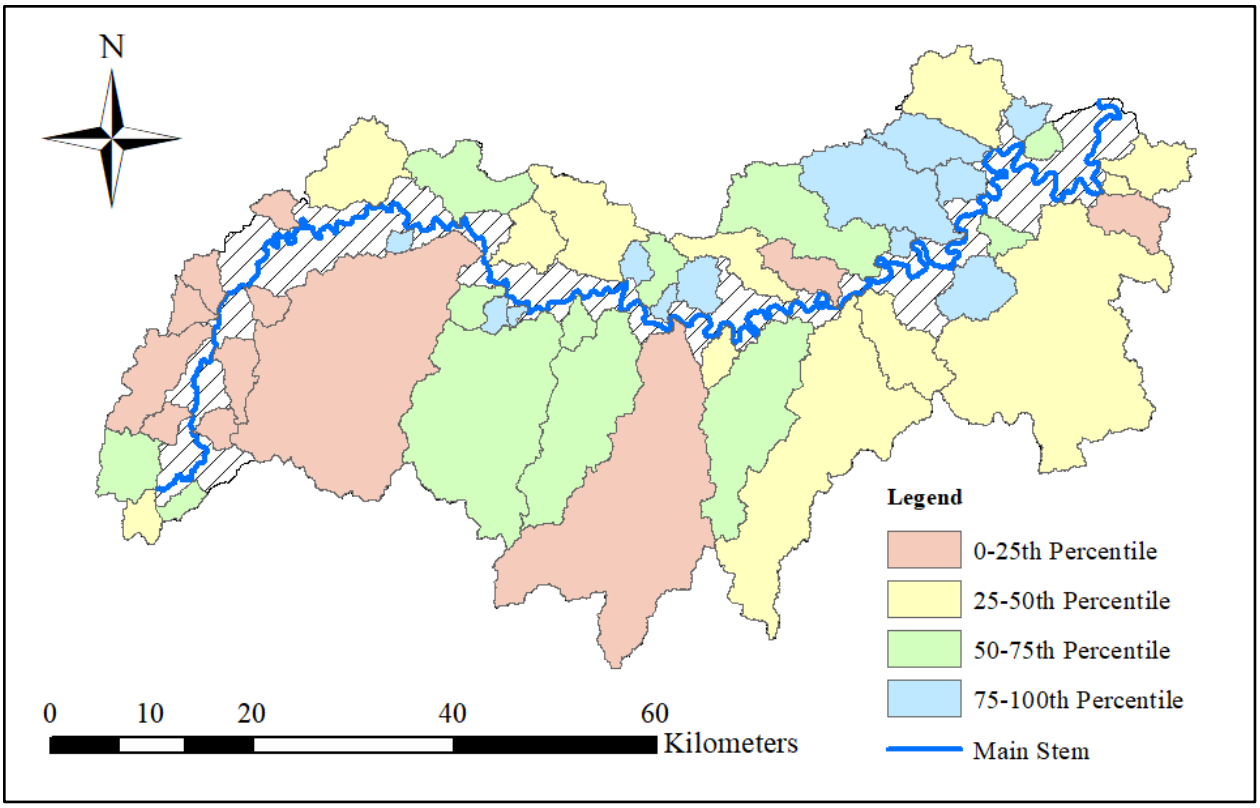

Figure 5.1: Dd percentile ranges of the 48 watersheds of third order or greater in the BNR watershed. Dd values for this figure and percentile cutoff values are provided in Appendix F.2.

Additionally, the balance of infiltration versus runoff in a basin (as inferred from Dd values) can influence sediment transport (Carlston, 1963; Strahler, 1964). If all other controls are equivalent, infiltration capacity and erosional resistance of the subsurface can control Dd (Horton, 1945), with lower Dd values indicating a subsurface with greater resistance or greater infiltration (Strahler, 1964). Increased infiltration of rainwater potentially limits the amount of stream discharge available for incision and sediment transport, thus decreasing stream competency and limiting local sediment transport. While the Mississippian-Pennsylvanian sandstones that dominate the majority of the Beech Creek tributary basin and Boston Mountain Plateau (Appendix A.1) (Hudson and Turner, 2007) are relatively permeable and resistant to erosion (Adamski et al., 1995; Chandler, 2015), impermeable shales cause the overall permeability of the area to be low

(Adamski et al., 1995). This impermeability does not follow common trends of lower Dd basins, as outlined by Strahler (1964). Since the other seven lowest-quartile Dd basins of the upper BNR are of similar lithologies, general impermeability is likely shared among them as well. For these reasons, it does not appear that groundwater infiltration controls Dd values in the BNR. Instead, the resistant nature of the Mississippian-Pennsylvanian sandstones that dominate these upper basins likely influence Dd values, as these units are simply more resistant to mechanical erosion (Adamski et al., 1995). The resistant subsurface here likely decreases the effectiveness of headward erosion, thus leading to a less complex stream network and, subsequently, lower Dd values in the upper portion of the watershed. This is supported by the previously addressed lowest-quartile Dd values in the upper reaches of the BNR (Figure 5.1). In contrast, BNR tributary watersheds in the Springfield Plateau have weak limestones and dolostones that fracture and dissolve, creating karst features that allow for greater incision and stream network complexity (Adamski et al., 1995; Chandler, 2015). Though ongoing work on heterogenous lithology in the BNR shows that the Boone and Everton Formations have near equal mechanical resistance, differences in susceptibility to dissolution and high fracture density may allow for greater incision in areas dominated by the Boone Formation (Keen-Zebert et al., 2017; Braun, 2021). Since the Calf and Cave Creek basins have much higher percentages of Boone Formation coverage than Beech Creek (Appendix A.1, B.1, C.1), it appears as though this unit allows for greater stream network complexity, as documented by the greater Dd values in these basins (Figure 5.1). Though it appears that differences in lithologic resistance may influence Dd values in the BNR, lithologic variability in each tributary basin makes this link difficult to fully support. While dominant lithologies in tributary basins can be compared, most (if not all) BNR tributaries have a variety of

different units exposed at the surface. Thus, Dd variability appears to be best linked to relative position in the watershed based on available data in this study.

Though underlying lithology may influence Dd differences, significant tributary sediment inputs were identified in both Boone and Everton reaches (as defined by Keen-Zebert et al., 2017). Therefore, our hypothesis of more pronounced tributary-derived sediment inputs in the wide and flat Boone reaches appears to be incorrect. While further studies would be necessary to quantify specific valley form controls on hillslope sediment inputs to the BNR, main stem valley width does not appear to dictate the prevalence of sediment input fingerprints in the main stem.

Additionally, though the literature states that basin shape - rounded versus elongated - influences peak flow discharges (Strahler, 1964), this study found that both elongated and rounded basins had distinguishable tributary-derived sediment inputs in the main stem. Thus, while peak flow discharges may be influenced by basin shape, it does not appear to greatly influence tributary sediment routing to the main stem in the BNR watershed.

Basin morphometric averages of the northern and southern tributary basins (of third order or greater) suggest physiographic controls on watershed area, as the southern basin areas are significantly larger than the northern basins on average (Table 4.3). Watershed scaling dynamics suggest that larger southern basins should have longer stream lengths, greater flow, and the potential to move more coarse sediment as compared to northern basins at the same position in the watershed. Since both of the southern study tributaries - Cave and Calf Creeks - had some of the strongest sediment signals in the main stem, basin area is interpreted as a primary control on sediment routing in the BNR. Since other north-south morphometric comparisons did not suggest considerably different mean values, it can be inferred that localized controls influence other morphometrics, as described in previous sections.

Transport in Beech Creek

Though Beech Creek's main stem sediment input signal is weak, the RFID pilot study captured considerable bedload sediment routing movements in Beech Creek over the sampling period. These data, paired with discharge data from the main stem, identified flow patterns necessary for coarse sediment entrainment and patterns of channelized gravel movements in relation to peak discharge events. As shown in Table 4.5, Figure 4.6, and Figure 4.7, coarse sediment entrainment in Beech Creek requires high peak flow discharges that are multiple logarithmic orders of magnitude above typical daily flows, with multiple peak flow events of this scale likely required for substantial coarse sediment transport. While gravel was sporadically distributed downstream of the placement area in response to one or both of the two peak discharge events in March, there appears to be two small clusters of 4 samples in portions of the stream that contain larger boulders (potentially areas of greater bed resistance). Thus, these clusters may provide evidence of temporary areas of deposition, as controlled by channel form. While this finding would be consistent with Pryce and Ashmore's (2003) documentation of holdover deposition locations in coarse sediment tracer studies, more data is needed to determine whether these two cluster areas serve as long-time holdover locations or not. Once the influence of additional peak flow discharge effects has been analyzed, this potential pattern will become clearer.

RFID gravel caliber data also suggests a trend in the average threshold size of gravel that will move in Beech Creek. As expected, the cobbles that moved the furthest (20+ meters downstream) had the smallest average medial axis, while those that moved 0-20 meters downstream had larger medial axes (Table 4.6). Of course, greater discharge events would mean that this caliber size threshold would increase, as shear stresses and force increase with increasing

flows (Wolman and Miller, 1960). It is also clear that while cobbles may shift a meter or two downstream from smaller peak discharge events, the majority of coarse sediment movements in Beech Creek occur in exceedingly large peak discharge events, which is consistent with the literature (Jacobson and Gran, 1999).

While coarse sediment caliber is an important consideration in sediment transport, the RFID data suggests a pattern in placement that influences the likelihood of entrainment. Figure 4.8 exemplifies how the majority of cobbles that moved the furthest were originally placed on the gently sloping stream bank on river left. In peak discharge events, the gravel bar on river left must become flooded, causing this edge of the main channel to receive some of the most turbulent flows. The cut bank side of the stream would also be expected to receive some of these most turbulent flows, though four cobbles on the cut bank side are missing location data to adequately support this assumption. Additionally, Figure 4.8 shows that most samples in the thalweg of the stream hardly moved. This result can likely be contributed to helical flow keeping these sediments armored in the thalweg, as this reach is a relatively deep and narrow, slightly bending channel that allows for helical flow to cause armoring (Matthes, 1947). Each of these findings are generally consistent with current theory on coarse sediment transport mechanics and entrainment by turbulent flow in natural channels.

Even with evidence of entrainment being greatest on the flanks of the channel, some smaller cobbles near the edge did not move in response to potentially greater turbulence in this area. Thus, the RFID data supports the presence and stark influence of vagaries in flow for entraining coarse sediment. This suggests that flow in natural channels is non-uniform - even within a specific cross-section or reach. Additionally, channel roughness and armoring may have trapped or buried smaller cobbles near their entrainment location, preventing further transport.

Previous studies have indicated that channel roughness is commonly underestimated in models of bedload transport dominated streams (Ferguson, 2017; Bartels et al., 2021), which supports this possibility. These findings support the fact that sediment transport is difficult to quantify due to the sporadic nature of turbulent flows and channel resistance.

Importantly, researchers have documented bedload material moving in waves of aggradation and degradation across various drainage basins in the Ozark region, including the BNR near Boxley (McKenney and Jacobson, 1996). Given the clear movements of cobbles away from the left flank of Beech Creek, it is assumed that further entrainment of sediments from this locality would eventually cause a local wave of channel degradation. Though localized waves could be partly supported by further RFID studies, the analysis of tributary basin-scale waves of aggradation and degradation requires multiple years of data collection to document bed-elevation changes over time. These analyses could be conducted in future studies.

As a pilot study, these data were helpful in determining streamflow variability and potential streamflow thresholds for coarse sediment movement in Beech Creek. Multiple years of RFID data paired with in situ streamflow measurements and rain gage data will be necessary to better quantify bedload sediment routing patterns at this location. Data collections from multiple water-years will allow for more peak flow discharge events to be evaluated and compared to one another for their effect on coarse sediment transport. This would then allow for the modeling of bedload transport in BNR tributaries, as evidenced by Bradley and Tucker (2012).

Conclusions

This study analyzed coarse sediment routing in a semi-controlled, gravel-mantled bedrock stream at both the tributary and watershed scale. Provenance and caliber datasets provided multiple

lines of evidence of tributary-derived sediment inputs in the main stem, which counters the theoretical downstream fining pattern caused by abrasion. These analyses helped elucidate specific basin morphometric controls on tributary-derived sediment transport in the BNR, which include basin area, stream order, drainage density, and position in the watershed. Though hillslope-derived sediment inputs are likely present in the main stem, tributary-derived sediment inputs had strong signals in the main stem of both Boone and Everton reaches. This result suggests that BNR main stem valley form does not influence the strength of tributary-derived sediment input signals in the main stem. Additionally, since strong sediment input signals were derived from both elongated and rounded basins, basin shape – as quantified by the elongation ratio - does not appear to be a primary control on tributary sediment routing in the BNR. The RFID pilot project on watershed-scale sediment routing patterns identified that most bedload movements occur in only the largest peak discharge events, which is consistent with the literature. Sediment caliber and channel flow patterns were found to have influenced localized sediment entrainment.

Future Directions

While this study identified primary controls on coarse sediment routing in tributaries of gravel-mantled bedrock streams, future studies could further analyze controls that were less-clear from this study's data. Specifically, future analyses of lithologic variability, hydrogeologic connectivity, as well as valley and channel form differences in tributaries could better constrain other controls on sediment routing processes in BNR tributaries. Comparing this in-situ study to gravel-mantled bedrock streams in the region that have managed flow, such as the Little Red River of north-central Arkansas, could allow for interesting comparisons between sediment routing controls of dammed and undammed fluvial systems in the Ozark Plateaus.

Though preliminary results from the RFID pilot project are promising in their ability to better constrain bedload transport, more data is needed to evaluate these trends over successive water-years and variable flow conditions. Continued monitoring of the previously placed gravel will provide better context for the extent to which varying peak discharge magnitudes influence sediment routing. Incorporating a streamflow datalogger in Beech Creek would also allow for specific entrainment streamflow thresholds to be recognized, which could allow for future modeling work and the identification of more pronounced routing patterns.

Significance

Coarse sediment routing in tributaries of gravel-mantled bedrock streams is critical for understanding channel and basin morphology in ever-changing fluvial systems. This study proves that the combination of caliber and provenance data can be utilized to identify tributary sediment input signals in the main stem. Identifying these signals contributes to our understanding of the controls on the connectivity between BNR tributaries and the main stem, as well as the availability of tools to incise the stream beds of each. Comparing the apparent influence of hillslope processes and tributaries to main stem sediment inputs allows us to better link these processes and understand the extent to which they influence the modern system, which has been anthropogenically altered through the region's logging history. This study's findings could aid future research in constraining natural and anthropogenic controls on sediment inputs at the watershed scale.

Additionally, gravel-mantled streams hold importance for the biosphere, providing aquatic habitat, nutrient cycling, and other ecosystem services (Boulton et al., 2008). Since gravel routing affects each of these environmental benefits, understanding long-term and short-term gravel

movement patterns in the greater BNR watershed helps to inform future river management plans. Plans associated with erosion control, biodiversity support, and more could be influenced by this project's conclusions.

References

Adamski, J.C., Petersen, J.C., Freiwald, D.A., and Davis, J.V., 1995, Environmental and hydrologic setting of the Ozark Plateaus study unit, Arkansas, Kansas, Missouri, and Oklahoma, Volume 94, No. 4022: Little Rock, AR, U.S. Geological Survey, Water-Resources Investigations Report, National Water-Quality Assessment Program.

Ansari, Z.R., Rao, L.A.K., and Yusuf, A., 2012, GIS based morphometric analysis of Yamuna drainage network in parts of Fatehabad area of Agra district, Uttar Pradesh: Journal of the Geological Society of India, v. 79, p. 505-514.

Araújo, J.C.D., 2007, Entropy-based equation to assess hillslope sediment production. Earth Surface Processes and Landforms, v. 32(13), p. 2005-2018, https://doi.org/10.1002/esp.1502.

Arkansas GIS Office, 2006, 2006 Five Meter Resolution Digital Elevation Model (raster): https://gis.arkansas.gov/product/2006-five-meter-resolution-digital-elevation-model-raster-new/.

Ausbrooks, S.M., Johnson, T.C., Nondorf, L.M., and Traywick, C.L., 2012a, Geologic Map of the Cozahome Quadrangle, Marion County, Arkansas: Arkansas Geological Survey, Digital Geologic Quadrangle Map DGM-AR-00187, scale 1:24,000.

Ausbrooks, S.M., Johnson, T.C., Nondorf, L.M., and Traywick, C.L., 2012b, Geologic Map of the Rea Valley Quadrangle, Marion County, Arkansas: Arkansas Geological Survey, Digital Geologic Quadrangle, Map DGM-AR-00730, scale 1:24,000.

Bagnold, R.A., 1960, Sediment discharge and stream power: a preliminary announcement, Volume 421: Washington, D.C., United States Department of the Interior, Geological Survey.

Bartels, G.K., dos Reis Castro, N.M., Collares, G.L., and Fan, F.M., 2021, Performance of bedload transport equations in a mixed bedrock–alluvial channel environment: Catena, v. 199, a. 105108.

Bartlett, M.S., 1937, Properties of sufficiency and statistical tests: Proceedings of the Royal Society of London, Series A-Mathematical and Physical Sciences, v. 160(901), p. 268-282.

Beer, A.R., and Turowski, J.M., 2015, Bedload transport controls bedrock erosion under sediment-starved conditions: Earth Surface Dynamics, v. 3(3), p. 291-309.

Beeson, H.W., McCoy, S.W., and Keen-Zebert, A., 2017, Geometric disequilibrium of river basins produces long-lived transient landscapes: Earth and Planetary Science Letters, v. 475, p. 34-43.

Begin, Z.B., and Schumm, S.A., 1979, Instability of alluvial valley floors: a method for its assessment: Transactions of the American Society of Agricultural and Biological Engineers, v. 22(2), p. 347-350, doi: 10.13031/2013.35018.

Bierman, P.R., and Montgomery, D.R., 2014, Key concepts in geomorphology: New York, W.H. Freeman and Company Publishers, 195 p.

Booth, D.B., 1990, Stream-Channel Incision Following Drainage-Basin Urbanization: Journal of the American Water Resources Association, v. 26, p. 407-417, https://doi.org/10.1111/j.1752-1688.1990.tb01380.x.

Boulton, A.J., Fenwick, G.D., Hancock, P.J., and Harvey, M.S., 2008, Biodiversity, functional roles and ecosystem services of groundwater invertebrates: Invertebrate Systematics, v. 22(2), p. 103-116.

Braden, A.K., Smith, J.M., 2004a, Geologic Map of the Lurton Quadrangle, Newton County, Arkansas, Map DGM-AR-00509: U.S. Geological Survey, scale 1:24,000.

Braden, A.K., Smith, J.M., 2004b, Geologic Map of the Moore Quadrangle, Newton and Searcy Counties, Arkansas: U.S. Geological Survey, Map DGM-AR-00579, scale 1:24,000.

Bradley, N.D., and Tucker, G.E., 2012, Measuring gravel transport and dispersion in a mountain river using passive radio tracers: Earth Surface Processes and Landforms, v. 37, p. 1034-1045. https://doi.org/10.1002/esp.3223.

Braun, J.N., 2021, Using Ground-Based LiDAR to Analyze Fracture Characteristics as Possible Controls on the Variability of Valley Morphology in the Buffalo River Watershed, Arkansas [M.S. Thesis]: Auburn University.

Burt, J.E., Barber, G.M., and Rigby, D.L. 2009, Elementary statistics for geographers: New York, Guilford Press, 114 & 393 p.

Caracciolo, L., 2020, Sediment generation and sediment routing systems from a quantitative provenance analysis perspective: Review, application and future development: Earth-Science Reviews, v. 209, a. 103226.

Carlston, C.W., 1963, Drainage density and streamflow: Washington, D.C., United States Government Printing Office.

Chandler, A.K., 2015, Arkansas Geology Outdoors: Exploring the Upper Buffalo River Region: Little Rock, AR, Arkansas Geological Survey, Educational Workshop Series 09.

Chandler, A.K., and Ausbrooks, S.M., 2015a, Geologic Map of the Eula Quadrangle, Newton and Searcy Counties, Arkansas: Arkansas Geological Survey, Map DGM-AR-00269, scale 1:24,000.

Chandler, A.K., and Ausbrooks, S.M., 2015b, Geologic Map of the Mt. Judea Quadrangle, Newton County, Arkansas: Arkansas Geological Survey, Map DGM-AR-00590, scale 1:24,000.

Chandler, A.K., and Ausbrooks, S.M., 2015c, Geologic Map of the Snowball Quadrangle, Searcy County, Arkansas: Arkansas Geological Survey, Map DGM-AR-00800, scale 1:24,000.

Cook, K.L., Turowski, J.M., and Hovius, N., 2012, A demonstration of the importance of bedload transport for fluvial bedrock erosion and knickpoint propagation: Earth Surface Processes and Landforms, v. 38(7), p. 683-695.

Cowan, W.L., 1956, Estimating hydraulic roughness coefficients: Agricultural engineering, v. 37(7), p. 473-475.

Das, B.C., Islam, A., and Sarkar, B., 2022, Drainage Basin Shape Indices to Understanding Channel Hydraulics: Water Resources Management, v. 36(8), p. 2523-2547.

Environmental Systems Research Institute (ESRI), 2021, ArcGIS Desktop: Release 10.8.2. Redlands, CA: Environmental Systems Research Institute.

Fenneman, N.M., 1928, Physiographic divisions of the United States: Annals of the Association of American Geographers, v. 18(4), p. 261-353.

Ferguson, R.I., Sharma, B.P., Hardy, R.J., Hodge, R.A., and Warburton, J., 2017, Flow resistance and hydraulic geometry in contrasting reaches of a bedrock channel: Water Resources Research, v. 53, p. 2278-2293, doi:10.1002/2016WR020233.

Fernández, R., Parker, G., and Stark, C.P., 2019, Experiments on patterns of alluvial cover and bedrock erosion in a meandering channel: Earth Surface Dynamics, v. 7(4), p. 949-968.

Foley, M.G., 1980, Bed-rock incision by streams: Geological Society of America Bulletin, v. 91(10, Part II), p. 2189-2213.

Gilbert, G.K., 1877, Report on the Geology of the Henry mountains: Washington, D.C., United States Government Printing Office.

Gilbert, G.K., and Murphy, E.C., 1914, The transportation of debris by running water, No. 86: Washington, D.C., United States Government Printing Office.

Giles, A.W., 1932, Textural features of the Ordovician sandstones of Arkansas: The Journal of Geology, v. 40(2), p. 97-118.

Google Earth, 2023, Google Earth Pro 7.3.6.9345 (64-bit): A computer program for visualizing geospatial data, Google Technology Company.

Gray, D.M., 1961, Interrelationships of watershed characteristics: Journal of Geophysical Research, v. 66(4), p. 1215– 1223, doi:10.1029/JZ066i004p01215.

Griffiths, R.E., and Topping, D.J., 2017, Importance of measuring discharge and sediment transport in lesser tributaries when closing sediment budgets: Geomorphology, v. 296, p. 59-73.

Hack, J.T., 1957, Studies of longitudinal stream profiles in Virginia and Maryland, Volume 294: Washington, D.C., United States Government Printing Office.

Hayes, S.K., Montgomery, D.R., and Newhall, C.G., 2002, Fluvial sediment transport and deposition following the 1991 eruption of Mount Pinatubo: Geomorphology, v. 45(3-4), p. 211-224.

Hicks, D.M., and Gomez, B., 2003, Sediment transport, *in* Kondolf, G.M., and Piégay, H., Tools in Fluvial Geomorphology: John Wiley & Sons, Ltd., p. 425-461.

Horton, R.E., 1932, Drainage-basin characteristics: Transactions of the American geophysical Union, v. 13(1), p. 350-361.

Horton, R.E., 1941, Sheet erosion: present and past: Transactions of the American Geophysical Union, v. 22, p. 299-305.

Horton, R.E., 1945, Erosional development of streams and their drainage basins: hydrophysical approach to quantitative morphology: Geological Society of America Bulletin, v. 56(3), p. 275-370.

Huang, C., Gascuel-Odoux, C., and Cros-Cayot, S., 2002, Hillslope topographic and hydrologic effects on overland flow and erosion: Catena, v. 46(2-3), p. 177-188.

Hudson, M.R., 2000, Coordinated strike-slip and normal faulting in the southern Ozark dome of northern Arkansas: Deformation in a late Paleozoic foreland: Geology, v. 28(6), p. 511-514.

Hudson, M.R., and Murray, K.E., 2003, Geologic map of the Ponca Quadrangle, Newton, Boone, and Carroll County, Arkansas: U.S. Geological Survey, Miscellaneous Field Studies Map MF-2412, scale 1:24,000.

Hudson, M.R., and Turner, K.J., 2007, Geologic map of the Boxley quadrangle, Newton and Madison Counties, Arkansas: U.S. Geological Survey, Scientific Investigations Map 2991, scale 1:24,000.

Hudson, M.R., and Turner, K.J., 2022, Late Paleozoic flexural extension and overprinting shortening in the southern Ozark dome, Arkansas, USA: Evolving fault kinematics in the foreland of the Ouachita orogen: Tectonics, v. 41(6), a. e2021TC006706.

Imhoff, K.S., and Wilcox, A.C., 2016, Coarse bedload routing and dispersion through tributary confluences: Earth Surface Dynamics, v. 4(3), p. 591-605.

Jacobson, R.B. and Gran, K.B., 1999, Gravel sediment routing from widespread, low-intensity landscape disturbance, Current River Basin, Missouri: Earth Surface Processes and Landforms, v. 24, p. 897-917.

James, L.A., 1997, Channel incision on the lower American River, California, from streamflow gage records: Water Resources Research, v. 33(3), p. 485-490.

Jarrett, R.D., 1984, Hydraulics of high-gradient streams: Journal of hydraulic engineering, v. 110(11), p. 1519-1539.

Keen-Zebert, A., Hudson, M.R., Shepherd, S.L., and Thaler, E.A., 2017, The effect of lithology on valley width, terrace distribution, and bedload provenance in a tectonically stable catchment with flat-lying stratigraphy: Earth Surface Processes and Landforms, v. 42(10), p. 1573-1587.

Knapp, R.T., 1938, Energy-balance in stream-flows carrying suspended load: Eos, Transactions American Geophysical Union, v. 19(1), p. 501– 505, doi:10.1029/TR019i001p00501.

Knighton, A.D., 1980, Longitudinal changes in size and sorting of stream-bed material in four English rivers: Geological Society of America Bulletin, v. 91(1), p. 55-62.

Knighton, A.D., 1999, Downstream variation in stream power: Geomorphology, v. 29(3-4), p. 293-306.

Knox, B.R., 1966, Pleistocene and recent geology of the southwest Ozark plateaus: The University of Iowa.

Komar, P.D., 1987, Selective gravel entrainment and the empirical evaluation of flow competence: Sedimentology, v. 34, p. 1165-1176, https://doi.org/10.1111/j.1365-3091.1987.tb00599.x.

Kondolf, G. M., Montgomery, D.R., Piégay, H., and Schmitt, L., 2003, Geomorphic classification of rivers and streams, *in* Kondolf, G.M., and Piégay, H., Tools in Fluvial Geomorphology: John Wiley & Sons, Ltd., p. 171-204.

Kumar, V., 2011, Elongation Ratio, in Singh, V.P., Singh, P., and Haritashya, U.K., 2011, Encyclopedia of Snow, Ice and Glaciers: Encyclopedia of Earth Sciences Series: New York, Springer, Dordrecht. https://doi.org/10.1007/978-90-481-2642-2_130.

Leopold, L.B., Wolman, M.G., and Miller, J.P., 1964, Fluvial Processes in Geomorphology: New York, Courier Dover Publications.

Limerinos, J.T., 1970, Determination of the Manning coefficient from measured bed roughness in natural channels, Volume 1898: Washington, D.C., United States Government Printing Office.

Lindsey, D.A., Langer, W.H., and Van Gosen, B.S., 2007, Using pebble lithology and roundness to interpret gravel provenance in piedmont fluvial systems of the Rocky Mountains, USA: Sedimentary Geology, v. 199(3-4), p. 223-232.

Magesh, N.S., Chandrasekar, N., and Soundranayagam, J.P., 2011, Morphometric evaluation of Papanasam and Manimuthar watersheds, parts of Western Ghats, Tirunelveli district, Tamil Nadu, India: a GIS approach: Environmental Earth Sciences, v. 64, p. 373-381.

Matthes, G.H., 1947, Macroturbulence in natural stream flow: Eos, Transactions American Geophysical Union, v. 28(2), p. 255-265.

Marcus, W.A., Roberts, K., Harvey, L., and Tackman, G., 1992, An evaluation of methods for estimating Manning's n in small mountain streams: Mountain Research and Development, v. 12(3), p. 227-239.

McFarland, J.D., 1998, Stratigraphic summary of Arkansas: Little Rock, Arkansas, Arkansas Geological Commission Information Circular, 36 & 39 p.

McKenney, R.A., and Jacobson, R.B., 1996, Erosion and deposition at the riffle-pool scale in gravel-bed streams, Ozark Plateaus, Missouri and Arkansas, 1990-95: Rolla, Missouri, United States Geological Survey. https://pubs.usgs.gov/of/1996/0655a/report.pdf.

McKnight, E.T, 1935, Zinc and lead deposits of northern Arkansas, No. 853: Washington, D.C., United States Government Printing Office.

Ott, R.L., and Longnecker, M., 2001, An introduction to Statistical Methods and Data Analysis – 5th ed.: Belmont, California, Dyxbury Thomson Learning, 308-314 p.

Panfil, M.S., and Jacobson, R.B., 2001, Relations Among Geology, Physiography, Land Use, and Stream Habitat Conditions in the Buffalo and Current River Systems, Missouri and Arkansas: USGS Biological Science Report, No. 2001-0005, https://www.cerc.usgs.gov/pubs/center/pdfdocs/BSR2001-0005.pdf.

Phillips, J.D., 1988, The role of spatial scale in geomorphic systems: Geographical Analysis, v. 20(4), p. 308-317.

Piégay, H., and Schumm, S.A., 2003, System approaches in fluvial geomorphology, *in* Kondolf, G.M., and Piégay, H., Tools in Fluvial Geomorphology: John Wiley & Sons, Ltd., 103-134 p.

Pizzuto, J.E., 1995, Downstream fining in a network of gravel-bedded rivers: Water Resources Research, v. 31(3), p. 753-759.

Prancevic, J.P., and Lamb, M.P., 2015, Unraveling bed slope from relative roughness in initial sediment motion: Journal of Geophysical Research: Earth Surface, v. 120(3), p. 474-489.

Purdue, A.H., and Miser, H.D., 1916, Description of the Eureka Springs and Harrison quadrangles. Arkansas-Missouri: United States Geological Survey, Atlas 202, 7.

Pyrce, R.S., and Ashmore, P.E., 2003, The relation between particle path length distributions and channel morphology in gravel-bed streams: a synthesis: Geomorphology, v. 56(1-2), p. 167-187.

Quinn, J.H., 1958, Plateau surfaces of the Ozarks: Journal of the Arkansas Academy of Science, v. 11(1), p. 36-43.

Rice, S., 1998, Which tributaries disrupt downstream fining along gravel-bed rivers?: Geomorphology, v. 22(1), p. 39-56.

Rice, S., and Church, M., 1998, Grain size along two gravel-bed rivers: statistical variation, spatial pattern and sedimentary links: Earth Surface Processes and Landforms, v. 23(4), p. 345-363.

Rigon, R., Rinaldo, A., Rodriguez-Iturbe, I., Bras, R.L., and Ijjasz-Vasquez, E., 1993, Optimal channel networks: A framework for the study of river basin morphology: Water Resources Research, v. 29, p. 1635– 1646, doi:10.1029/92WR02985.

Roberts, M.C., and Archibold, O.W., 1978, Variation of drainage density in a small British Columbia watershed: Journal of the American Water Resources Association, v. 14(2), p. 470-476.

Rodrigues, K., Keen-Zebert, A., Shepherd, S., Hudson, M.R., Bitting, C.J., Johnson, B.G., and Langston, A., 2023, The role of lithology and climate on bedrock river incision and terrace development along the Buffalo National River, Arkansas: Quaternary Research, p. 1-15.

RStudio Team, 2021, RStudio v. 4.1.2: Integrated Development for R. RStudio, PBC, Boston, MA: http://www.rstudio.com/.

Scheidegger, A.E., 1965, The algebra of stream-order numbers, *in* U.S. Geological Survey, Geological Survey Research 1965: Chapter B., Part 2, p. 187-189.

Schumm, S.A., 1954, The relation of drainage basin relief to sediment loss: International Association of Scientific Hydrology, v. 36(1), p. 216-219.

Schumm, S.A., 1956, Evolution of drainage systems and slopes in badlands at Perth Amboy, New Jersey: Geological society of America bulletin, v. 67(5), p. 597-646.

Schumm, S.A., 1963, A tentative classification of alluvial river channels: an examination of similarities and differences among some Great Plains rivers, Volume 477: Washington, D.C., United States Department of the Interior, Geological Survey, 8 p.

Schumm, S.A., 1977, The Fluvial System: New York, John Wiley & Sons, 58-93 p.

Schumm, S.A., 1985, Patterns of alluvial rivers: Annual Review of Earth and Planetary Sciences, v. 13(1), p. 5-27.

Scott, H.D., and Udouj, T.H., 1999, Spatial and temporal characterization of land-use in the Buffalo National River Watershed: Environmental Conservation, v. 26(2), p. 94-101. doi:10.1017/S0376892999000144.

Shapiro, S.S., and Wilk, M.B., 1965, An analysis of variance test for normality (complete samples): Biometrika, v. 52(3/4), p. 591-611.

Shreve, R.L., 1969, Stream Lengths and Basin Areas in Topologically Random Channel Networks: The Journal of Geology, v. 77(4), p. 397–414, https://doi.org/10.1086/628366.

Smith, D.K., and Hutton, R.S., 2007, Geologic Map of the Witts Springs Quadrangle, Searcy County, Arkansas: U.S. Geological Survey, Map DGM-AR-00927, scale 1:24,000.

Sólyom P.B., and Tucker G.E., 2004, Effect of limited storm duration on landscape evolution, drainage basin geometry, and hydrograph shapes: Journal of Geophysical Research: Earth Surface, v. 109(F3), https://doi.org/10.1029/2003JF000032.

Strahler, A.N., 1957, Quantitative analysis of watershed geomorphology: Eos, Transactions American Geophysical Union, v. 38(6), p. 913-920.

Strahler, A.N., 1964, Quantitative Geomorphology of Drainage Basins and Channel Networks, *in* Chow, V.T., Handbook of Applied Hydrology: A Compendium of Water-Resources Technology: New York, McGraw-Hill Book Company, p. 439-476.

Sukristiyanti, S., Maria, R., and Lestiana, H., 2018, Watershed-based morphometric analysis: a review: IOP Conference Series: Earth and Environmental Science, v. 118(1), a. 012028.

Tarboton, D.G., Bras, R.L., and Rodriguez-Iturbe, I., 1992, A physical basis for drainage density: Geomorphology, v. 5(1-2), p. 59-76.

U.S. Geological Survey (USGS), 2011, Rea Valley Quadrangle, Arkansas, 7.5-minute series: U.S. Geological Survey, scale 1:24,000.

U.S. Geological Survey (USGS), 2014, Eula Quadrangle, Arkansas, 7.5-minute series: U.S. Geological Survey, scale 1:24,000.

U.S. Geological Survey (USGS), 2014, Snowball Quadrangle, Arkansas, 7.5-minute series: U.S. Geological Survey, scale 1:24,000.

U.S. Geological Survey (USGS), 2017, Boxley Quadrangle, Arkansas, 7.5-minute series: U.S. Geological Survey, scale 1:24,000.

U.S. Geological Survey (USGS), 2023a, Buffalo River Near Boxley, AR – 07055646: https://waterdata.usgs.gov/monitoring-location/07055646/ (accessed June 2023).

U.S. Geological Survey (USGS), 2023b, Buffalo River Near Ponca, AR – 07055660: https://waterdata.usgs.gov/monitoring-location/07055660/ (accessed June 2023).

Verstraeten, G., 2006, Regional scale modelling of hillslope sediment delivery with SRTM elevation data: Geomorphology, v. 81(1-2), p. 128-140.

Wentworth, C.K., 1922, A scale of grade and class terms for clastic sediments: The Journal of Geology, v. 30(5), p. 377-392.

Whipple, K.X., 2004, Bedrock rivers and the geomorphology of active orogens: Annual Review of Earth and Planetary Sciences, v. 32, p. 151-185.

Wilcock, P.R., 2001, Toward a practical method for estimating sediment-transport rates in gravel-bed rivers: Earth Surface Processes and Landforms, v. 26(13), p. 1395-1408.

Wolman, M.G., 1954, A method of sampling coarse river-bed material: EOS, Transactions American Geophysical Union, v. 35(6), p. 951-956.

Wolman, M.G., and Miller, J.P., 1960, Magnitude and frequency of forces in geomorphic processes: The Journal of Geology, v. 68(1), p. 54-74.

Yang, C.T., and Sayre, W.W., 1971, Stochastic model for sand dispersion: Journal of the Hydraulics Division, v. 97(2), p. 265-288.

APPENDICIES

APPENDIX A:

Beech Creek

Appendix A.1: Geologic map of the Beech Creek tributary basin and surrounding area. Geologic map overlay acquired from Hudson and Turner (2007).

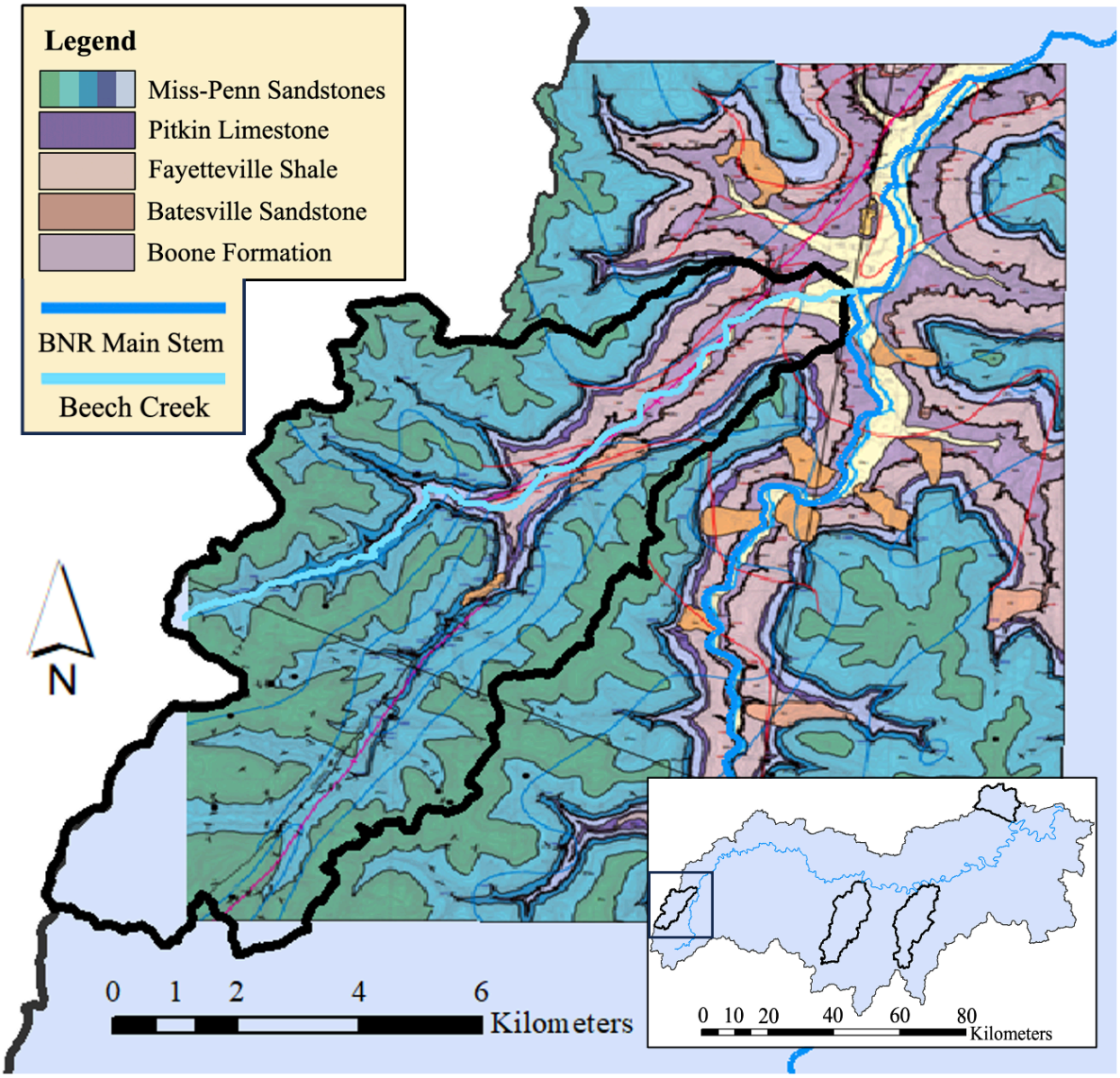

Appendix A.2: Satellite imagery of the Beech Creek confluence area and sampled gravel bars. Beech Creek flows West to East into the BNR main stem, which is flowing South to North in the eastern portion of this map. Each approximate gravel bar area is denoted in the table. **Bar A**: Beech Creek gravel bar 1; **Bar B**: Beech Creek gravel bar 2; **Bar C**: BNR main stem bar just upstream of the Beech Creek confluence; **Bar D**: BNR main stem bar just downstream of the Beech Creek confluence. Gravel bar provenance data is contained in Appendix A.4-7. Satellite imagery from Google Earth Pro (v. 7.3.6.9345), July 10, 2022 (Google Earth, 2023).

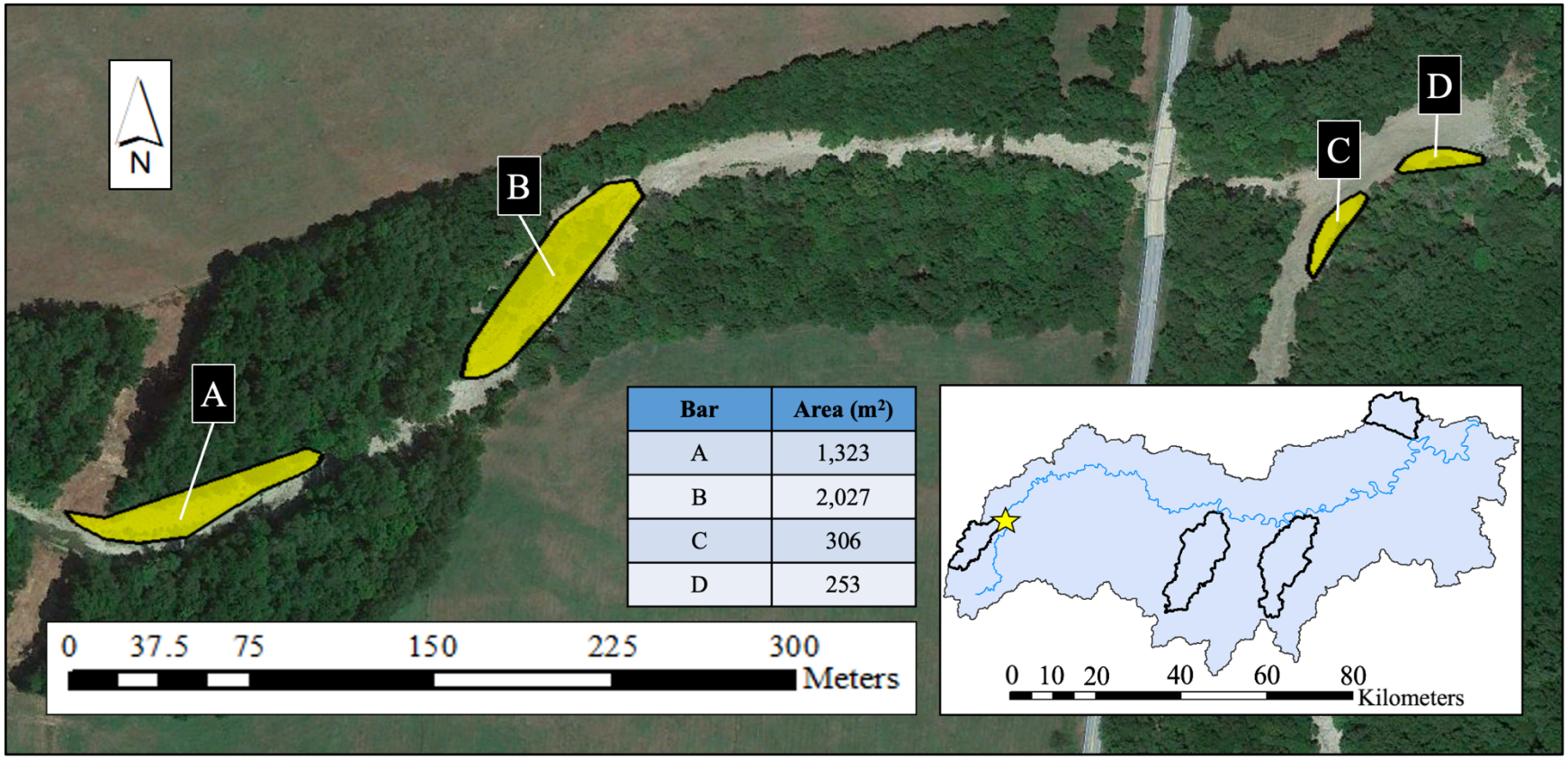

Bar	Area (m²)
A	1,323
B	2,027
C	306
D	253

Appendix A.3: Field images from each gravel bar in Appendix A.2. Arrows in each image denote flow direction. **Image A**: Looking downstream on Beech Creek gravel bar 1 (Appendix A.2: Bar A). Bucket in the bottom left corner for scale. Image date: 5/30/2022. **Image B**: Looking upstream on Beech Creek gravel bar 2 (Appendix A.2: Bar B). People for scale. Image date: 6/1/2022. **Image C**: Looking downstream from the BNR bar upstream of the Beech confluence (Appendix A.2: Bar C). Rock hammer for scale. Image date: 7/18/2022. **Image D**: Looking upstream from the BNR bar downstream of the Beech confluence (Appendix A.2: Bar D). James for scale. Image date: 7/26/2022.

Appendix A.4: Beech Creek bar 1 provenance data (Bar A in Appendix A.2). These 60 samples were analyzed on the upper, middle, and lower portions of the bar, respectively. *Miss-Penn* meaning *Mississippian-Pennsylvanian*; *Ss* meaning *sandstone*; *Ls* meaning *limestone*. While not included in these data, small (1-5 cm) shales were present in the gravel bar.

Beech Creek Bar 1: Upper Bar Provenance

#	Size (cm)	Size (mm)	Lithology/Unit
1	16.6	166	Batesville
2	3.1	31	Miss-Penn Chert
3	4.2	42	Miss-Penn Ss
4	3.5	35	Miss-Penn Ss
5	5.4	54	Batesville Ss
6	5.3	53	Batesville Ss
7	5.1	51	Batesville Ss
8	7.3	73	Batesville Ss
9	3.6	36	Bloyd Ss
10	3.5	35	Ordovician Ss
11	7	70	Batesville Ss
12	2.5	25	Miss-Penn Ss
13	6.4	64	Batesville Ss
14	5.6	56	Bloyd Ss
15	5.9	59	Miss-Penn Chert
16	3.8	38	Limestone
17	7.4	74	Batesville Ss
18	5	50	Batesville Ss
19	1.8	18	Miss-Penn Ss
20	4.7	47	Batesville Ss

Beech Creek Bar 1: Middle Bar Provenance

#	Size (cm)	Size (mm)	Lithology/Unit
1	11	110	Batesville Ss
2	6.9	69	Bloyd Ss
3	4.3	43	Miss-Penn Chert
4	9.5	95	Batesville Ss
5	15.8	158	Batesville Ss
6	5.2	52	Batesville Ss
7	8	80	Batesville Ss
8	3	30	Batesville Ss
9	7.7	77	Batesville Ss
10	6.2	62	Miss-Penn Chert
11	4.6	46	Miss-Penn Chert
12	2.8	28	Miss-Penn Chert
13	8.5	85	Batesville Ss
14	2	20	Batesville Ss
15	5.2	52	Miss-Penn Ss
16	3.3	33	Miss-Penn Ss
17	3.9	39	Batesville Ss
18	2.9	29	Batesville Ss
19	4.7	47	Miss-Penn Chert
20	2.3	23	Miss-Penn Ss

Beech Creek Bar 1: Lower Bar Provenance

#	Size (cm)	Size (mm)	Lithology/Unit
1	4.8	48	Miss-Penn Ss
2	3.6	36	Ls
3	8.8	88	Shale (dark)
4	4.2	42	Miss-Penn Ss
5	3.7	37	Ls
6	3.3	33	Bloyd Ss
7	4.6	46	Bloyd Ss
8	4.6	46	Miss-Penn Ss
9	4	40	Miss-Penn Ss
10	5.9	59	Ls
11	7.9	79	Batesville Ss
12	1.8	18	Ls (dark colored)
13	4.4	44	Batesville Ss
14	4.6	46	Miss-Penn Chert
15	3	30	Batesville Ss
16	6.3	63	Ls
17	3.9	39	Miss-Penn Ss
18	3.9	39	Batesville Ss
19	6.2	62	Miss-Penn Chert
20	5.1	51	Miss-Penn Chert

Appendix A.5: Beech Creek bar 2 provenance data (Bar B in Appendix A.2). These 60 samples were analyzed on the upper, middle, and lower portions of the bar, respectively. *Miss-Penn* meaning *Mississippian-Pennsylvanian*; *Ss* meaning *sandstone*; *Ls* meaning *limestone*; *bv* meaning *Batesville Sandstone*. While not included in these data, small (1-5 cm) shales were present in the gravel bar.

Beech Creek Bar 2: Upper Bar Provenance

#	Size (cm)	Size (mm)	Lithology/Unit	Notes
1	4.5	45	Bloyd Ss	
2	13.3	133	Batesville Ss	
3	4.6	46	Batesville Ss	
4	4	40	Miss-Penn Ss	dark
5	4.3	43	Batesville Ss	
6	5.1	51	Miss-Penn Chert	
7	4.5	45	Miss-Penn Chert	
8	1.6	16	Bloyd Ss	
9	3.5	35	Miss-Penn Ss	
10	3.1	31	Miss-Penn Ss	
11	5	50	Batesville Ss	
12	3.9	39	Ls	
13	3.9	39	Miss-Penn Ss	large-grained bv possible
14	3.5	35	Miss-Penn Chert	
15	2.6	26	Miss-Penn Ss	
16	2.4	24	Miss-Penn Ss	
17	3.4	34	Miss-Penn Ss	
18	4.4	44	Miss-Penn Ss	
19	4.2	42	Batesville Ss	
20	6.3	63	Miss-Penn Ss	potentially bv, large grains, clean

Beech Creek Bar 2: Middle Bar Provenance

#	Size (cm)	Size (mm)	Lithology/Unit	Notes
1	3.9	39	Ls	
2	4.2	42	Miss-Penn Chert	
3	4.7	47	Miss-Penn Shale	
4	5.9	59	Miss-Penn Ss	
5	5.6	56	Miss-Penn Shale	
6	4.1	41	Batesville Ss	
7	5.1	51	Bloyd Ss	
8	6.2	62	Miss-Penn Ss	
9	8.9	89	Miss-Penn Ss	
10	3	30	Miss-Penn Chert	
11	14.1	141	Miss-Penn Ss	Fine-grained
12	5.6	56	Miss-Penn Ss	
13	4.5	45	Miss-Penn Ss	
14	5.6	56	Ls	dark
15	2.6	26	Ls	
16	3	30	Miss-Penn Ss	Potentially Batesville
17	6.8	68	Miss-Penn Ss	dark, poor sorted, angular, iron banding, iron-rich
18	3.2	32	Miss-Penn Shale	
19	4	40	Miss-Penn Ss	
20	9.4	94	Calcite	quartz vein, geode, black chert surrounding euhedral crystals

Beech Creek Bar 2: Lower Bar Provenance

#	Size (cm)	Size (mm)	Lithology/Unit	Notes
1	5.7	57	Miss-Penn Chert	
2	10.5	105	Batesville Ss	slightly larger grain than typical Batesville, well sorted, iron banding, oxidized grains throughout
3	6.6	66	Batesville Ss	Iron-rich
4	2.7	27	Miss-Penn Ss	well sorted, looks b before broken, 90% quartz 10% oxides
5	5.1	51	Miss-Penn Chert	
6	5.2	52	Miss-Penn Chert	
7	4.8	48	Miss-Penn Ss	bv possible, decently sorted
8	2.1	21	Shale	dark
9	3.5	35	Ls	
10	4	40	Batesville Ss	oxidation in some grains
11	2.8	28	Ls	
12	5.4	54	Miss-Penn Shale	large grains, muscovite
13	6.9	69	Miss-Penn Shale	dark, almost siltstone
14	1.4	14	Miss-Penn Shale	dark, almost siltstone
15	2.2	22	Miss-Penn Shale	dark, almost siltstone
16	3.6	36	Batesville Ss	blue inside
17	3.4	34	Miss-Penn Chert	dark (grey)
18	4.9	49	Miss-Penn Chert	
19	3.9	39	Miss-Penn Ss	95% quartz, well sorted, subrounded
20	5.7	57	Miss-Penn Ss	

Appendix A.6: Main stem of the BNR just upstream of the Beech Creek confluence provenance data (Bar C in Appendix A.2). These 60 samples were analyzed on the upper, middle, and lower portions of the bar, respectively. *Miss-Penn* meaning *Mississippian-Pennsylvanian*; *Ss* meaning *sandstone*; *Ls* meaning *limestone*.

Main Stem Bar Upstream of Beech Confluence: Upper Bar Provenance

#	Size (cm)	Size (mm)	Lithology/Unit	Notes	Sample?
1	4.3	43	Miss-Penn Ss	dark, coarse	
2	10.1	101	Batesville Ss	mostly quartz	
3	4.5	45	Miss-Penn Ss		
4	3.1	31	Batesville Ss		
5	5.3	53	Ls	white/light grey, Boone	
6	4.4	44	Bloyd/Miss-Penn Ss	reddish	
7	6.3	63	Miss-Penn Ss		
8	3.1	31	Ls	dark, grey with quartz clasts	#10-1
9	1.7	17	Ls	white	
10	5.2	52	Batesville Ss		
11	2.9	29	Miss-Penn Ss	iron included	
12	9.7	97	Miss-Penn Ss	dark colored, similar to black Ls	#10-2
13	9	90	Ls	white	
14	3.7	37	Miss-Penn Ss	very fine grained	
15	6.4	64	Batesville Ss		
16	6	60	Miss-Penn Ss	0.5-1mm quartz module grains	
17	4.8	48	Miss-Penn Ss	dark	#10-3 *may also be labeled as #10-2
18	12	120	Miss-Penn Ss	coarse grained, tan, dark on weathered & fresh facies	
19	3.9	39	Miss-Penn Ss	same as #17 (#10-3)	
20	4.7	47	Ss	dark, Fe-rich Ss	

Main Stem Bar Upstream of Beech Confluence: Middle Bar Provenance

#	Size (cm)	Size (mm)	Lithology/Unit	Notes	Sample?
1	5.9	59	Batesville Ss	very fine, tan Ss	#11-1
2	7.1	71	Ss	medium coarse, greyish tan	
3	9.3	93	Ls	white	
4	9.7	97	Shale	dark, not well-defined grains	
5	7.4	74	Ss	very red colored	#11-2
6	8.3	83	Ss	tan	
7	5.9	59	Miss-Penn Ss	tan-dark colored, fine grains	#11-3
8	4	40	Ss	reddish	
9	4.2	42	Ss	fine & coarse grains, red	
10	5.6	56	Batesville Ss	coarse grained	
11	7.7	77	Ss	grey	
12	4	40	Batesville Ss	fine-grained siltstone? Shale?	#11-4
13	4.4	44	Ss	dark on fresh, white on weathered	
14	6.4	64	Miss-Penn Ss	iron nodule	#11-5
15	4.8	48	Ss	brown, dirty	
16	4.2	42	Ss	orange/brown, dirty Ss, sandy	
17	7.2	72	chert	white	
18	4.5	45	Ls	grey	
19	5.7	57	Ss	dark colored on fresh & weathered	
20	6.1	61	Ss	tan w/ Fe nodule	

Main Stem Bar Upstream of Beech Confluence: Lower Bar Provenance

#	Size (cm)	Size (mm)	Lithology/Unit	Notes	Sample?
1	3.5	35	Batesville Ss		
2	7	70	Ss	coarse Ss, friable, Bloyd w/ burrow-like features	
3	6.5	65	Ss	reddish, fine grained Ss	
4	5.3	53	Bloyd Ss		#12-1
5	4.9	49	Miss-Penn Ss	dark, grains	#12-2
6	9.9	99	Miss-Penn Ss	Batesville? Light tan, weathered	
7	4.7	47	Ss	tan Ss w/ large Fe nodule	
8	10.7	107	cherty Ls		
9	4.7	47	Ss	dark & dirty	
10	7.2	72	Ls	dark	#12-3
11	5.4	54	Ss	light tan Ss	#12-4
12	4	40	Batesville Ss		
13	7.8	78	Ss	fine grained Ss - Fe band	
14	3.2	32	Middle Bloyd Ss		#12-5
15	4.2	42	Ss	medium grained, light tan Ss	
16	3.3	33	Ss	reddish brown, fine grained	
17	9.8	98	Batesville Ss		
18	3.3	33	Ls	fine grained & dark Ls, different	
19	2.5	25	Batesville Ss		#12-6
20	5	50	Batesville Ss	clean	

Appendix A.7: Main stem of the BNR just downstream of the Beech Creek confluence provenance data (Bar D in Appendix A.2). These 40 samples were analyzed on the upper and lower portions of the bar, respectively. *Miss-Penn* meaning *Mississippian-Pennsylvanian*; *Ss* meaning *sandstone*; *Ls* meaning *limestone*.

Main Stem Bar Downstream of Beech Confluence: Upper Bar Provenance

#	Size (cm)	Size (mm)	Lithology/Unit	Notes	Sample?
1	5.4	54	Limestone	fine grain, white to light grey	
2	4.8	48	Miss-Penn Ss	shiny, tan to brown, subrounded, fine grain, iron rich	
3	3.6	36	Chert	white in and out, gritty, fine grained, broken down	B1-1
4	2	20	Boone Ls (fossiliferous)	light grey in white out, fossil, reacts with HCl as well	
5	3.6	36	Limestone	fossiliferous, fibrous matrix, white to tan in and out	
6	3	30	Shale	very fine grain, dark grey	B1-2
7	1.5	15	Chert	black out in	
8	2.2	22	Chert	white out, white in	
9	2.5	25	Miss-Penn Ss	sandy, tan to brown, not well sorted, medium grains	
10	2.2	22	Miss-Penn Ss	fine grain, brown, well sorted	
11	4.1	41	Cherty Limestone	white out and in, grainy, effervesces with HCl, same outside & inside as B1-1 (minus the cherty part)	
12	2.9	29	Miss-Penn Ss	orangish brown due to iron	B1-3
13	4.2	42	Limestone (Boone)	fossiliferous, white to light grey, no grains	
14	3	30	limestone	dirty white, orange and black, fibrous matrix	
15	2.9	29	Boone Ls	white to tan out, white-light grey in, no grains	
16	1.1	11	Chert	white	
17	2.8	28	Miss-Penn Ss	orange to brown color, fine-medium grains	
18	3.3	33	Cherty Limestone (Boone)	some grain sections, some not, white-light grey in	
19	3	30	Miss-Penn Ss (Bloyd)	dark color (orange-brown), quartz grains, iron rich	
20	2.4	24	Chert	white	

Main Stem Bar Downstream of Beech Confluence: Lower Bar Provenance

#	Size (cm)	Size (mm)	Lithology/unit	Notes	Sample?
1	8.3	83	Miss-Penn Ss	brown color, fine grained	
2	4.9	49	Batesville Ss	tan, fine grain	
3	6.4	64	Miss-Penn Ss	iron rich, brown-purple, quartz rich	B2-1
4	5.4	54	Miss-Penn Ss	iron stained, large quartz grain, poorly sorted	
5	2.9	29	Miss-Penn Ss	dark grey out, green in, sub-angular grains	B2-2
6	7	70	Miss-Penn Ss	brown with greenish tint, poorly sorted	
7	3.1	31	Chert	white	
8	4.9	49	Batesville Ss	Dirty, tan-light brown, shiny, well-sorted, subangular	
9	2.6	26	Cherty Ls	very fine grain, white out and in	
10	3.8	38	Batesville Ss	Dirty, tan with iron band	
11	5.7	57	Miss-Penn Ss	dark, dark grey, very fine grain (same as 11-4)	B2-3
12	3	30	Miss-Penn Ss	dark grey with green tint (dark grey on out and in), very fine grained, no reaction with HCl	
13	3.7	37	Limestone (Boone)	white to light grey, large calcite crystals	
14	2.9	29	Miss-Penn Ss	brown with green tint, poorly sorted	
15	5.3	53	Miss-Penn Ss	sandy, large grains, tan color, subangular	
16	2.5	25	Miss-Penn Ss	dark grey to purplish-grey, fine grained	
17	4	40	Miss-Penn Ss	tan-grey with greenish tint, medium grains	
18	2.3	23	Boone Ls	classic medium-grey outside & inside	
19	2.7	27	Miss-Penn Ss		
20	5.2	52	Batesville Ss	brown fine-grained	

APPENDIX B:

Cave Creek

Appendix B.1: Geologic map of the Cave Creek tributary basin and surrounding area. Geologic map overlays acquired from Braden and Smith (2004a, 2004b) & Chandler and Ausbrooks (2015a, 2015b).

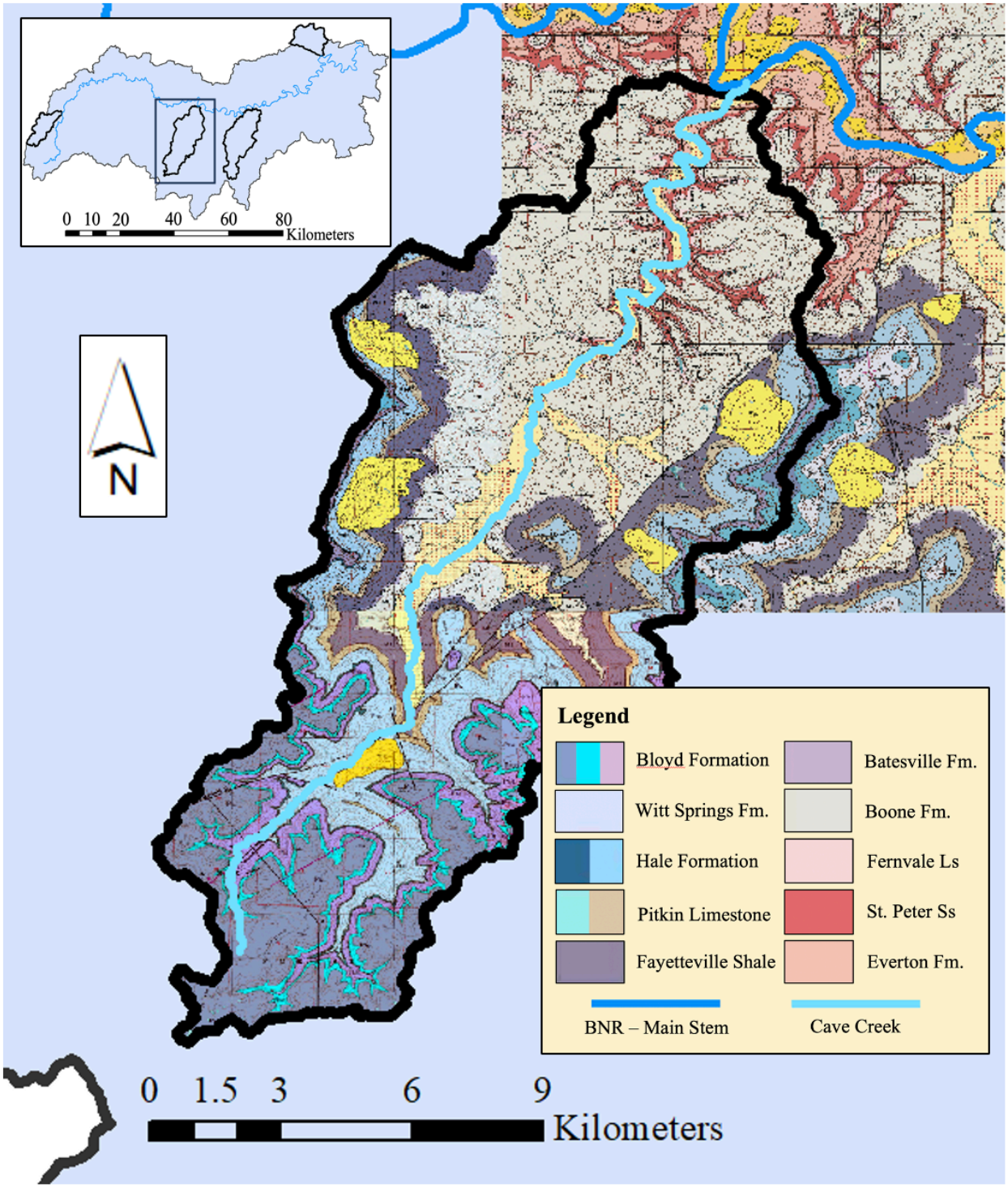

Appendix B.2: Satellite imagery of the Cave Creek confluence area and sampled gravel bars. Cave Creek flows South to North into the BNR main stem, which is flowing West to East in the image. Each approximate gravel bar area is denoted in the table. **Bar A**: BNR main stem bar just upstream of the Cave Creek confluence; **Bar B**: Cave Creek gravel bar; **Bar C**: BNR main stem bar just downstream of the Cave Creek confluence. Gravel bar provenance data is contained in Appendix B.4-6. Satellite imagery from Google Earth Pro (v. 7.3.6.9345), July 10, 2022 (Google Earth, 2023).

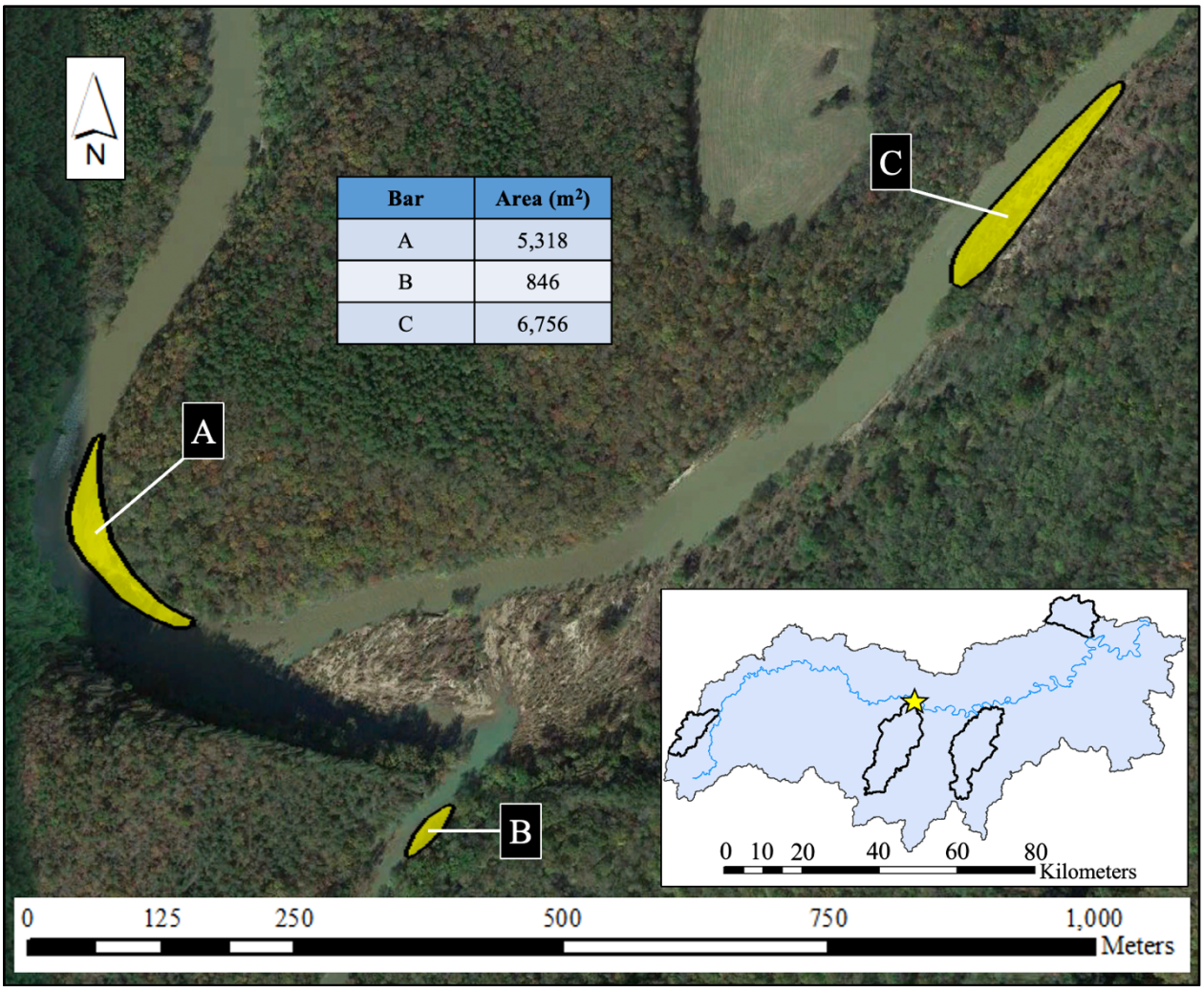

Appendix B.3: Field images from each gravel bar in Appendix B.2. Arrows in each image denote flow direction. **Image A**: Looking downstream on the BNR bar upstream of the Cave confluence (Appendix B.2: Bar A). James and his kayak for scale. Image date: 6/26/2022. **Image B**: Looking downstream on the Cave Creek gravel bar (Appendix B.2: Bar B). James for scale. Image date: 6/26/2022. **Image C**: Looking downstream from the BNR bar downstream of the Beech confluence (Appendix B.2: Bar C). James for scale. Image date: 7/24/2022.

Appendix B.4: Main stem of the BNR just upstream of the Cave Creek confluence provenance data (Bar A in Appendix B.2). These 60 samples were analyzed on the upper, middle, and lower portions of the bar, respectively. *Miss-Penn* meaning *Mississippian-Pennsylvanian*; *Ss* meaning *sandstone*; *Ls* meaning *limestone*; *Dolo* meaning *dolostone*; *Ord.* meaning *Ordovician.*

Main Stem Bar Upstream of Cave Confluence: Upper Bar Provenance

#	Size (cm)	Size (mm)	Lithology/Unit	Notes	Sample?
1	5.2	52	Ls/Dolo	fossiliferous, white out & in, gritty, no HCl reaction	
2	2.8	28	Miss-Penn Ss	Sandy, brown color, not well sorted	
3	4.8	48	Ls	light grey in, white out, fossiliferous	
4	4.5	45	Batesville Ss	tan color	
5	2.2	22	Chert	white, Fe-rich (Fe nodule present)	
6	4.4	44	Ls/Dolo	smooth, white in & out, no reaction with HCl	#25-1
7	7.7	77	Ls	shiny, white in & out (w/ some tan in), same as #25-1, effervesces with HCl	
8	3.8	38	Ss	dark Ss, sub-angular, coarse grained	
9	4.9	49	Chert	Light grey in	
10	4.3	43	Ls/Dolo	white, gritty, fossiliferous	#25-2
11	2.8	28	Ss	tan & red in, very fine grained	
12	4	40	Ls/Dolo	light grey, chert nodules, no HCl reaction	
13	3.4	34	Ls/Dolo	white out & in, no reaction with HCl	#25-3
14	4.8	48	Ss	Fe-rich, dark color, multiple Fe nodules	
15	4	40	Miss-Penn Ss	coarse grained, tan/brown in, all qtz, sub-rounded	#25-4
16	3.5	35	Chert	medium grey	
17	3.4	34	Ls/Dolo	white/tan out, white in	
18	4.1	41	Ls/Dolo	White out & in	#25-5
19	3.5	35	Ls/Dolo	Big shale inclusion, fossil, light grey Ls?	#25-6
20	2.5	25	Miss-Penn Ss	Poorly sorted, Fe-rich, subangular, Bloyd look	

Main Stem Bar Upstream of Cave Confluence: Middle Bar Provenance

#	Size (cm)	Size (mm)	Lithology/unit	Notes	Sample?
1	6.7	67	Batesville Ss	Brown to tan, sub-rounded, shiny	
2	3.1	31	Ord. Ss	brown to black, fine grained, clean	#26-1
3	6.8	68	Ls	fossiliferous, effervesces with HCl, white/black in, gritty	
4	4.5	45	Everton Ss	tan outer, tan/yellow in, sandy	
5	4.9	49	Ls/Dolo	very fossilized, white, does not react with HCl	
6	3.7	37	Ls/Dolo	light grey in, white out, no reaction with HCl	
7	3	30	Miss-Penn Ss	all quartz, dirty, well-sorted, sub-rounded, pink & tan tint, white out, tan in, coarse-grained	#26-2
8	3.6	36	Ss	dark grey out, black in, fine grained	#26-3
9	2.4	24	Batesville Ss		
10	2.7	27	Chert	black	
11	3.3	33	Cherty Ls	white out, light grey in	
12	5	50	Ls/Dolo	white, gritty, no reaction with HCl, very fine-grained	
13	5.1	51	Ord. Ss	tan out, light grey & tan in	
14	3	30	Chert	light grey	
15	3.9	39	Ls	tan out, white in, flakey & gritty, fine-grained	
16	3.1	31	Batesville Ss	very fine grained, brown to grey color	
17	3.1	31	Miss-Penn Ss	poorly sorted, all quartz	
18	6.5	65	Ls	white out, light grey in, looks like Boone	
19	2.9	29	Ls	white	
20	3.2	32	Cherty Ls	fossiliferous	#26-4

Main Stem Bar Upstream of Cave Confluence: Lower Bar Provenance

#	Size (cm)	Size (mm)	Lithology/Unit	Notes	Sample?
1	5.3	53	Ls	light grey, slightly effervesces with HCl	
2	4.5	45	Miss-Penn Ss	conglomerate-type matrix, poorly sorted	
3	3	30	Boone Ls	classic medium grey out & in	
4	2.5	25	Chert	black	
5	4.7	47	Miss-Penn Ss	brown/tan out & in, sub-rounded, coarse-grained, sandy	#27-1
6	6	60	Ls/Dolo	white/peach Ls	
7	2.3	23	Chert	white to light grey in	
8	2.2	22	Ls	Black Ls, grains	
9	3.2	32	Ord. Ss	Brown color, medium-grained	#27-2
10	4.5	45	Ord. Ss	Same as #27-2, large quartz grains in few spots	
11	4.4	44	Ls	light grey/white in, Fernvale?	#27-3
12	4	40	Ls	White Ls with Fe	
13	5.6	56	Batesville Ss	brown to tan in, quartz grains, dirty, variable sizes in different bands	
14	3.2	32	Ss	dark grey to black in/out, coarse grains	#27-4
15	3.2	32	Cherty Ls	tan out, white in	
16	3.5	35	Ls	dark grey out/in	
17	4.7	47	Ls	fossil, tan/white out & in	#27-5
18	3.5	35	Ss	very fine grained, dark grey out, brown in	#27-6
19	3.5	35	Chert	medium grey	
20	2.9	29	Ls	white out & in, gritty	

Appendix B.5: Cave Creek bar provenance data (Bar B in Appendix B.2). These 60 samples were grouped into two groups due to sample collection bag issues: upper and middle provenance data (40 samples), and lower bar provenance data (20 samples). *Miss-Penn* meaning *Mississippian-Pennsylvanian*; *Ss* meaning *sandstone*; *Ls* meaning *limestone*; *Dolo* meaning *dolostone*; *Ord.* meaning *Ordovician.*

Cave Creek Bar: Upper and Middle Bar Provenance

#	Size (cm)	Size (mm)	Lithology/Unit	Notes	Sample?
1	8.7	87	Ss	Lineations, brown, fine grained	CV1-1
2	6.2	62	Miss-Penn Ss (Bloyd?)	Brown to Purple-Red, Medium grain, Sub Angular, lots of cavities	CV1-2
3	7.6	76	Ord. Ss	sandy, light brown/tan, fine-grained	
4	10.7	107	Ord. Ss	sandy, white-brown-tan, sugary, Everton	
5	5.5	55	Batesville Ss	brown, fine grained, same as CV 1-1, lineations	
6	5.3	53	Ord. Ss	sugary, tan, sub-rounded, fine to medium, frosty	
7	4.2	42	Ls	tan to white inside, gritty, fine grained	
8	4.5	45	Ls/Dolo	white, gritty, no reaction with HCl	
9	4.6	46	Cherty Ls	chert nodule present	CV1-3
10	5.4	54	Chert	dark grey, conchoidal fracture	
11	5.3	53	Chert	dark grey, conchoidal fracture	
12	3.5	35	Chert	dark grey	
13	5.4	54	Ord. Ss	dirty, tan, subrounded	
14	4.8	48	Ss	black-purple, lineations	CV1-4
15	4.6	46	Ss	green tint to tan-brown color, Fe-rich, similar to CV-4, sub-rounded quartz grains, St. Peter Ss?	CV1-5
16	4.8	48	Ord. Ss	clean, tan-brown	
17	3.7	37	Ls	light grey-dark grey	
18	3.8	38	Ord. Ss	weathered, brown	
19	3.7	37	Chert	light grey	
20	4.2	42	Miss-Penn Ss	friable, coarse, sub-angular	

#	Size (cm)	Size (mm)	Lithology/Unit	Notes	Sample?
21	4.2	42	Ss	fine-grained, sub-angular, tan to brown, Batesville?	CV1-6
22	3.6	36	Ord. Ss	weathered, frosted	
23	4.8	48	Ord. Ss	iron bands, green tint, light-tan rock, coarse grains, sub-rounded, sparkles	CV1-7
24	8.2	82	Ss	Reddish-brown, shale nodule, fine to medium grains, rounded, similar to CV1-4 with more red/less layers	CV1-8
25	3.6	36	Ord. Ss		
26	4.2	42	Chert	dark-grey to black chert	
27	5.2	52	Ord. Ss	friable, tan, sub-rounded, medium grained	
28	3.5	35	Ord. Ss	very fine grains & medium grains, calcite cement	CV1-9
29	5.5	55	Everton Dolo	dark grey, lightly effervesces with HCl	
30	4.6	46	Ord. Ss	weathered, fine-grained, cavities, sub-rounded, tan	CV1-10
31	6	60	Ss	fine-grained, same as CV1-6 (should be Ord.)	CV1-11
32	4	40	Fernvale Ls	pink tint	CV1-12
33	4.8	48	Ls	light grey with green tint, gritty	CV1-13
34	3.8	38	Ord. Ss	friable, lots of cavities, weathered, medium grains, sub-rounded	
35	4.1	41	Chert	grey with quartz vein	
36	4.1	41	Ord. Ss	very weathered, friable	
37	5.1	51	Fernvale Ls	white-light grey, gritty	
38	4.9	49	Ord. Ss	tan-brown, sandy	
39	4.5	45	Miss-Penn Ss	large pebbles up to 6mm, sub-angular, coarse	
40	5.9	59	Ord. Ss	sandy, gravel, weathered, tan, sub-rounded, medium grained, dirty	

Cave Creek Bar: Lower Bar Provenance

#	Size (cm)	Size (mm)	Lithology/unit	Notes	Sample?
1	6.5	65	Batesville Ss		
2	5.4	54	Ss	brown, fine-grained, Batesville?	CV2-1
3	4.5	45	?	weathered bad, black colored, fine-grained	CV2-2
4	5.9	59	Ss	poor sorting, sub-angular to sub-rounded grains, grey, small shale, nodules	CV2-3
5	8.7	87	Ord. Ss	friable	
6	4.5	45	Ss	same as CV1-6, but with green shale nodule	CV2-4
7	4.7	47	Ss	lineations, cavities present (fossils), light tan, rounded grains, some shale perhaps	CV2-5
8	5.9	59	Ord. Ss	thin shale layers, fine grained, dark brown	CV2-6
9	7.3	73	Ord. Ss	tan-brown, medium grained, sub-rounded	
10	5	50	Ord. Ss	green tint, medium grains, sub-rounded, St. Peter Ss	
11	4.3	43	Ord. Ss	sandy, light tan, clean, frosted, Everton Ss	
12	5.4	54	Ord. Ss	medium grey, medium grains, sub-rounded	CV2-7
13	5	50	Batesville Ss	very fine graine, shale layers, tan	
14	5.4	54	Ord. Ss	same look as CV2-6, but shinier	CV2-8
15	4.4	44	Miss-Penn Ss	black-maroon, shiny, sub-angular, similar to a Buff bar sample from downstream of here	CV2-9
16	6	60	Ord. Ss	dirty, sandy, friable	
17	4.4	44	Ord. Ss	grey with green tint, medium grains, sub-rounded-rounded	
18	5.5	55	Chert	medium grey	
19	4	40	Ord. Ss		
20	5	50	Ord. Ss	grey	

Appendix B.6: Main stem of the BNR just downstream of the Cave Creek confluence provenance data (Bar C in Appendix B.2). These 60 samples were analyzed on the upper, middle, and lower portions of the bar, respectively. *Miss-Penn* meaning *Mississippian-Pennsylvanian*; *Ss* meaning *sandstone*; *Ls* meaning *limestone*; *Dolo* meaning *dolostone*; *Ord.* meaning *Ordovician.*

Main Stem Bar Downstream of Cave Confluence: Upper Bar Provenance

#	Size (cm)	Size (mm)	Lithology/Unit	Notes	Sample?
1	9.5	95	Ss	Fe-rich, brown in & out, quartz	#28-1
2	4.9	49	Batesville Ss	fine-grained, well-sorted, lineations	
3	4.6	46	Miss-Penn Ss	sub-angular, coarse-grained, brown	#28-2
4	9.5	95	Ss	sugary, tan color	#28-3
5	4.2	42	Cherty Ls	medium grey in, brown out	
6	5	50	Ss	red to purple in, fine-grained, well sorted, sub-rounded	#28-4
7	5.6	56	Everton Ss		
8	5.5	55	Everton Ss	Brown to tan, sandy, medium-grained	
9	6.5	65	Ss	Fe-rich, dark grey, fine-grained, sub-rounded	#28-5
10	7.1	71	Ls	light grey in, smooth-like	
11	4.3	43	Ls	white, gritty, fine-grained	
12	4.5	45	Ss	Fe strands alternating with tan bands, all quartz, sub-rounded	#28-6
13	3.8	38	Ls	light grey to tan in	
14	8.3	83	Ls	dark grey to black	
15	7.5	75	Ss	fine-grained, all quartz, sub-rounded	#28-7
16	6.5	65	Miss-Penn Ss	Brown-black, green-blue shale inclusion, sub-angular	#28-8
17	8.9	89	Ls/Dolo	tan in	#28-9
18	3.8	38	Ls	medium grey in, no grains, no reaction with HCl	
19	5	50	Everton Ss		
20	4.3	43	Ss	thin sheet-like pebble, dark out & in, similar to #27-4	#28-10

Main Stem Bar Downstream of Cave Confluence: Middle Bar Provenance

#	Size (cm)	Size (mm)	Lithology/unit	Notes	Sample?
1	4.6	46	Ls	white, gritty, fine-grained	#29-1
2	4.4	44	Ls	fossiliferous, tan color	
3	5.5	55	Ls	medium grey to dark grey, effervesces with HCl, no grains, tan outside	
4	3.5	35	Ls	white inside and out, fine-grained, peach tinge	#29-2
5	3.9	39	Ss	shiny brown, shiny quartz, medium grained, decently sorted	#29-3
6	1.7	17	Chert	white	
7	3.7	37	Ls/Dolo	medium gray in, no reaction with HCl	
8	3.6	36	Ls/Dolo	light grey	#29-4
9	3.1	31	Ls	brownish-tan, fossiliferous	
10	11	110	Everton Ss	sandy, tan, friable	
11	8.9	89	Ss	well-sorted, black band through middle	#29-5
12	3.5	35	Ls	white in/out, gritty, fine-grained	#29-6
13	3.5	35	Ls	fossiliferous, light gray to white, sharp	
14	4.2	42	Chert	medium gray	
15	4.3	43	Ss	Lineations, tan in brown out, fine grained	#29-7
16	5.8	58	Cherty Ls/Dolo	medium gray	#29-8
17	2.1	21	Ss	brown, very fine-grained	#29-9
18	8.7	87	Miss-Penn Ss	tan to grey, shiny, poorly sorted	
19	11.5	115	Boone Ls	light to medium grey in & out	
20	2.1	21	Bloyd Ss	Bloyd-looking, angular grains	

Main Stem Bar Downstream of Cave Confluence: Lower Bar Provenance

#	Size (cm)	Size (mm)	Lithology/Unit	Notes	Sample?
1	3	30	Chert	Smooth, white	
2	4.4	44	Everton Ss		
3	5	50	Miss-Penn Ss	brownish-gray, medium sorted, dirty	
4	4.1	41	Miss-Penn Ss	very green tint to it, medium gray in, sub-angular	
5	2.9	29	Ls	gritty, white w/ red out, no reaction with HCl	#30-1
6	4.9	49	Chert	white in & out	
7	3.8	38	Chert	light to dark gray in & out	
8	5.6	56	Ss	shale interbeds within, brownish color	#30-2
9	2.9	29	Cherty Ls	white	#30-3
10	4.8	48	Everton Ss		
11	7.3	73	Everton Ss	dirty Fe localities	
12	4.1	41	Miss-Penn Ss	fossiliferous, Fe, black, poorly sorted	
13	3.3	33	Ss	maroon in & out, very fine grained	#30-4
14	6.2	62	Ss	yellow/tan in	#30-5
15	5.6	56	Miss-Penn Ss	coarse-grained, purple to black, all quartz, well-sorted	#30-6
16	3	30	Ls/Dolo	light gray in, smooth	#30-7
17	3.7	37	Ss	tan color, fine grained, well-sorted	#30-8
18	6.5	65	Ss	tannish-brown w/ green tint, sub-angular	#30-9
19	5.2	52	Ss	same as previous (#30-9)	
20	6.1	61	Everton Ss		

APPENDIX C:

Calf Creek

Appendix C.1: Geologic map of the Calf Creek tributary basin and surrounding area. Geologic map overlays acquired from Smith and Hutton (2007) & Chandler and Ausbrooks (2015a, 2015c).

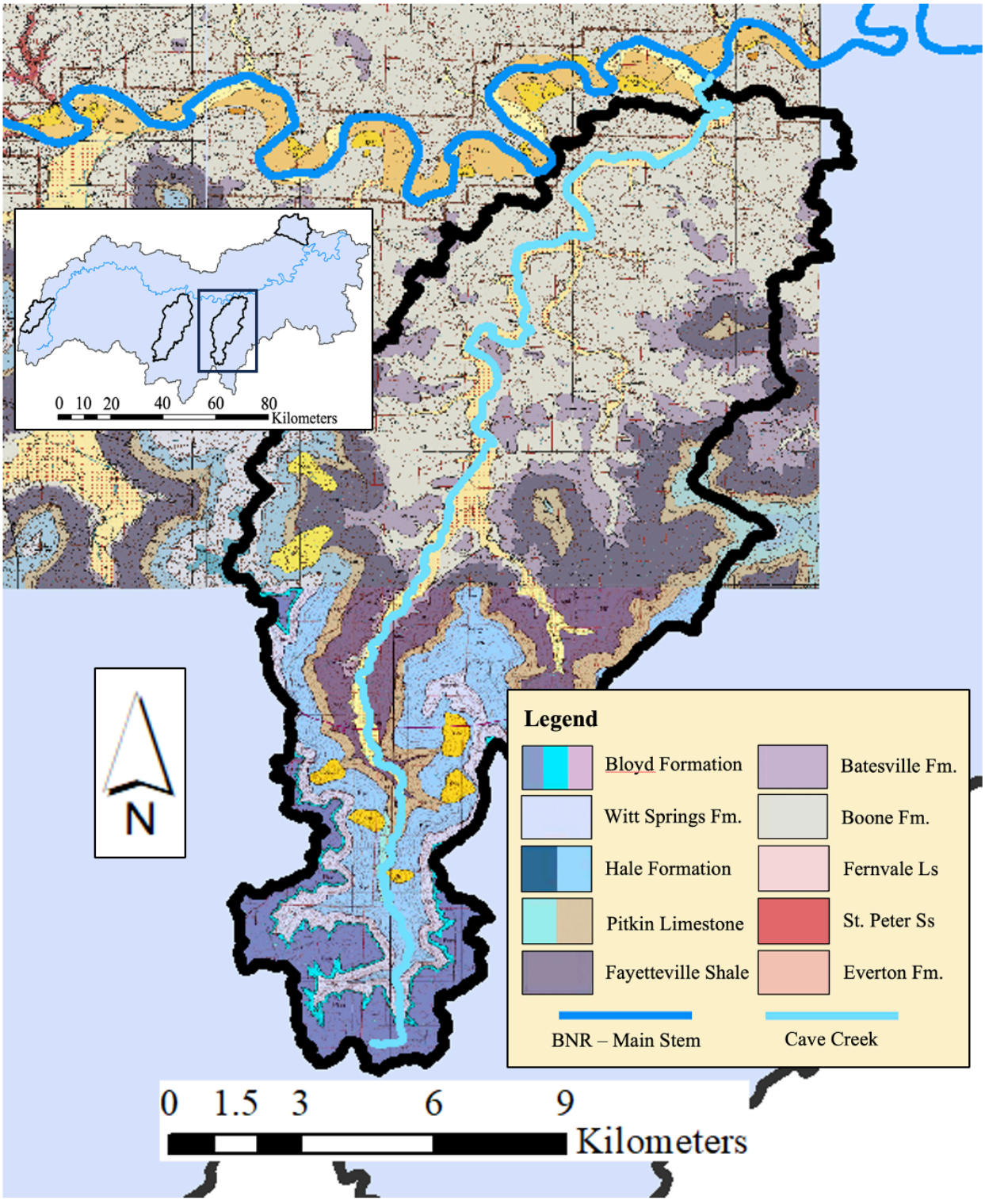

Appendix C.2: Satellite imagery of the Calf Creek confluence area and sampled gravel bars. Calf Creek flows South to North into the BNR main stem, which is flowing West to East in the image. Each approximate gravel bar area is denoted in the table. **Bar A**: BNR main stem bar just upstream of the Calf Creek confluence; **Bar B**: Calf Creek gravel bar; **Bar C**: BNR main stem bar just downstream of the Calf Creek confluence. The most upstream portion of this gravel bar was omitted from provenance analyses, as it is too close to the confluence to likely be influenced by Calf Creek inputs. Gravel bar provenance data is contained in Appendix C.4-6. Satellite imagery from Google Earth Pro (v. 7.3.6.9345), January 4, 2023 (Google Earth, 2023).

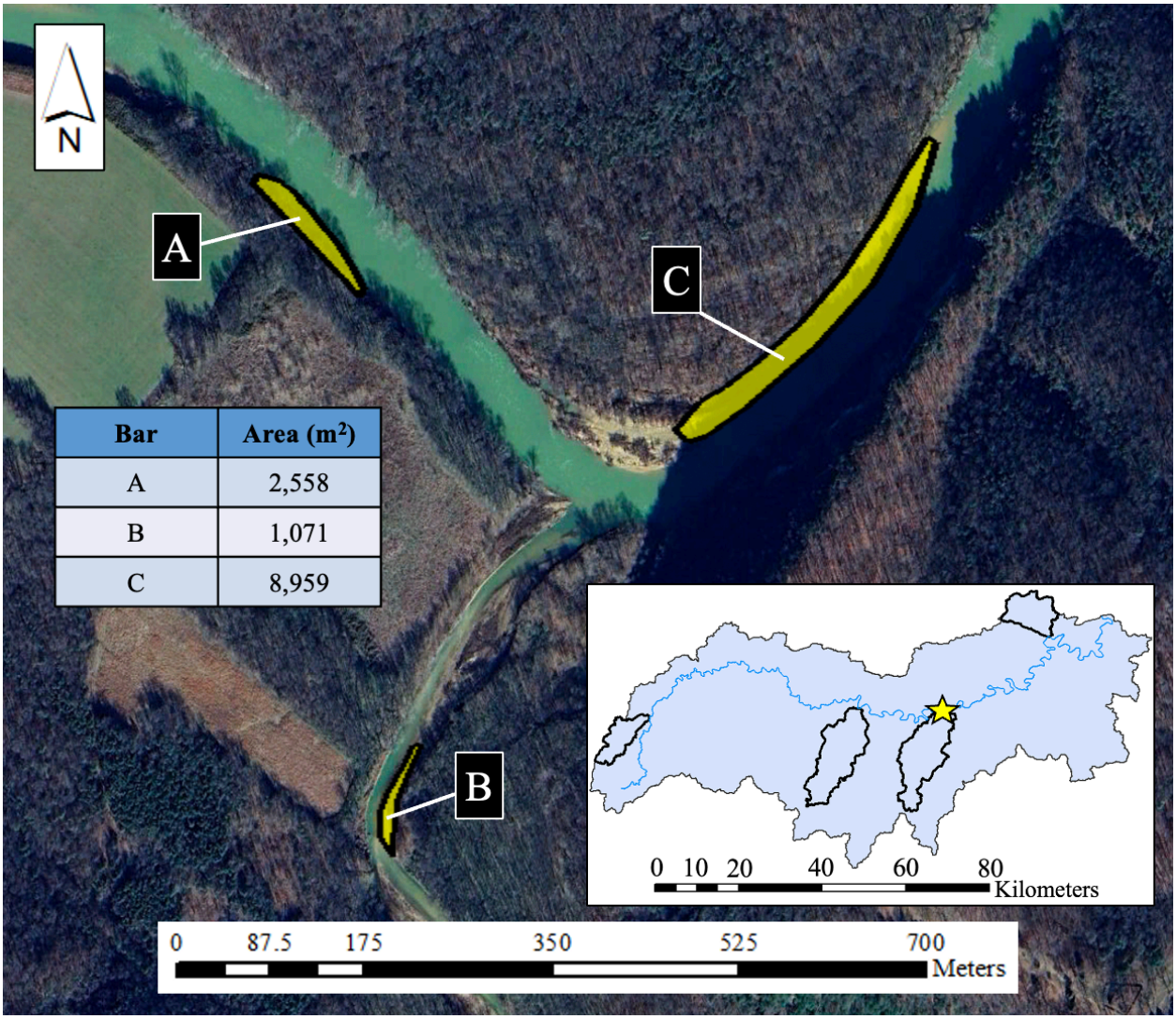

Appendix C.3: Field images from each gravel bar in Appendix C.2. Arrows in each image denote flow direction. All images were captured on 7/17/2022. **Image A**: Looking downstream on the BNR bar upstream of the Calf confluence (Appendix C.2: Bar A). Kayaks for scale. **Image B**: Looking downstream on the Calf Creek gravel bar (Appendix C.2: Bar B). **Image C**: Looking roughly upstream from the large BNR bar downstream of the Calf confluence (Appendix C.2: Bar C). Field equipment for scale.

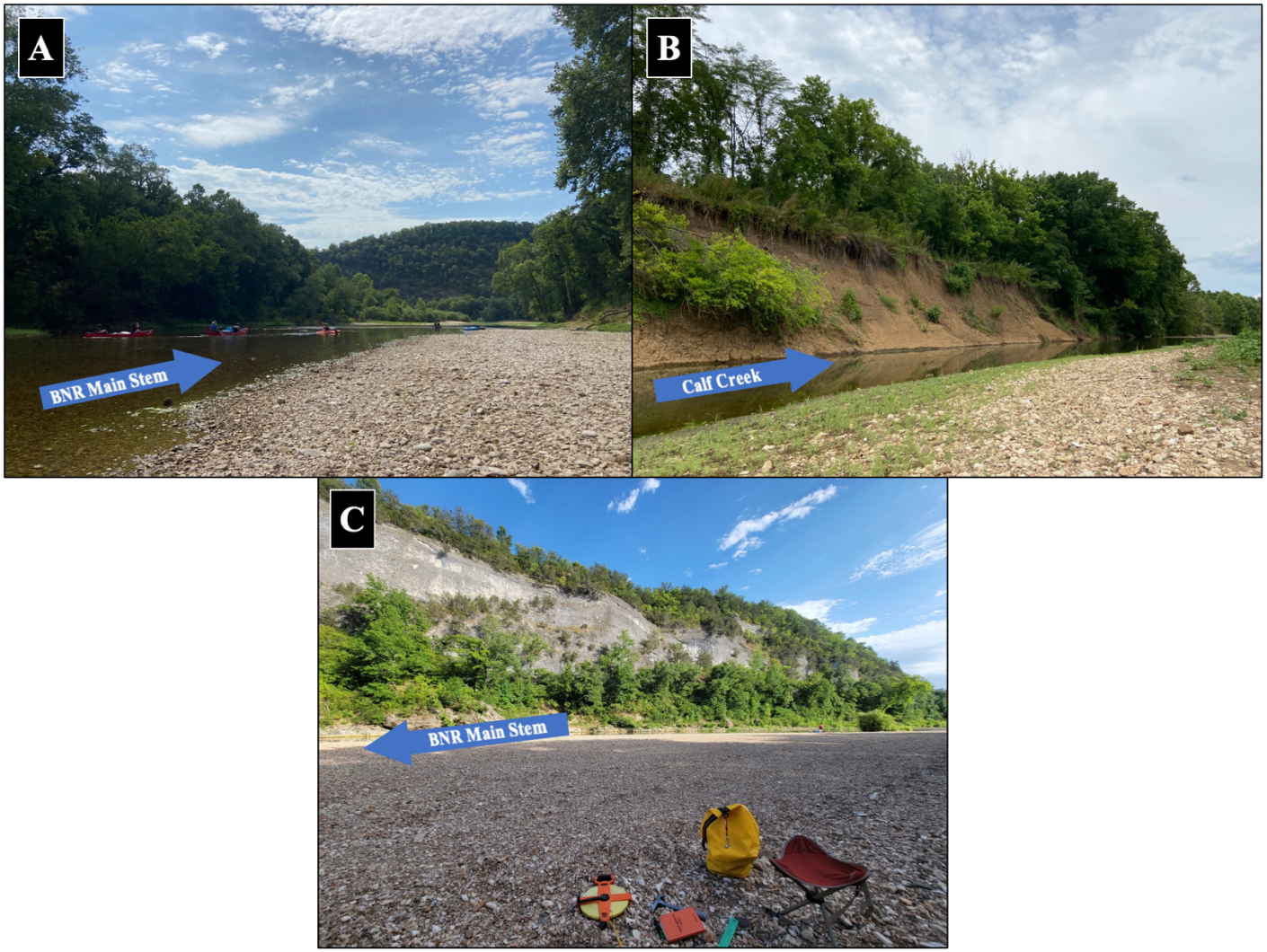

Appendix C.4: Main stem of the BNR just upstream of the Calf Creek confluence provenance data (Bar A in Appendix C.2). These 60 samples were analyzed on the upper, middle, and lower portions of the bar, respectively. *Miss-Penn* meaning *Mississippian-Pennsylvanian*; *Ss* meaning *sandstone*; *Ls* meaning *limestone*.

Main Stem Bar Upstream of Calf Confluence: Upper Bar Provenance

#	Size (cm)	Size (mm)	Lithology/Unit	Notes	Sample?
1	8.3	83	Miss-Penn Ss	Batesville Ss, white on fresh facies, super sugary	
2	10.7	107	Miss-Penn Ss	Batesville Ss	
3	5.3	53	Limestone	Boone Ls, dark limestone	#3-1
4	2.5	25	Miss-Penn Ss		
5	7.2	72	Ordovician Ls		#3-2
6	4	40	Ordovician Ls		
7	3.7	37	Ordovician Ss	Everton Ss	
8	4.4	44	Miss-Penn Ss		
9	3.8	38	Chert		
10	4.5	45	Chert		
11	3.3	33	Miss-Penn Ss		
12	8.1	81	Ordovician Ls	white	
13	4.5	45	Limestone	white	#3-3
14	7.3	73	Ordovician Ss	Everton Ss	
15	5.2	52	Miss-Penn Ss		
16	3	30	Chert		
17	5.5	55	Miss-Penn Ss	Batesville Ss	
18	4.9	49	Ordovician Ss		
19	3.4	34	Chert		
20	3.5	35	Ordovician Ss		

Main Stem Bar Upstream of Calf Confluence: Middle Bar Provenance

#	Size (cm)	Size (mm)	Lithology/unit	Notes	Sample?
1	4.8	48	Miss-Penn Ss	Sugary (friable)	
2	5.2	52	Miss-Penn Ss	dark brown inside (fresh facies), grey outside	
3	6	60	Limestone		
4	5.7	57	Chert		
5	4.2	42	Limestone		
6	6.2	62	Ordovician Ss	Everton Ss	
7	4.1	41	Limestone	white	
8	3.8	38	Chert		
9	3	30	Chert		
10	4.5	45	Limestone	white	
11	3.8	38	Chert		
12	3.6	36	Ordovician Ss	Everton Ss	
13	4.6	46	Chert		
14	5.8	58	Miss-Penn Ss	Batesville Ss	
15	6.4	64	Ordovician Ss	Everton Ss	
16	5.3	53	Ordovician Ss	Everton Ss	
17	3.6	36	Limestone		
18	5	50	Ordovician Ss	Everton Ss	
19	4	40	Limestone		
20	3.5	35	Chert		

Main Stem Bar Upstream of Calf Confluence: Lower Bar Provenance

#	Size (cm)	Size (mm)	Lithology/Unit	Notes	Sample?
1	4.3	43	Chert		
2	5.3	53	Chert		
3	4.3	43	Miss-Penn Ss	Sub-angular, perhaps dirty Batesville Ss sample	#1-1
4	3.5	35	Chert		
5	5.6	56	Ordovician Ss	likely Everton Ss	#1-2
6	4.6	46	Ordovician Ss	Everton Ss	
7	3.1	31	Chert		
8	2.6	26	Chert		
9	3.6	36	Dolostone		#1-3
10	5.2	52	Limestone/dolostone	light/white	#1-4
11	2.7	27	Miss-Penn Ss	Sugary (friable), shiny	
12	3.4	34	Chert		
13	3.4	34	Miss-Penn Ss	Batesville Ss	
14	5.5	55	Chert		
15	3.1	31	Limestone/dolostone		
16	3.8	38	Limestone		
17	2.6	26	Miss-Penn Ss		
18	12	120	Limestone	Boone Ls? Light grey matrix	#1-5
19	4.9	49	Ordovician Ss	Everton Ss	
20	9	90	Ordovician Ss	Batesville Ss	

Appendix C.5: Calf Creek bar provenance data (Bar B in Appendix C.2). These 60 samples were analyzed on the upper, middle, and lower portions of the bar, respectively. *Miss-Penn* meaning *Mississippian-Pennsylvanian*; *Ss* meaning *sandstone*; *Ls* meaning *limestone*.

Calf Creek Bar: Upper Bar Provenance

#	Size (cm)	Size (mm)	Lithology/Unit	Notes	Sample?
1	12.5	125	Cherty Limestone	intermingling	
2	6.4	64	Chert		
3	3.8	38	Limestone	white	
4	3	30	Miss-Penn Ss	dark Batesville Ss	
5	3.5	35	Limestone	dark tan Ls, possibly coarse	
6	2.4	24	Limestone	grey	
7	9.7	97	Limestone		
8	5.5	55	Limestone	dark grey, with iron	
9	6	60	Limestone	dark tan Ls	
10	5.8	58	Miss-Penn Ss	Batesville Ss	
11	6.7	67	Limestone	white	
12	5.2	52	Miss-Penn Ss	Batesville Ss	
13	2.2	22	Limestone	white	
14	4.5	45	Miss-Penn Ss	Batesville Ss, dark outside tan inside	
15	3	30	Chert		
16	12.8	128	Limestone	fossiliferous	
17	6.4	64	Limestone		
18	5.5	55	Limestone	fossiliferous	
19	4.5	45	Chert		
20	5.1	51	Limestone	fossiliferous	

Calf Creek Bar: Middle Bar Provenance

#	Size (cm)	Size (mm)	Lithology/unit	Notes	Sample?
1	8.2	82	Limestone	white/clean	
2	7	70	Limestone	white/clean	
3	5.2	52	Limestone	coarse-grained w/ some angular quartz grains	#5-1
4	6.5	65	Chert		
5	4.4	44	Limestone	light grey, clean	
6	4.2	42	Miss-Penn Ss		#5-2
7	4.2	42	Chert		
8	3.6	36	Miss-Penn Ss	Batesville Ss	
9	3.9	39	Limestone	Slightly red colored	
10	4.5	45	Limestone	light grey limestone with white exterior	
11	5.7	57	Miss-Penn Ss	granular Ss	#5-3
12	4.9	49	Chert		
13	4.6	46	Limestone	light grey limestone	
14	3.9	39	Limestone		
15	5.8	58	Limestone		
16	5.7	57	Limestone		
17	5.1	51	Chert		
18	7.9	79	Chert		
19	4.5	45	Chert		
20	6.2	62	Limestone		

Calf Creek Bar: Lower Bar Provenance

#	Size (cm)	Size (mm)	Lithology/Unit	Notes	Sample?
1	4.7	47	Boone Ls	light grey limestone	
2	5.4	54	Boone Ls	white on weathered & fresh surfaces	
3	10.1	101	Miss-Penn Ss	Batesville Ss	
4	4.8	48	Limestone	Peach colored, interesting fiber-like matrix	
5	3.4	34	Boone Ls	Light grey limestone	
6	3.5	35	Limestone	Light colored	
7	3.5	35	Limestone	Light colored: white/light grey	
8	4.8	48	Limestone		#4-1
9	3.5	35	Cherty Limestone		#4-2
10	4.6	46	Limestone?	peach-orange colored, interesting/complex matrix	#4-3
11	3	30	Limestone	peach colored, interesting matrix	
12	3.1	31	Miss-Penn Ss	Dark on fresh & weathered facies, iron-bearing	#4-4
13	3	30	Limestone	Peach & white. Coarse peach w/ white intermingling colors, fine	
14	4.6	46	Miss-Penn Ss	Dirty Batesville Ss	
15	4.8	48	Limestone	White Ls with heavy iron on one side	
16	3.5	35	Limestone	Dark on fresh & weathered facies	
17	4	40	Limestone	Light colored	
18	4.2	42	Miss-Penn Ss	Batesville Ss	
19	1.5	15	Limestone		
20	3.6	36	Limestone	peach-colored	

Appendix C.6: Main stem of the BNR just downstream of the Calf Creek confluence provenance data (Bar C in Appendix C.2). These 60 samples were analyzed on the upper, middle, and lower portions of the bar, respectively. *Miss-Penn* meaning *Mississippian-Pennsylvanian*; *Ss* meaning *sandstone*; *Ls* meaning *limestone*; *FV* meaning *Fayetteville Shale*.

Main Stem Bar Downstream of Calf Confluence: Upper Bar Provenance

#	Size (cm)	Size (mm)	Lithology/Unit	Notes	Sample?
1	5.1	51	Ls	white	
2	3.6	36	Ls	white	
3	3.6	36	Ls	white	
4	4.1	41	Ls	white	
5	3.7	37	Chert		
6	4	40	Ls		
7	3.4	34	Chert		
8	3.1	31	Ss	w/ green tint	#7-1
9	4	40	Ls	white	
10	4.1	41	Ls	white	
11	3.2	32	Chert		
12	3.4	34	Ls	peachy/dirty	
13	3.7	37	Ls	white	
14	1.8	18	Batesville Ss	dirty	
15	2	20	Batesville Ss		
16	7.5	75	Ls	white Ls, shiny fine grains	
17	4.4	44	Chert		
18	2.5	25	Batesville Ss		
19	1.8	18	Chert		
20	3.4	34	Ls		

Main Stem Bar Downstream of Calf Confluence: Middle Bar Provenance

#	Size (cm)	Size (mm)	Lithology/unit	Notes	Sample?
1	6.5	65	Ls	white	
2	3.4	34	Chert	white	
3	4	40	Chert	white	
4	3.6	36	Chert	white	
5	5	50	Ls	white	
6	3.5	35	Ls	fossiliferous	
7	3.8	38	Ls	white	
8	4	40	Miss-Penn Ss	coarse, reddish	
9	2.6	26	Miss-Penn Ss	dark w/ iron	
10	3	30	Chert		
11	4.4	44	Chert	fossiliferous	#8-1
12	3	30	Ls	white	
13	2.2	22	Ls	white	
14	5.3	53	Ls	dark on weathered & fresh facies	#8-2
15	3	30	Miss-Penn Ss		
16	2.7	27	Miss-Penn Ss	Very dark colored, perhaps dark Ls/shale?	#8-3
17	3.2	32	Batesville Ss		
18	2.8	28	Chert		
19	4.3	43	Chert		
20	1.9	19	Chert	black	

Main Stem Bar Downstream of Calf Confluence: Lower Bar Provenance

#	Size (cm)	Size (mm)	Lithology/Unit	Notes	Sample?
1	3.9	39	Ls	peach/dirty, fossils & iron as well	
2	2.9	29	Ls	white	
3	3.3	33	Miss-Penn Ss	Bloyd?	
4	2.9	29	Chert	tan outer, white inner	
5	2.7	27	Ls	white	
6	2.7	27	Ls w/ Chert nodule	dark colored	#9-1
7	2.9	29	Chert		
8	3.9	39	Ls	white; effervesces with HCl	
9	3.5	35	Ls	white	
10	2.5	25	Ls	white	
11	2.1	21	Ls	white	
12	3.5	35	Chert		
13	3.5	35	Chert	white	
14	4.3	43	Ls	white	
15	2.7	27	Chert	tan	
16	3.2	32	Miss-Penn Ss	thin black, sheet-like (FV Shale? Dark Ls?)	#9-2
17	2.8	28	Ls	dirty, weathered Ls	
18	2.5	25	Ls	fossiliferous	
19	2.4	24	Ls	fossiliferous	
20	2.8	28	Ls	dirty	

APPENDIX D:

Clabber Creek

Appendix D.1: Geologic map of the Clabber Creek tributary basin and surrounding area. Geologic map overlays acquired from Ausbrooks et al. (2012a, 2012b).

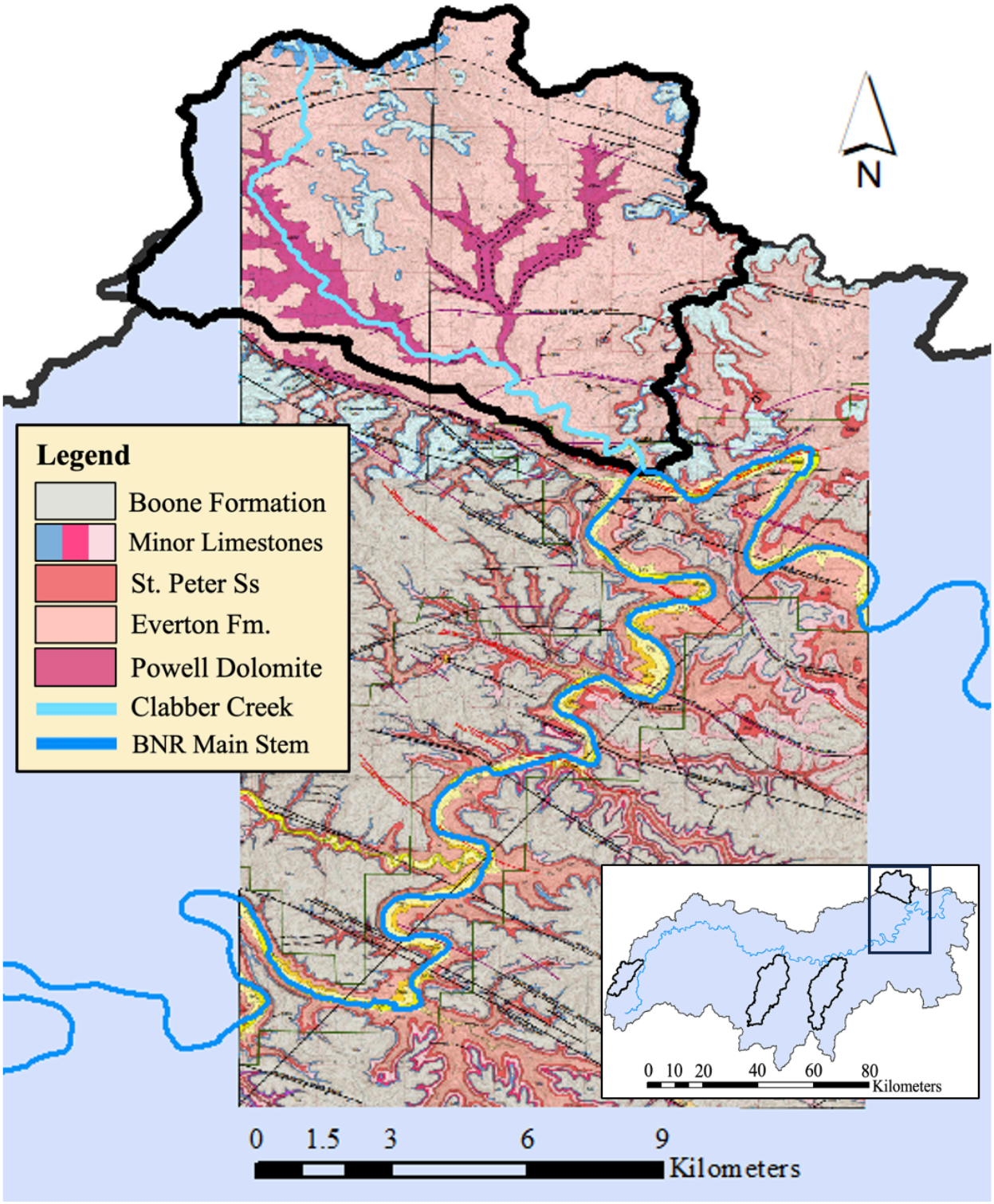

Appendix D.2: Satellite imagery of the Clabber Creek confluence area and sampled gravel bars. Clabber Creek flows North to South into the BNR main stem, which is flowing West to East in the southern portion of the image. Each approximate gravel bar area is denoted in the table. **Bar A**: Clabber Creek gravel bar; **Bar B**: BNR main stem bar just upstream of the Clabber Creek confluence; **Bar C**: BNR main stem bar just downstream of the Clabber Creek confluence. Gravel bar provenance data is contained in Appendix D.4-6. Satellite imagery from Google Earth Pro (v. 7.3.6.9345), May 4, 2014 (Google Earth, 2023).

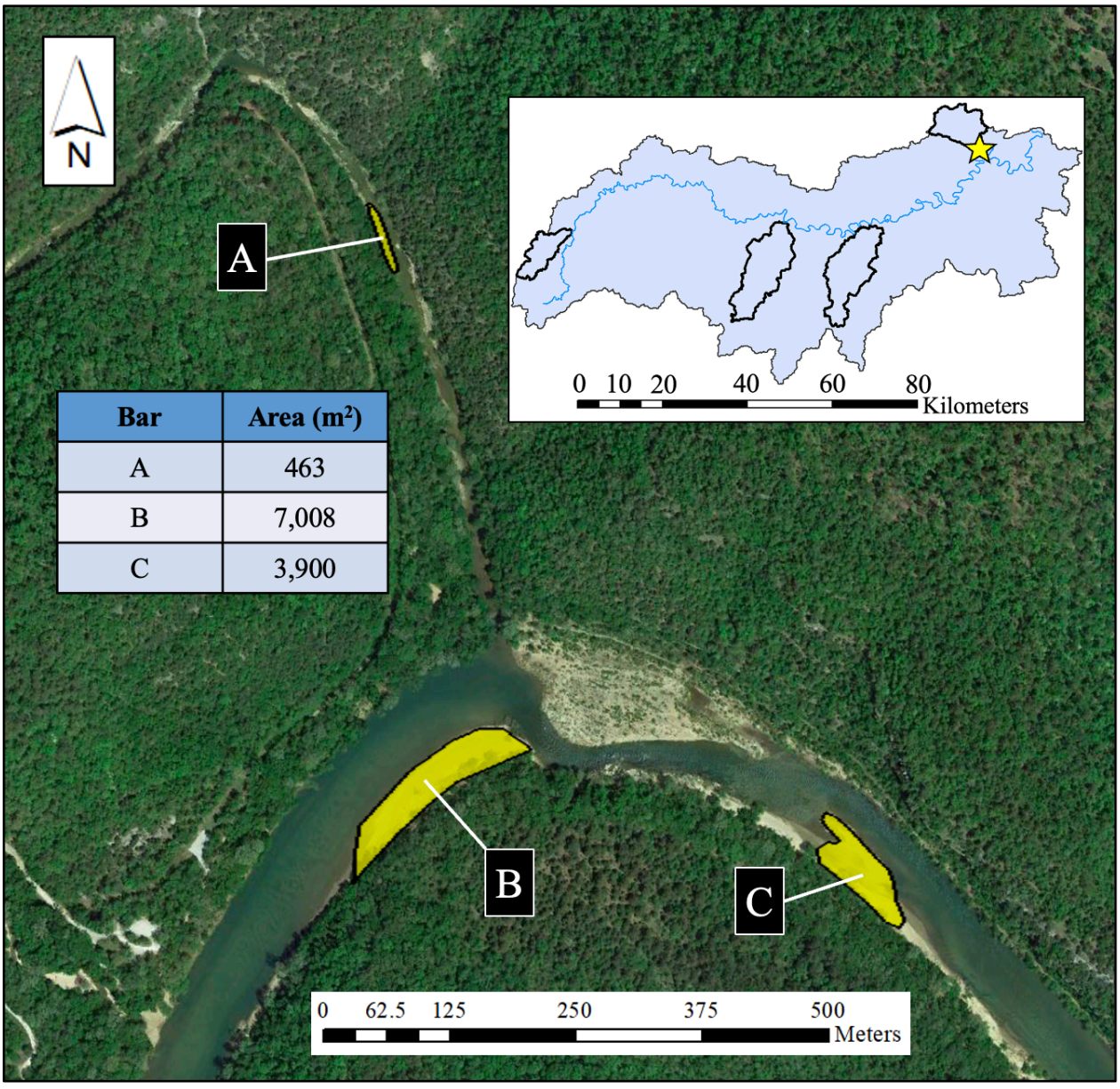

Bar	Area (m²)
A	463
B	7,008
C	3,900

Appendix D.3: Field images from each gravel bar in Appendix D.2. Arrows in each image denote flow direction. All images were captured on 7/23/2022. **Image A**: Looking downstream on the Clabber Creek gravel bar (Appendix D.2: Bar A). James for scale. **Image B**: Looking upstream from the BNR bar upstream of the Clabber confluence (Appendix D.2: Bar B). James and field equipment for scale. **Image C**: Looking downstream from the BNR bar downstream of the Calf confluence (Appendix D.2: Bar C). James for scale.

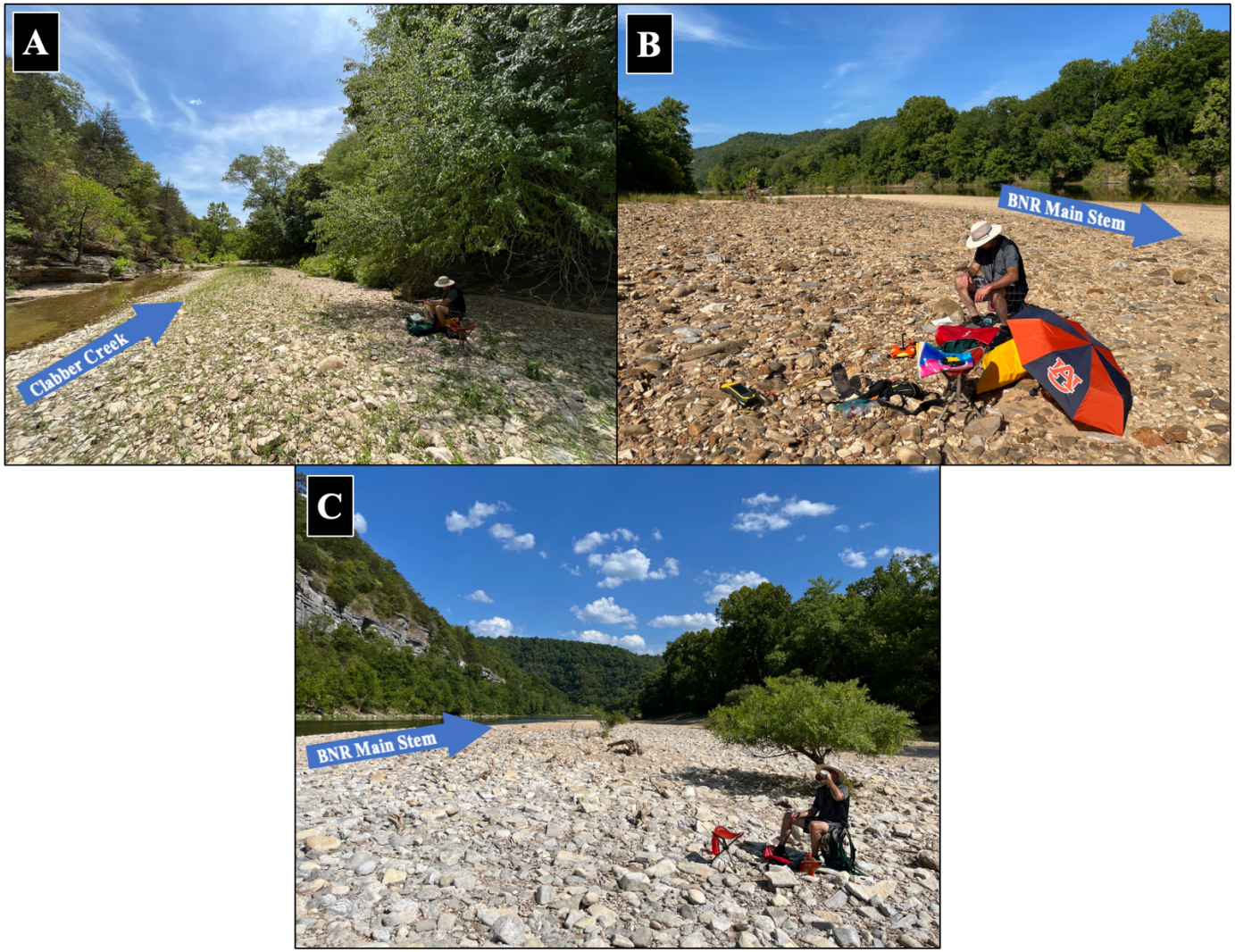

Appendix D.4: Clabber Creek bar provenance data (Bar A in Appendix D.2). These 60 samples were analyzed on the upper, middle, and lower portions of the bar, respectively. *Miss-Penn* meaning *Mississippian-Pennsylvanian*; *Ss* meaning *sandstone*; *Ls* meaning *limestone*; *dolo* meaning *dolostone*.

Clabber Creek Bar: Upper Bar Provenance

#	Size (cm)	Size (mm)	Lithology/Unit	Notes	Sample?
1	7.6	76	Everton Ss	coarse-grained, light tan outside, white/tan inside, all quartz, clean	
2	6.9	69	Ls/Dolo	tan-gray color, visibly effervesces w/ HCl	
3	5	50	Powell Shale	tan outside, greenish tan inside	#19-1
4	4.8	48	Powell Dolo	white like Ls, but no reaction with HCl	#19-2
5	5.3	53	Powell Dolo	thin, light grey/tan outside, white/light grey inside	#19-3
6	5.4	54	Dolostone	light grey color	#19-4
7	3	30	Everton Dolo	medium grey inside	
8	7.3	73	Everton Ss	shiny, all quartz grains, white to medium grey color	
9	2.9	29	Everton Dolo/Ls	medium grey, effervesces with HCl	
10	4	40	Everton Dolo	large white crystal pockets that react with HCl, dark grey color, calcite pockets react with HCl, chert nodules present	
11	3.5	35	Powell Dolo	light grey to tan	
12	3.7	37	Dolomite?	tan to medium grey	#19-5
13	3.9	39	Chert	translucent grey chert	#19-6
14	2.6	26	Everton Dolo	dark grey inside	
15	3.6	36	Dolomite?	dark to light tan in, weak HCl reaction (held up to ear)	#19-7
16	4.7	47	Powell Dolo	clean white in, white to tan out. Weak HCl reaction (held up to ear)	#19-8
17	8.7	87	Everton Ss	coarse quartz, clean, white to tan to greyish	
18	2.7	27	Chert	medium grey	
19	3.1	31	Powell Dolo	Fe-rich, white to black inside	
20	5.2	52	Powell Dolo	pink tint, grainy	#19-9

Clabber Creek Bar: Middle Bar Provenance

#	Size (cm)	Size (mm)	Lithology/unit	Notes	Sample?
1	6.4	64	Powell Dolo	white, gritty	
2	4	40	Everton Dolo	medium to dark grey	
3	3.1	31	Chert	light tan, conchoidal fracture	
4	4.6	46	Everton Dolo	light to medium grey	
5	2.6	26	Everton Dolo	Fe-nodules, medium grey	
6	6.2	62	Dolostone?	tan to brown inside	#20-1
7	2.5	25	Chert	tan color - similar to sample #20-1	
8	3.5	35	Dolostone	similar to previous two	
9	3	30	Dolostone (Everton?)	light grey	#20-2
10	6.4	64	Dolostone	pink tint, grains present	#20-3
11	4.4	44	Cherty dolo?	dark grey, translucent, similar to previous, translucent	#20-4
12	4.9	49	Dolostone	dark grey, shiny, reacts w/ HCl well	
13	3.3	33	Dolostone	light grey, reacts w/ HCl well	
14	5.4	54	Ss	crystal, small grains, light grey	
15	3.9	39	Cherty dolo	black/brown out, tan to brown inside	
16	5	50	Everton Dolo	dark grey cherty nodules	
17	3.8	38	Dolostone	greenish tint to tan to light grey inside, effervesces w/ HCl well	
18	5.8	58	Dolostone	light to medium grey, smooth inside, effervesces w/ HCl, white outside	#20-5
19	6.2	62	Cherty Dolo	light grey inside	
20	4.3	43	Dolostone	tan to medium grey	#20-6

Clabber Creek Bar: Lower Bar Provenance

#	Size (cm)	Size (mm)	Lithology/Unit	Notes	Sample?
1	5.5	55	Dolostone Everton	dark grey outside & inside	
2	3.5	35	Powell Dolo	pink tint, chert-like fracture	
3	4.5	45	Powell Dolo	white, gritty, pink tint out	
4	6.1	61	Everton Dolo	fossiliferous, translucent appearance in dark grey	
5	5.5	55	Everton Dolo	grey out, dark grey in, no grains, classic look, vigorously effervesces w/ HCl	
6	5.1	51	Everton Ss	Fe-band, pink to tan to white inside, fine grained	#21-1
7	4.2	42	Everton Dolo	medium grey, classic look, no grains	
8	3.3	33	Everton Dolo		
9	5.1	51	Everton Dolo	medium grey, classic look	
10	5.7	57	Everton Ss	shiny, sandy quartz grains, white with tan	
11	3.6	36	Everton Dolo	medium grey	
12	6.2	62	Powell Dolo	white	#21-2
13	3.1	31	Dolo/Ls (Boone? Everton?)	classic look, medium grey out & in, effervesces well w/ HCl	#21-3
14	5.4	54	Cherty Dolo	pink tint, white, cherty	
15	4.2	42	Everton Dolo	medium grey, fossiliferous, reacts well w/ HCl	
16	4	40	Everton Dolo	same as 15, weathered granular bands	#21-4
17	2.3	23	Chert	white inside	
18	3.7	37	Everton Dolo	medium grey outside, dark grey inside, shiny	
19	3.5	35	Chert	tan outside & inside	
20	5.8	58	Everton Dolo	light grey, smooth, weak HCl reaction (can hear when held up to ear)	#21-5

Appendix D.5: Main stem of the BNR just upstream of the Clabber Creek confluence provenance data (Bar B in Appendix D.2). These 60 samples were analyzed on the upper, middle, and lower portions of the bar, respectively. *Miss-Penn* meaning *Mississippian-Pennsylvanian*; *Ss* meaning *sandstone*; *Ls* meaning *limestone*; *dolo* meaning *dolostone*.

Main Stem Bar Upstream of Clabber Confluence: Upper Bar Provenance

#	Size (cm)	Size (mm)	Lithology/Unit	Notes	Sample?
1	3.3	33	Chert	white outside & inside	
2	4.5	45	Ss	brown outside, dark grey inside	
3	4.7	47	Chert	light gray, conchoidal fracture	
4	6.4	64	Ls/dolo	pink tint, geode band, white inside	#18-1
5	3.4	34	Shale	black	
6	4	40	Ss	dark grey outside & inside	
7	7.2	72	Chert	tan outside, white inside	
8	6.7	67	Everton Ss	clean, all quartz, tan/white inside, sandy	
9	3.1	31	Chert	white outside & inside	
10	3.2	32	Ls?	dark grey out/in, fine grained, no reaction with HCl	#18-2
11	4.5	45	Miss-Penn Ss	very coarsely grained, shiny, dark tan in, dirty & sandy	
12	1.8	18	Shale	black	
13	2.3	23	Chert	dark grey, conchoidal fracture	
14	5.7	57	Ss	Fe-bands, yellow/tan/white in, all quartz	
15	6.1	61	Everton Ss	extremely sandy (friable), white/tan on fresh surface	
16	10.4	104	Ss	large grains, coarse, sub-angular, Fe bits, light gray, greenish tint	
17	3.4	34	Chert	white	
18	4.9	49	Ss	green tint in specific area, light grey/brown in, fine-grained	
19	1.2	12	Ls	dark grey outside & inside	
20	4.5	45	Cherty Ls	zebra-looking	

Main Stem Bar Upstream of Clabber Confluence: Middle Bar Provenance

#	Size (cm)	Size (mm)	Lithology/unit	Notes	Sample?
1	5.5	55	Dolostone ?	tan out, dark grey inside	#17-1
2	3.3	33	Ls	zebra-looking, zebra color inside, white Ls	#17-2
3	9.4	94	Ls/Dolo	light tan outside, white inside. Doesn't react with HCl well	#17-3
4	4.3	43	Ss	dark grey outside & inside	
5	5.5	55	Everton Ss	Fe nodules, all quartz (quartz-arenite)	
6	3.9	39	Chert	tan outside, white inside	
7	6.6	66	Ss	dark tan/dark grey	
8	6.2	62	Cherty Ls	white/tan color	
9	5.6	56	Chert	white inside, tan outside	
10	7.7	77	Ls?	medium grey outside & inside, coarse quartz grains, sub-rounded, reacts well with HCl (calcite cement?)	#17-4
11	3.6	36	Ss	dark grey outside & inside, Fe-rich, lightly effervesces with HCl	
12	4.3	43	Ls	white to light tan color	
13	4.8	48	Everton Ss	clean, sugary, light tan out, light tan/white inside. all quartz, fine grained	
14	5.1	51	Ss	tan to medium grey inside, sub-angular grains, medium grains	
15	6.1	61	Chert	white	
16	3.5	35	Ls	white outside & inside	
17	7	70	Ss	dark yellow/tan on fresh surface, fine grained	
18	2.5	25	Ss	dark grey/tan on fresh surface, shiny	
19	2.5	25	Ls	white to light orange on fresh surface	
20	2.8	28	Chert	white on fresh surface	

Main Stem Bar Upstream of Clabber Confluence: Lower Bar Provenance

#	Size (cm)	Size (mm)	Lithology/Unit	Notes	Sample?
1	7.8	78	Ls	white outside & inside	
2	6.7	67	Ls/Dolo	medium grey, quartz grains, gray outside & inside	#16-1
3	4.3	43	Chert	dark tan out, white in	
4	3.9	39	Ls	white color	
5	2.8	28	Ls	white, fossiliferous (crinoids?)	
6	9.3	93	Ls (Boone?)	classic, medium grey outside & inside, seeing this a lot	#16-2
7	2.8	28	Cherty Ls	tan outside & inside	
8	2.1	21	Ss	dark sandstone, calcite cement, quartz grains, Fe nodule	#16-3
9	4.7	47	Quartz-Arenite Ss	dark tan out, dark in, fine-grained	
10	3.4	34	Ls	white outside/inside	
11	5.2	52	Ls	white outside/inside	
12	10.7	107	Ss (Everton?)	very sandy, tan out, med grey in (grey/white). Quartz-Arenite	#16-4
13	4.5	45	Chert/Cherty Ls	tan out, white in	
14	6.9	69	Ss	tan in, sandy, quartz-arenite	#16-5
15	6.5	65	Ls	classic, medium gray outside & inside	
16	4.4	44	Ss	gray/tan outside & inside, slight green tint	
17	4.4	44	Ls	coarse, grey	
18	3.3	33	Cherty Ls	tan/white outside, white inside	
19	13.6	136	Ls	dark grey out, medium grey in. quartz crystals, same as #17	
20	3.1	31	Dolo?	white out & in, fiber-like matrix	#16-6

Appendix D.6: Main stem of the BNR just downstream of the Clabber Creek confluence provenance data (Bar C in Appendix D.2). These 60 samples were analyzed on the upper, middle, and lower portions of the bar, respectively. *Ss* meaning *sandstone*; *Ls* meaning *limestone*; *dolo* meaning *dolostone*.

Main Stem Bar Downstream of Clabber Confluence: Upper Bar Provenance

#	Size (cm)	Size (mm)	Lithology/Unit	Notes	Sample?
1	16.5	165	Ls/dolo	light grey out, dark grey in, shiny, fizzes well, classic dark grey	#22-1
2	6	60	Ss	red sandstone, fine grained	
3	4.7	47	Ss?	quartz crystals, all white	#22-2
4	5	50	Ss (Batesville?)	gold color, sugary Ss, fine grained	#22-3
5	5	50	Ls	fossiliferous, light grey to tan	
6	4.4	44	Everton Dolo	light grey, fine grained	
7	4.2	42	Ss (Batesville?)	gold color, sugary, same as #22-3	
8	4.4	44	Ss (Batesville?)	same as above	
9	16.2	162	Everton Ss	white, sugary	
10	11.2	112	Ls/dolo	laminated, fine grained, classic medium grey out & in. Looks like stuff from Clabber	#22-4
11	3.9	39	Ls	black Ls with green tint	
12	11.2	112	Ls	classic grey look, same as #22-1	
13	4	40	Dolostone	white to light grey color, very fine grained	#22-5
14	8.3	83	Dolostone	classic light grey color, no grains, fizzes lightly	#22-6
15	10	100	Dolostone	light grey, same as previous, as #22-6. Both this one & the last one are like #20-5 from earlier	
16	2.1	21	Chert	white in	
17	3	30	Dolostone	light grey	
18	7.2	72	Ss	tan, same as #16-5 & #22-3	
19	3	30	Everton Ss	tan/white, sandy, medium grained	
20	3.5	35	Chert	chert with quartz veins	

Main Stem Bar Downstream of Clabber Confluence: Middle Bar Provenance

#	Size (cm)	Size (mm)	Lithology/unit	Notes	Sample?
1	5.2	52	Ss	black Ss, dark inner, grains, calcite cement	#23-1
2	6.1	61	Ss	dark grey/black in, fine grained	#23-2
3	4.7	47	Everton Dolo	light grey to medium grey	
4	6	60	Chert	dark grey in	
5	12.8	128	Dolostone	classic grey, coarse grained, medium grey	#23-3
6	3.7	37	Cherty Dolo	light grey/white w tan, gritty	
7	2.1	21	Ss	dark grey/tan, fine grained	
8	5.8	58	Ss	same as above, shiny, sub-angular grains, sandy	
9	4.6	46	Dolostone	gritty, light grey to tan	
10	9.1	91	Ls/dolo	light grey white out, lightly fizzes	#23-4
11	4.4	44	Ss (quartz-arenite)	sandy, tan, medium grained	
12	9.5	95	Ls	classic look, medium grey, fizzes a lot, same as #22-1 (only lighter, same matrix)	
13	7.5	75	Ls	classic look, medium grey out & in, same as #22-1	
14	4.4	44	Ss	sandy, tan, like other Ss	
15	6	60	Ss	brown color, fine grained	#23-5
16	5.3	53	Dolostone	light grey, fine grained	
17	3.6	36	Ss	dark, black	#23-6
18	4.8	48	Ls	classic look, medium grey out & in, heavy fizz	
19	2.9	29	Chert	medium grey in	
20	2.8	28	Everton Ss		

Main Stem Bar Downstream of Clabber Confluence: Lower Bar Provenance

#	Size (cm)	Size (mm)	Lithology/Unit	Notes	Sample?
1	3.3	33	Dolostone	white	
2	11.9	119	Ls	classic look, light grey out & in, effervesces w/ HCl well, medium grey in, similar to #22-1	#24-1
3	1.8	18	Chert	tan	
4	5.1	51	Everton Ss	sandy, coarse grained, tan	
5	4.2	42	Dolostone	fiber-like appearance, white in, no fizz	#24-2
6	3.2	32	Dolostone	white in, a few coarse grains	
7	2.5	25	Dolostone	white outside & inside, gritty, very fine grained, no fizz	#24-3
8	5.5	55	Everton Ss	white/tan, sandy	
9	3.2	32	Chert	white/tan	
10	2	20	Dolostone?	fossiliferous	#24-4
11	2.8	28	Cherty Ls		
12	4.5	45	Dolo/Ls	no fizz, white to tan	#24-5
13	3.5	35	Ls	red, fizzes, fiber-like matrix, has grains	#24-6
14	5.3	53	Chert	white	
15	11.8	118	Ls/Dolo	classic medium grey out & in, vigorously effervesces w/ HCl	
16	3.2	32	Chert		
17	4	40	Chert	grey, conchoidal fracture	
18	2.6	26	Dolo/Ls	white outside & inside, Ls appearance, fossil present, same as #24-4	
19	3.5	35	Dolostone	white to light grey out/in	
20	3.8	38	Dolo/Ls?	same as #24-4	

APPENDIX E:

Caliber Statistics

Appendix E.1: RStudio statistical functions utilized in this study's caliber data analyses.

Name	Function	Citation
Mean Function	Determine average cobble sizes	-
Variance Function	Determine range in cobble sizes	Burt et al. (2009)
Shapiro-Wilk Test	Statistically inspect for normality	Shapiro and Wilk (1965)
Bartlett Test	Statistically test if groups have equal variance	Bartlett (1937)
Kruskal-Wallis Test	Non-parametric one-way analysis of variance (ANOVA)	Burt et al. (2009)
Wilcoxon Rank Sum Test	Non-parametric pairwise test to detect significantly different medians	Ott and Longnecker (2001)

Appendix E.2: RStudio example script to run statistical analyses on confluence gravel size distribution data. Though this script is specific to the Cave Creek confluence, it is easily applied to each study confluence with minor modifications.

```
#Script to analyze cave creek pebble count data

#Import data
CaveCreek <- read.csv("CaveCreek_forR_NA.csv")

mean(CaveCreek$CaveBar_cm,na.rm = TRUE)
mean(CaveCreek$BuffDown_cm,na.rm = TRUE)
mean(CaveCreek$BuffUp_cm,na.rm = TRUE)

var(CaveCreek$CaveBar_cm,na.rm = TRUE)
var(CaveCreek$BuffDown_cm,na.rm = TRUE)
var(CaveCreek$BuffUp_cm,na.rm = TRUE)

#visually inspect data for normality
hist(CaveCreek$CaveBar_cm)
hist(CaveCreek$?..BuffUp_cm)

#test if data is normal
#p-value <0.05 means not normal
shapiro.test(CaveCreek$CaveBar_cm)

#test if groups have equal variance
#p-value <0.05 means variances not equal
bartlett.test(CaveCreek)

#non-parametric anova
#p-value <0.05 means at least one group is significantly different
kruskal.test(CaveCreek)

#pairwise tests to determine if groups are different
wilcox.test(CaveCreek$CaveBar_cm,CaveCreek$BuffDown_cm)
wilcox.test(CaveCreek$CaveBar_cm,CaveCreek$BuffUp_cm)
wilcox.test(CaveCreek$BuffDown_cm,CaveCreek$BuffUp_cm)
```

Appendix E.3: RStudio statistical analysis results for each confluence.

	Beech Creek		Cave Creek	Calf Creek	Clabber Creek
Mean - Buff Up	3.43		1.9	2.62	4.47
Mean – Tributary Bar(s)	Bar 1	5.71	4.27	3.25	3.10
	Bar 2	4.64			
Mean - Buff Down	3.22		4.25	2.93	3.93
Variance - Buff Up	11.86		2.10	2.95	15.22
Variance – Tributary Bar(s)	Bar 1	35.31	9.95	3.44	4.50
	Bar 2	21.07			
Variance - Buff Down	3.38		8.23	2.63	15.09
Shapiro-Wilk Test - Tributary Bar(s)	Bar 1	W = 0.83 p-value = 2.13e-09	W = 0.92 p-value = 1.78e-07	W = 0.94 p-value = 8.88e-05	W = 0.91 p-value = 3.14e-06
	Bar 2	W = 0.79 p-value = 3.06e-12			
Bartlett Test	K^2 = 1643.3 df = 4 p-value <2.2e-16		K^2 = 2348.5 df = 3 p-value < 2.2e-16	K^2 = 2400.8 df = 3 p-value < 2.2e-16	K^2 = 1674.7 df = 3 p-value < 2.2e-16
Kruskal-Wallis Test	X^2 = 413.97 df = 4 p-value <2.2e-16		X^2 = 454.52 df = 3 p-value < 2.2e-16	X^2 = 400.27 df = 3 p-value <2.2e-16	X^2 = 384.93 df = 3 p-value < 2.2e-16

Appendix E.4: RStudio Wilcoxon Rank Sum Test results for each confluence area.

Beech Creek confluence area			
Bar	*Bar*	*W*	*P-Value*
Buff Bar - upstream	Beech Bar 1	3912.5	0.007834
Buff Bar - upstream	Beech Bar 2	5261	0.01677
Buff Bar - upstream	Buff Bar - downstream	3388	0.2751
Beech Bar 1	Beech Bar 2	6674.5	0.6523
Beech Bar 1	Buff Bar - downstream	4135	0.2462
Beech Bar 2	Buff Bar - downstream	5149	0.4442
Cave Creek confluence area			
Bar	*Bar*	*W*	*P-Value*
Cave Bar	Buff Bar - downstream	11022	0.917
Cave Bar	Buff Bar - upstream	22089	3.84e-15
Buff Bar - upstream	Buff Bar - downstream	23165	<2.2e-16
Calf Creek confluence area			
Bar	*Bar*	*W*	*P-Value*
Calf Bar	Buff Bar - downstream	11418	0.1219
Calf Bar	Buff Bar - upstream	9371	0.003996
Buff Bar - upstream	Buff Bar - downstream	13226	0.05831
Clabber Creek confluence area			
Bar	*Bar*	*W*	*P-Value*
Clabber Bar	Buff Bar - downstream	5836.5	0.7287
Clabber Bar	Buff Bar - upstream	7633.5	0.0008339
Buff Bar - upstream	Buff Bar - downstream	14378	0.003003

Legend:

Denotes significant difference detected (<0.05)	Denotes very significant difference detected (<0.01)

APPENDIX F:

Basin Morphometrics

Appendix F.1: Basin morphometric data calculated for all 48 BNR tributary basins of third order (Strahler) or greater. Basins are organized by pour order, or the order in which they are introduced into the main stem. Big Buffalo Creek and Reeves Fork have pour orders of zero, as the convergence of these two basins form the beginnings of the BNR. Numbers at the end of tributary names denote the second, third, etc. use of the same tributary name in the watershed. *Dd* stands for *drainage density*; *Rc* stands for *circularity ratio*; *Re* stands for *elongation ratio*; *Rr* stands for *relief ratio*. Asterisk (*) denotes study tributary.

Watershed	Pour Order	N or S of BNR	Strahler Order	Area (sq. km)	Perimeter (km)	Slope mean (degrees)	Flowline Length Total (km)	Main Stem Length (km)	Max Basin Length (km)	Dd	Rc	Re	Rr
Big Buffalo Creek	0	N	4	36.07	30.83	12.98	55.33	11.06	7.69	1.53	0.48	0.88	0.04
Reeves Fork	0	S	3	14.56	19.67	11.32	20.67	6.77	5.41	1.42	0.47	0.80	0.05
Adkins Creek	1	S	3	9.75	16.47	10.45	14.64	5.96	4.91	1.50	0.45	0.72	0.05
Boen Gulf Branch	2	S	3	11.81	17.18	10.66	14.05	5.40	4.03	1.19	0.50	0.96	0.07
Whitaker Creek	3	N	3	12.17	18.53	12.29	14.22	6.35	5.48	1.17	0.45	0.72	0.07
Smith Creek	4	S	3	22.41	27.40	12.92	28.42	9.56	8.13	1.27	0.38	0.66	0.05
Beech Creek*	5	N	3	50.88	46.13	13.03	63.44	12.26	10.55	1.25	0.30	0.76	0.04
Moore Creek	6	N	3	14.34	21.19	12.38	15.47	6.40	5.58	1.08	0.40	0.77	0.06
Whiteley Creek	7	N	3	15.90	20.99	12.96	17.43	8.24	4.99	1.10	0.45	0.90	0.07
Running Creek	8	S	3	11.33	15.75	14.47	13.16	6.86	4.62	1.16	0.57	0.82	0.08
Sneeds Creek	9	N	3	11.53	16.39	18.36	11.62	5.53	5.24	1.01	0.54	0.73	0.09
Cecil Creek	10	N	4	59.26	41.29	11.70	79.03	12.60	7.42	1.33	0.44	1.17	0.06
Sawmill Hollow	11	S	3	5.02	10.15	12.80	9.45	3.07	2.88	1.88	0.61	0.88	0.14

Watershed	Pour Order	N or S of BNR	Strahler Order	Area (sq. km)	Perimeter (km)	Slope mean (degrees)	Flowline Length Total (km)	Main Stem Length (km)	Max Basin Length (km)	Dd	Rc	Re	Rr
Mill Creek	12	N	4	54.66	45.69	10.42	81.41	11.97	8.59	1.49	0.33	0.97	0.05
Little Buffalo River	13	S	5	371.18	109.89	13.08	480.65	34.10	27.13	1.29	0.39	0.80	0.02
Wells Creek	14	N	4	31.38	32.91	11.76	45.41	9.00	8.20	1.45	0.36	0.77	0.05
Rock Creek	15	S	3	15.91	20.71	13.35	24.56	6.87	6.19	1.54	0.47	0.73	0.07
Sheldon Branch	16	S	3	7.50	14.61	12.74	16.09	4.43	3.97	2.15	0.44	0.78	0.11
Elm Spring Hollow	17	S	3	2.72	8.32	10.32	6.95	3.04	2.40	2.55	0.49	0.77	0.05
Big Creek	18	S	5	236.00	88.72	13.31	367.97	27.06	23.88	1.56	0.38	0.73	0.02
Lick Creek	19	S	3	11.49	17.82	11.36	17.98	6.76	5.37	1.56	0.45	0.71	0.06
Davis Creek	20	N	4	72.40	52.47	10.91	106.17	23.28	14.68	1.47	0.33	0.65	0.03
Mill Branch	21	N	3	9.59	15.16	13.78	16.13	4.71	3.92	1.68	0.52	0.89	0.06
Cave Creek*	22	S	4	135.46	74.48	12.55	209.75	29.36	21.97	1.55	0.31	0.60	0.02
Cane Branch	23	N	3	19.71	26.55	15.59	29.52	8.55	7.33	1.50	0.35	0.68	0.03
Roughedge Hollow	24	N	3	5.26	12.18	14.37	9.46	3.76	3.66	1.80	0.45	0.71	0.05
Richland Creek	25	S	5	337.52	126.99	12.23	429.59	51.04	33.62	1.27	0.26	0.62	0.01
Jamison Creek	26	N	3	19.45	22.00	12.95	32.76	7.77	5.89	1.68	0.50	0.85	0.03
Slay Branch	27	S	3	13.88	19.70	10.39	19.98	6.56	5.39	1.44	0.45	0.78	0.08
Calf Creek*	28	S	4	127.39	77.95	9.76	198.60	31.39	23.14	1.56	0.26	0.55	0.02
Mill Creek (2)	29	N	3	36.74	45.77	10.32	50.12	17.24	13.45	1.36	0.22	0.51	0.02

Watershed	Pour Order	N or S of BNR	Strahler Order	Area (sq. km)	Perimeter (km)	Slope mean (degrees)	Flowline Length Total (km)	Main Stem Length (km)	Max Basin Length (km)	Dd	Rc	Re	Rr
Dry Creek (3)	30	N	4	27.25	34.06	7.63	36.10	12.35	9.12	1.33	0.30	0.65	0.03
Bear Creek (2)	31	S	5	239.09	124.32	10.80	342.39	52.91	35.17	1.43	0.19	0.50	0.01
Brush Creek	32	S	3	51.63	45.65	11.86	74.38	15.40	12.33	1.44	0.31	0.66	0.03
Tomahawk Creek	33	N	4	95.18	67.07	10.35	145.64	25.77	16.68	1.53	0.27	0.66	0.02
Green Haw Hollow	34	N	3	5.87	12.17	13.82	10.07	2.85	2.79	1.72	0.50	0.98	0.05
Spring Creek (2)	35	S	4	34.04	29.22	14.10	55.31	7.13	6.11	1.62	0.50	1.08	0.04
Water Creek	36	N	4	99.10	61.56	11.21	181.15	24.43	17.56	1.83	0.33	0.64	0.01
Rock Creek (2)	37	S	3	11.95	19.49	15.17	18.52	6.96	5.52	1.55	0.40	0.71	0.04
Panther Creek	38	N	3	17.11	22.11	12.75	27.38	7.50	5.65	1.60	0.44	0.83	0.04
Rush Creek	39	N	3	38.24	38.14	13.36	66.52	16.67	12.63	1.74	0.33	0.55	0.02
Clabber Creek*	40	N	4	68.44	43.08	10.55	97.49	16.09	11.60	1.42	0.46	0.80	0.02
Cedar Creek	41	N	3	11.90	17.65	14.34	19.92	5.12	4.67	1.67	0.48	0.83	0.05
Boat Creek	42	N	3	10.05	14.24	14.53	14.98	4.27	3.83	1.49	0.62	0.93	0.06
Big Creek (2)	43	S	5	347.45	132.99	11.97	480.19	45.74	19.71	1.38	0.25	1.07	0.02
Middle Creek	44	S	3	28.96	30.30	16.02	33.68	9.74	7.13	1.16	0.40	0.85	0.04
Short Creek	45	S	3	5.09	11.34	16.62	7.29	3.76	3.56	1.43	0.50	0.71	0.07
Leatherwood Creek (2)	46	S	3	32.96	34.90	16.59	44.34	12.66	9.70	1.34	0.34	0.67	0.03

Appendix F.2: Drainage density (Dd) calculated and grouped into percentiles for all 48 BNR tributary basins of third order (Strahler) or greater (Figure 5.1). Basins are organized by pour order, or the order in which they are introduced into the main stem. Color key is located on the next page, though colors used here coordinate with those used in Figure 5.1. Asterisk (*) denotes study tributary.

Watershed	Pour Order	Drainage Density
Reeves Fork	0	1.42
Big Buffalo Creek	0	1.53
Adkins Creek	1	1.50
Boen Gulf Branch	2	1.19
Whitaker Creek	3	1.17
Smith Creek	4	1.27
Beech Creek*	5	1.25
Moore Creek	6	1.08
Whiteley Creek	7	1.10
Running Creek	8	1.16
Sneeds Creek	9	1.01
Cecil Creek	10	1.33
Sawmill Hollow	11	1.88
Mill Creek	12	1.49
Little Buffalo River	13	1.29
Wells Creek	14	1.45
Rock Creek	15	1.54
Sheldon Branch	16	2.15
Elm Spring Hollow	17	2.55
Big Creek	18	1.56
Lick Creek	19	1.56
Davis Creek	20	1.47
Mill Branch	21	1.68
Cave Creek*	22	1.55
Cane Branch	23	1.50
Roughedge Hollow	24	1.80
Richland Creek	25	1.27
Jamison Creek	26	1.68
Slay Branch	27	1.44
Calf Creek*	28	1.56
Mill Creek (2)	29	1.36
Dry Creek (3)	30	1.33

Watershed	Pour Order	Drainage Density
Bear Creek (2)	31	1.43
Brush Creek	32	1.44
Tomahawk Creek	33	1.53
Green Haw Hollow	34	1.72
Spring Creek (2)	35	1.62
Water Creek	36	1.83
Rock Creek (2)	37	1.55
Panther Creek	38	1.60
Rush Creek	39	1.74
Clabber Creek*	40	1.42
Cedar Creek	41	1.67
Boat Creek	42	1.49
Big Creek (2)	43	1.38
Middle Creek	44	1.16
Short Creek	45	1.43
Leatherwood Creek (2)	46	1.34

Legend:	
0-25th percentile	between 1.008 and 1.327
25-50th percentile	between 1.328 and 1.478
50-75th percentile	between 1.479 and 1.591
75-100th percentile	between 1.592 and 2.552

APPENIX G:

RFID Data

Appendix G.1: RFID gravel numbers, their corresponding PIT tag ID's, and their b-axis (cm) lengths. PIT tag ID's here are the final three digits in each ID.

ORDER #	PIT ID	B-AXIS (CM)
1	999	9.8
2	996	7.5
3	995	8.8
4	981	11.5
5	986	9
6	988	6.8
7	980	9
8	990	9.9
9	992	11.7
10	993	8.5
11	983	8.8
12	994	5.4
13	982	9.1
14	979	8.9
15	978	9
16	977	11.5
17	987	5.5
18	984	9
19	985	10.5
20	997	9.5
21	976	12
22	989	11
23	991	6.8
24	975	6.5
25	973	8
26	974	9.2
27	967	10
28	966	8.5
29	968	10.5
30	971	15.5
31	969	7.5
32	970	8.7
33	972	7.4

Appendix G.2: RFID gravel detection record from each return trip, organized by PIT tag ID. Color key located on next page.

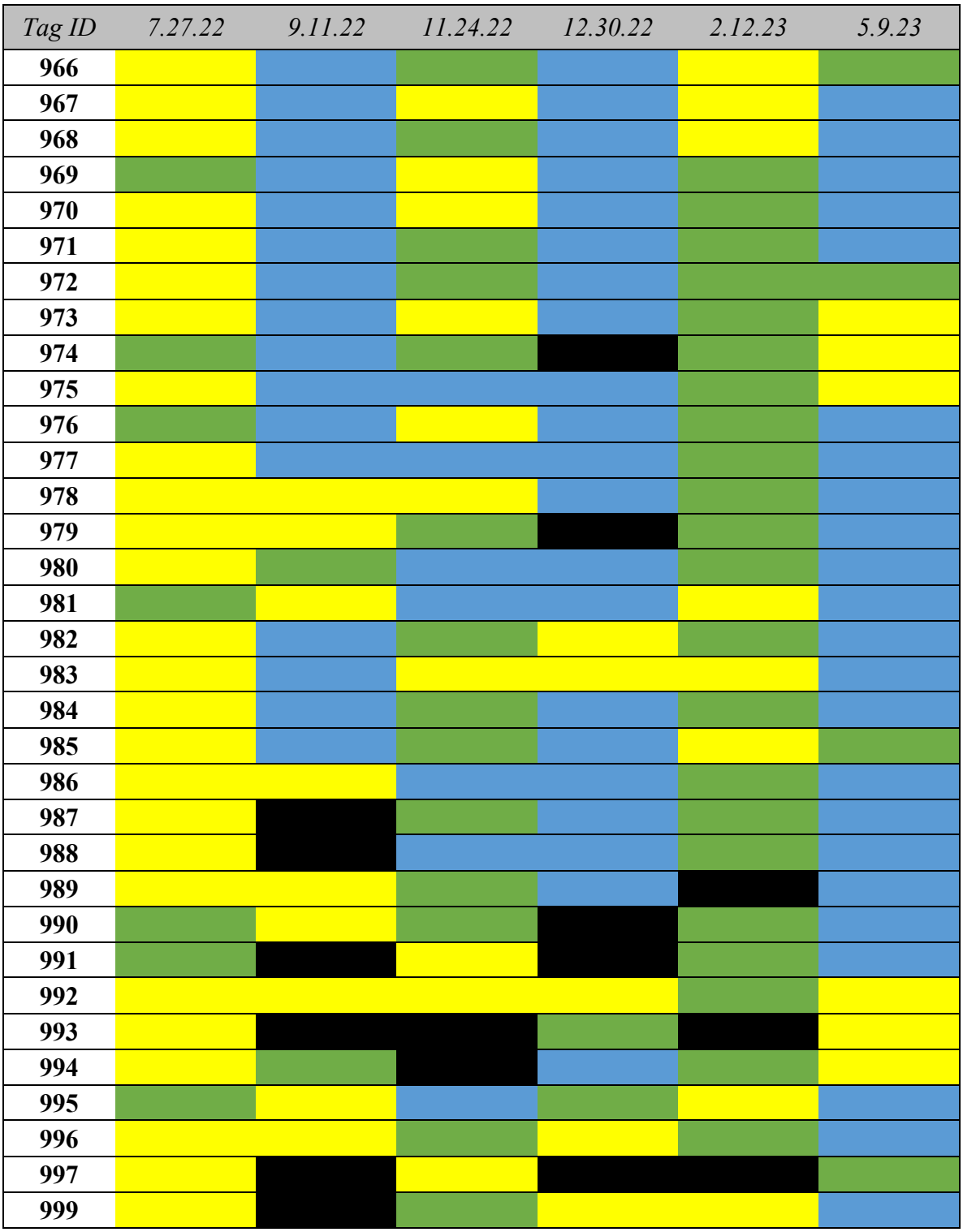

Totals:

Date	Blue	Green	Yellow	Black
7.27.22	0	7	26	0
9.11.22	16	2	9	6
11.24.22	7	14	10	2
12.30.22	21	2	5	5
2.12.23	0	22	8	3
5.9.23	23	4	6	0

Blue	Denotes detection(s) with precise coordinates (including elevation)
Green	Denotes at least one detection with coordinates, but detection may not be precise (elevation missing, or other problem)
Yellow	Denotes detected tags, but no coordinates found
Black	Denotes no detection found.

Appendix G.3: Total RFID gravel downstream movements from 7.27.2022 to 5.9.2023. Colors follow those used in Figure 4.8. Cobble sizes are also organized by distance traveled in the table below the color legend (data used in Table 4.6).

PIT Tag ID	Downstream Movement (m)
999	0.6
996	0.6
995	7.2
981	5.8
986	43.5
988	70.1
980	35.6
990	17.8
992	-
993	-
983	0.9
994	106 (approx.)
982	19.7
979	14.3
978	35.6
977	2.5
987	6.1
984	13.1
985	0.7
997	2.8
976	0.2
989	3.5
991	2.0
975	147 (approx.)
973	-
974	-
967	7.5
966	0.0
968	5.1
971	5.5
969	2.3
970	41.2
972	2.4

- Minimal/none (0-1 M)
- 1-5 M movement
- 5-20 M movement
- 20+ M movement
- Unknown

Cobble Size (cm.)			
0-1 m	1-5 m	5-20 m	20+ m
7.5	6.8	5.5	5.4
8.5	7.4	8.8	6.5
8.8	7.5	8.9	6.8
9.8	9.5	9.0	8.7
10.5	11	9.1	9.0
12	11.5	9.9	9.0
		10	9.0
		10.5	
		11.5	
		15.5	

Appendix G.4: Locations of USGS BNR main stem gages above and below Beech Creek (*Buffalo River Near Boxley, AR – 07055646* and *Buffalo River Near Ponca, AR – 07055660*). Data from these gage locations were extracted to create daily peak discharge graphs (Figure 4.7; USGS, 2023a, 2023b).

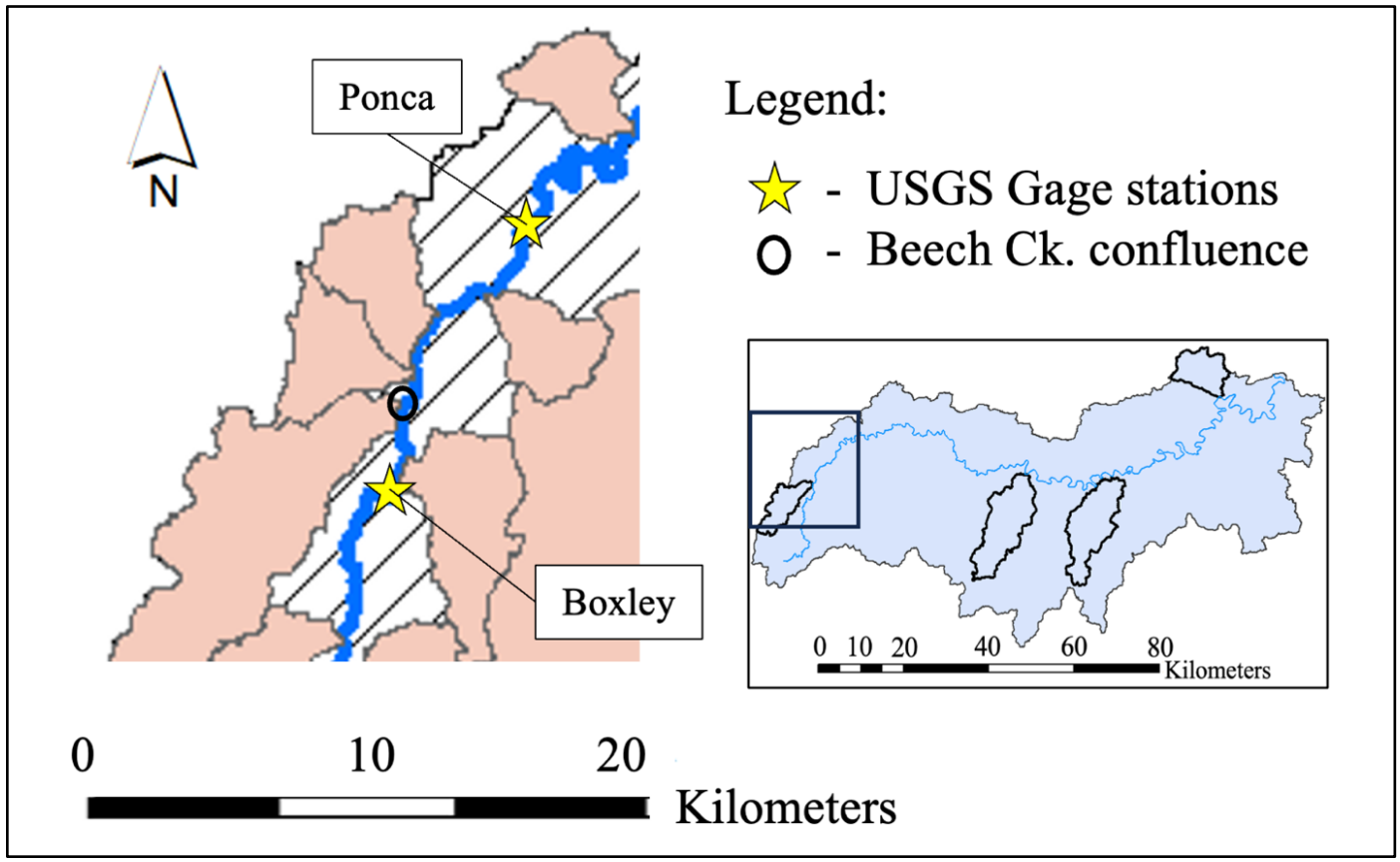

Appendix G.5: Final OregonRFID location data from surveys two through six. Survey one data is not included here, as this survey's data was extracted from the Trimble GPS unit. Data is organized by PIT tag ID. Each of these 109 data points were carefully curated from 785 detection records. Asterisk (*) denotes approximated coordinates from survey six. These data are plotted in Figure 4.6.

Date	Duration	PIT Tag ID	Gravel #	Latitude (Y)	Longitude (X)	Altitude
9/11/22	00:01.8	900_228000757966	28	35.96532	-93.40955	341
12/30/22	00:04.2	900_228000757966	28	35.96530	-93.40951	350
5/9/23	00:02.1	900_228000757966	28	35.96532	-93.40959	n/a
9/11/22	00:11.1	900_228000757967	27	35.96529	-93.40954	341
12/30/22	00:02.8	900_228000757967	27	35.96528	-93.40952	349
5/9/23	00:14.2	900_228000757967	27	35.96529	-93.40947	342
9/11/22	00:01.2	900_228000757968	29	35.96531	-93.40952	339
11/24/22	00:00.8	900_228000757968	29	35.96528	-93.40957	n/a
12/30/22	00:02.5	900_228000757968	29	35.96531	-93.40954	346
5/9/23	00:02.5	900_228000757968	29	35.96527	-93.40950	n/a
9/11/22	00:02.7	900_228000757969	31	35.96533	-93.40953	341
12/30/22	00:05.1	900_228000757969	31	35.96534	-93.40955	349
2/12/23	00:00.7	900_228000757969	31	35.96533	-93.40956	n/a
5/9/23	00:03.1	900_228000757969	31	35.96528	-93.40952	340
9/11/22	00:01.4	900_228000757970	32	35.96533	-93.40953	342
12/30/22	00:03.0	900_228000757970	32	35.96534	-93.40953	347
2/12/23	00:00.9	900_228000757970	32	35.96534	-93.40956	n/a
5/9/23	00:26.9	900_228000757970	32	35.96539	-93.40910	341
9/11/22	00:01.5	900_228000757971	30	35.96532	-93.40955	341
11/24/22	00:00.2	900_228000757971	30	35.96529	-93.40956	n/a
12/30/22	00:01.0	900_228000757971	30	35.96531	-93.40955	347
2/12/23	00:02.4	900_228000757971	30	35.96533	-93.40955	n/a
5/9/23	00:48.4	900_228000757971	30	35.96533	-93.40949	342

Date	Duration	PIT Tag ID	Gravel #	Latitude (Y)	Longitude (X)	Altitude
9/11/22	00:02.3	900_228000757972	33	35.96531	-93.40955	339
11/24/22	00:05.5	900_228000757972	33	35.96527	-93.40956	n/a
12/30/22	00:03.3	900_228000757972	33	35.96530	-93.40954	347
2/12/23	00:01.9	900_228000757972	33	35.96530	-93.40957	n/a
5/9/23	00:00.4	900_228000757972	33	35.96526	-93.40954	n/a
9/11/22	00:06.4	900_228000757973	25	35.96531	-93.40955	342
12/30/22	00:02.7	900_228000757973	25	35.96528	-93.40952	350
2/12/23	00:00.8	900_228000757973	25	35.96529	-93.40957	n/a
9/11/22	00:01.9	900_228000757974	26	35.96528	-93.40954	341
11/24/22	00:00.3	900_228000757974	26	35.96526	-93.40953	n/a
2/12/23	00:00.6	900_228000757974	26	35.96529	-93.40957	n/a
9/11/22	00:02.9	900_228000757975	24	35.96533	-93.40952	341
11/24/22	00:00.1	900_228000757975	24	35.96527	-93.40955	329
12/30/22	00:03.7	900_228000757975	24	35.96533	-93.40955	346
2/12/23	00:00.2	900_228000757975	24	35.96534	-93.40956	n/a
5/9/23	01:39.4	900_228000757975	24	35.96581*	-93.40803*	n/a
9/11/22	00:03.4	900_228000757976	21	35.96531	-93.40952	339
12/30/22	00:02.2	900_228000757976	21	35.96533	-93.40953	347
2/12/23	00:01.0	900_228000757976	21	35.96530	-93.40955	n/a
5/9/23	00:00.3	900_228000757976	21	35.96533	-93.40954	334
9/11/22	00:02.0	900_228000757977	16	35.96532	-93.40952	339
11/24/22	00:02.0	900_228000757977	16	35.96527	-93.40954	329
12/30/22	00:01.9	900_228000757977	16	35.96534	-93.40952	346
2/12/23	00:05.8	900_228000757977	16	35.96535	-93.40953	n/a
5/9/23	00:06.2	900_228000757977	16	35.96529	-93.40950	349
12/30/22	00:00.6	900_228000757978	15	35.96532	-93.40952	346

Date	Duration	PIT Tag ID	Gravel #	Latitude (Y)	Longitude (X)	Altitude
2/12/23	00:00.8	900_228000757978	15	35.96533	-93.40954	n/a
5/9/23	00:40.3	900_228000757978	15	35.96540	-93.40914	340
11/24/22	00:01.5	900_228000757979	14	35.96531	-93.40953	n/a
2/12/23	00:02.7	900_228000757979	14	35.96531	-93.40954	n/a
5/9/23	00:17.4	900_228000757979	14	35.96530	-93.40937	344
9/11/22	00:01.2	900_228000757980	7	35.96530	-93.40950	n/a
11/24/22	00:00.8	900_228000757980	7	35.96527	-93.40953	329
12/30/22	00:02.1	900_228000757980	7	35.96534	-93.40951	346
2/12/23	00:03.4	900_228000757980	7	35.96535	-93.40951	n/a
5/9/23	00:25.7	900_228000757980	7	35.96539	-93.40913	343
11/24/22	00:01.1	900_228000757981	4	35.96524	-93.40951	330
12/30/22	00:00.9	900_228000757981	4	35.96531	-93.40952	345
5/9/23	00:13.7	900_228000757981	4	35.96532	-93.40946	344
9/11/22	00:04.5	900_228000757982	13	35.96530	-93.40952	338
11/24/22	00:02.5	900_228000757982	13	35.96530	-93.40953	n/a
2/12/23	00:02.2	900_228000757982	13	35.96531	-93.40952	n/a
5/9/23	00:11.3	900_228000757982	13	35.96533	-93.40931	344
9/11/22	00:01.0	900_228000757983	11	35.96530	-93.40951	338
5/9/23	00:16.5	900_228000757983	11	35.96531	-93.40951	341
9/11/22	00:03.7	900_228000757984	18	35.96529	-93.40952	339
11/24/22	00:01.2	900_228000757984	18	35.96524	-93.40954	n/a
12/30/22	00:01.9	900_228000757984	18	35.96530	-93.40954	348
2/12/23	00:00.3	900_228000757984	18	35.96530	-93.40955	n/a
5/9/23	00:18.2	900_228000757984	18	35.96527	-93.40939	341
9/11/22	00:01.5	900_228000757985	19	35.96527	-93.40952	338
11/24/22	00:00.7	900_228000757985	19	35.96525	-93.40954	n/a

Date	Duration	PIT Tag ID	Gravel #	Latitude (Y)	Longitude (X)	Altitude
12/30/22	00:02.2	900_228000757985	19	35.96531	-93.40954	347
5/9/23	00:00.8	900_228000757985	19	35.96525	-93.40955	n/a
11/24/22	00:00.7	900_228000757986	5	35.96525	-93.40952	329
12/30/22	00:02.8	900_228000757986	5	35.96532	-93.40952	346
2/12/23	00:03.7	900_228000757986	5	35.96533	-93.40951	n/a
5/9/23	00:20.2	900_228000757986	5	35.96540	-93.40905	345
11/24/22	00:00.5	900_228000757987	17	35.96526	-93.40955	n/a
12/30/22	00:01.7	900_228000757987	17	35.96529	-93.40954	347
2/12/23	00:00.1	900_228000757987	17	35.96529	-93.40957	n/a
5/9/23	00:03.7	900_228000757987	17	35.96528	-93.40948	344
11/24/22	00:00.3	900_228000757988	6	35.96525	-93.40952	329
12/30/22	00:01.1	900_228000757988	6	35.96534	-93.40951	345
2/12/23	00:04.3	900_228000757988	6	35.96533	-93.40949	n/a
5/9/23	00:06.0	900_228000757988	6	35.96554	-93.40878	342
11/24/22	00:01.8	900_228000757989	22	35.96528	-93.40955	n/a
12/30/22	00:01.7	900_228000757989	22	35.96534	-93.40953	347
5/9/23	00:18.5	900_228000757989	22	35.96534	-93.40950	340
11/24/22	00:01.3	900_228000757990	8	35.96530	-93.40950	n/a
2/12/23	00:03.8	900_228000757990	8	35.96532	-93.40949	n/a
5/9/23	00:08.1	900_228000757990	8	35.96535	-93.40932	343
2/12/23	00:00.7	900_228000757991	23	35.96532	-93.40952	n/a
5/9/23	00:06.0	900_228000757991	23	35.96534	-93.40952	341
2/12/23	00:01.2	900_228000757992	9	35.96526	-93.40954	n/a
12/30/22	00:03.0	900_228000757993	10	35.96529	-93.40952	n/a
12/30/22	00:01.9	900_228000757994	12	35.96530	-93.40951	345
5/9/2023	01:37.9	900_228000757994	12	35.96574*	-93.40849*	n/a

Date	Duration	PIT Tag ID	Gravel #	Latitude (Y)	Longitude (X)	Altitude
11/24/22	00:01.3	900_228000757995	3	35.96528	-93.40948	333
12/30/22	00:02.3	900_228000757995	3	35.96530	-93.40951	n/a
5/9/23	00:37.6	900_228000757995	3	35.96532	-93.40944	347
2/12/23	00:00.6	900_228000757996	2	35.96527	-93.40952	n/a
5/9/23	00:11.3	900_228000757996	2	35.96530	-93.40952	339
5/9/23	00:06.9	900_228000757997	20	35.96524	-93.40951	n/a
11/24/22	00:00.7	900_228000757999	1	35.96526	-93.40952	n/a
5/9/23	00:08.8	900_228000757999	1	35.96529	-93.40952	338